Annals of Physics **295**, 136–193 (2002)
doi:10.1006/aphy.2001.6219, available online at http://www.idealibrary.com on IDEAL®

Two-Loop Correction to the Orthopositronium Decay Rate

Gregory S. Adkins

Franklin and Marshall College, Lancaster, Pennsylvania 17604

Richard N. Fell

Brandeis University, Waltham, Massachusetts 01742

and

J. Sapirstein

Department of Physics, University of Notre Dame, Notre Dame, Indiana 46556

Received June 27, 2001; revised September 24, 2001

We give a detailed description of our calculation of the $O(\alpha^2)$ correction to the orthopositronium decay rate. The resulting correction is 45.06(26) in units of $(\alpha/\pi)^2$ times the lowest order rate. When combined with other known corrections, the theoretical prediction for the decay rate is 7.039979(11) μs^{-1}, where the leading uncalculated term makes an estimated contribution of roughly 0.00002 μs^{-1}. Our result is in significant disagreement with two of the four highest precision measurements (at about the 5σ level), but does not contradict the others. The experimental uncertainties ($\approx$0.002 μs^{-1}) are much larger than the remaining theoretical uncertainties. We also calculate the one-photon-annihilation contribution to the positronium hyperfine structure at $O(m\alpha^6)$. This calculation is closely analogous to the decay rate calculation. Our agreement with prior results for this hyperfine structure contribution demonstrates the soundness of our approach.

I. INTRODUCTION

Positronium was discovered by M. Deutsch in 1951 [1]. Its discovery hinged on the development of experimental methods during the war years and shortly thereafter. (See [2, 3] for accounts of this story by Deutsch.) The notion that electrons and positrons could form a quasistable bound state had been in the air for several years. The existence of the positron had been predicted by Dirac and discovered in 1932 by Anderson through a study of cosmic rays [4]. In 1934, the spectrum of positronium was discussed by Mohorovičić [5]. The name positronium originated with Ruark in 1945, who also made note of some of its properties [6]. Detailed predictions of properties, and in particular the decay rate of the spin singlet state (parapositronium: p-Ps), were published by Wheeler [7] and by Pirenne [8] in 1946 and 1947. The spin triplet (orthopositronium: o-Ps) decay rate, which is more difficult to calculate, was first obtained correctly by Ore and Powell in 1949 [9].

There are a number of useful review articles devoted to positronium. We mention those of DeBenedetti and Corben (1954) [10], Maglic (1975) [11], Stroscio (1975) [12], Berko and Pendleton (1980) [13], Rich (1981) [14], Mills and Chu (1990) [15], Rich *et al*. (1990) [16], Dvoeglazov *et al*. (1993) [17], and Dobroliubov *et al*. (1993) [18].

0003-4916/02 $35.00

TABLE I

Experimental Determinations of the Orthopositronium Decay Rate

Year	Rate (in μs^{-1})	Type	Authors	Reference
1968	7.29(3)	Gas	Beers and Hughes	[20]
1973	7.275(15)	Gas	Hughes	[21]
1973	7.262(15)	Gas	Coleman and Griffith	[22]
1976	7.104(6)	Powder	Gidley, Marko, and Rich	[23]
1976	7.09(2)	Vacuum	Gidley, Zitzewitz, Marko, and Rich	[24]
1977	7.058(15)	Gas	Griffith and Heyland	[25]
1978	7.122(12)	Vacuum	Canter, Clark, and Rosenberg	[26]
1978	7.056(7)	Gas	Gidley, Rich, Zitzewitz, and Paul	[27]
1978	7.067(21)	Powder	Gidley, Rich, Zitzewitz, and Paul	[27]
1978	7.050(13)	Vacuum	Gidley and Zitzewitz	[28]
1978	7.045(6)	Gas	Griffith, Heyland, Lines, and Twomey	[29]
1982	7.051(5)	Gas	Gidley, Rich, Sweetman, and West	[30]
1987	7.031(7)	Vacuum	Hasbach, Hilkert, Klempt, and Werth	[31]
1989	7.0514(14)	Gas	Westbrook, Gidley, Conti, and Rich	[32, 33]
1990	7.0482(16)	Vacuum	Nico, Gidley, Rich, and Zitzewitz	[34]
1995	7.0398(29)	Powder	Asai, Orito, and Shinohara	[35]
2000	7.0399(26)	Powder	Jinnouchi, Asai, and Kobayashi	[36]

A. Experiment

A few months after the discovery of positronium, Deutsch reported the first measurement of the orthopositronium decay rate [19]. He formed o-Ps in freon (CCl_2F_2) and showed that the decay rate in the gas, $\Gamma(\text{gas})$, depends on gas pressure p according to $\Gamma(\text{gas}) = \Gamma + \beta p$. For the vacuum rate Γ he found

$$\Gamma = 6.8(7)\,\mu s^{-1}. \tag{1.1}$$

All subsequent o-Ps decay rate measurements are listed in Table I. Three types of experiments have been performed: gas, powder, and vacuum. In the gas experiments, positrons from the beta decay of Na^{22} or Ge^{68} were used. The start signal either was the 1.28 MeV gamma which accompanies each Na^{22} positron with a delay of $\approx 10^{-4}$ ns or was obtained by having the emitted positron pass through a thin scintillator. Positronium was formed on collision with the gas molecules. The stop signal came when one or more of the final state photons were detected. An extrapolation to zero gas pressure was then carried out. Powder experiments use a similar positron source arrangement, but use SiO_2 powder as the medium instead of gas. In vacuum experiments slow positrons (several hundred eV) enter a chamber and strike the cone of a channel electron multiplier (CEM) and emerge as positronium. Secondary electrons provide the start signal. The positronium atom bounces around in the chamber until it decays.

There is an interesting history of orthopositronium measurements. All measurements subsequent to the original Deutsch result and the various theoretical predictions are depicted in Fig. 1 by year. The 1968 measurement of Beers and Hughes [20] was well above the lowest order theory of Ore and Powell [9]. However, the theory value quoted by Beers and Hughes was inaccurate, apparently through use of an early, inaccurate value of the fine structure constant α. This lowest order value was improved by incorporating an improved value of α in about 1970 [25]. In the early 1970s two more gas experiments were performed [21, 22], with results consistent with the first. A calculation of the $O(\alpha)$ correction to the rate by Stroscio and Holt [37] led to improved but not satisfactory agreement between theory and experiment. This discrepancy was rendered moot in 1976, when

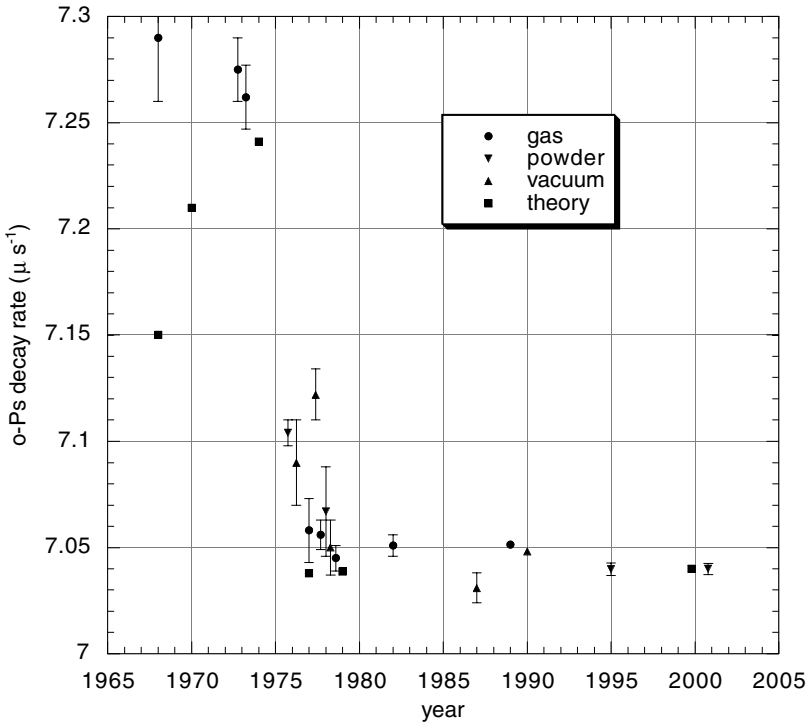

FIG. 1. All experimental and theoretical o-Ps decay rate results are shown except for the original 1951 measurement of Deutsch. The 1968 theory value is just the lowest-order Ore and Powell result as quoted by Beers and Hughes in that year. The 1970 theory is the same Ore and Powell formula but with an improved value for the fine structure constant α. The 1974 theory value is the one-loop result of Stroscio and Holt. The 1977 theory value is the corrected one-loop result of Caswell, Lepage, and Sapirstein. The $\alpha^2 \ln \alpha$ correction of Caswell and Lepage was included in 1979. The 2000 theory value contains the α^2 correction of Adkins, Fell, and Sapirstein, as well as the $O(\alpha^3)$ logarithmic corrections. The experimental results are listed in Table I.

new powder [23] and vacuum [24] results by the Michigan group lowered the measured rate by well over 10 σ. A gas experiment [25] reported shortly thereafter confirmed the dramatic shift and continued the downward trend of decay rate results. A recalculation of the $O(\alpha)$ correction by Caswell *et al*. [38] gave a new theoretical prediction below, but much closer to, the newer experimental results. Subsequent theoretical refinements shifted the result only slightly. Since 1980, all measured results have fallen into two disjoint and mutually inconsistent groups: those clustered around the theoretical prediction of 7.040 μs^{-1} [31, 35, 36] and those near 7.050 μs^{-1} [30, 32–34]. The two most precise results are the 200 ppm Michigan gas [32, 33] and vacuum [34] results of 1989 and 1990, which are in the latter group. Improved measurements by both the Tokyo [36] and the Michigan [39] groups are in the works, and the inconclusive experimental situation might soon be improved.

B. Theory

The calculation of radiative corrections to the o-Ps decay rate has a long history as well. The theoretical result for the o-Ps decay rate can be written as

$$\Gamma = \left\{1 + A\frac{\alpha}{\pi} + \frac{\alpha^2}{3}\ln\alpha + B\left(\frac{\alpha}{\pi}\right)^2 - \frac{3\alpha^3}{2\pi}\ln^2\alpha + C\frac{\alpha^3}{\pi}\ln\alpha + D\left(\frac{\alpha}{\pi}\right)^3 + \cdots\right\}\Gamma_0, \quad (1.2)$$

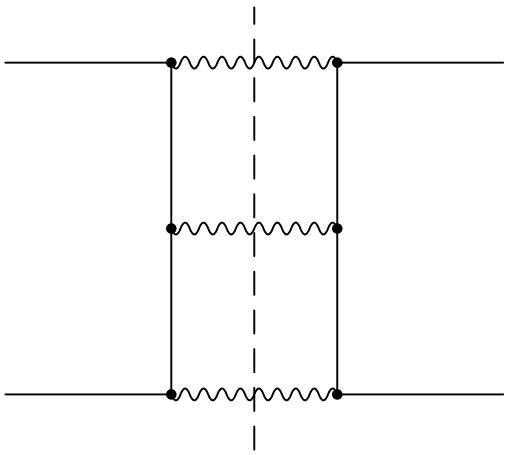

FIG. 2. QED graph contributing to the three-photon-annihilation decay rate. The dashed vertical line represents a Cutkosky cut through the three-photon intermediate state used to find the imaginary part. Time is taken to run horizontally (from right to left).

where

$$\Gamma_0 = \frac{2}{9}(\pi^2 - 9)\frac{m\alpha^6}{\pi} = 7.2111670(1)\ \mu s^{-1} \tag{1.3}$$

is the Ore and Powell result (1949) for the lowest order decay rate [9, 40]. The Feynman graph representing the lowest order decay is shown in Fig. 2.

Calculations of the one-loop $O(\alpha)$ corrections to the o-Ps decay rate were not attempted for many years—well after the 0.4% measurement of Beers and Hughes in 1968 [20]. This long delay can be attributed to the relative difficulty of the o-Ps calculation, since the one-loop correction to the p-Ps rate was worked out in 1957 [41]. The difference in difficulty is due to the structure of the final states. For p-Ps decay, charge parity conservation restricts the final state to an even number of photons, and two is preferred by two powers of α. These two photons go off back-to-back, each with nearly an electron mass of energy. The phase space is therefore trivial, and the calculation can be done readily by hand. For o-Ps decay, the preferred final state consists of three photons. There is a nontrivial two-dimensional phase space integration to be done, and the integrand is significantly more complicated than that of the two photon case.

The first one-loop correction completed was that involving an internal annihilation to a single photon (see Fig. 3f). This annihilation graph by itself forms a gauge invariant set. The contribution of the annihilation graph, worked out in 1970 by Pascual and de Rafael [42], is

$$A_A = -0.741(17). \tag{1.4}$$

The first complete one-loop calculation (see Fig. 3) was done in 1974 by Stroscio and Holt [37]. They redid the annihilation graph and worked out all the others as well. Their results are presented in Table II (and are shown in Fig. 1). Of particular interest is the ladder graph (Fig. 3e) which contains a binding singularity regulated by the nonzero relative speed v of the electron and positron. This $1/v$ singular term is subtracted in order to avoid double counting the effect of binding. The ladder graph can be expressed as a sum of an infrared divergent part and a finite part. The divergent part has the

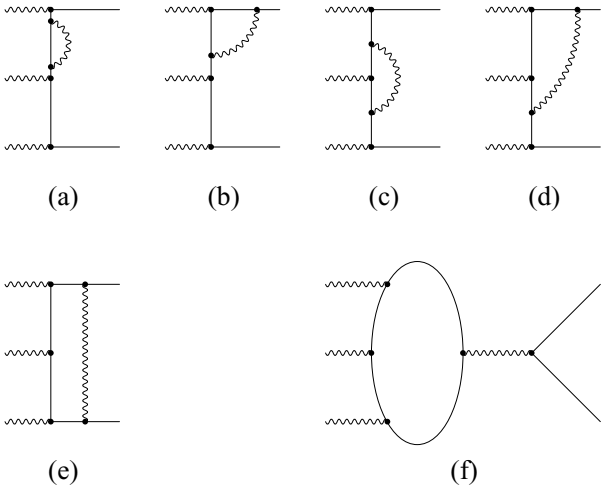

FIG. 3. One-loop QED graphs contributing to the orthopositronium decay rate. They are (a) the self-energy graph, (b) the outer vertex graph, (c) the inner vertex graph, (d) the double vertex graph, (e) the ladder graph, and (f) the annihilation graph.

form [38]

$$\Gamma_L^{IR} = \left\{ \frac{\pi^2}{v} + 2\ln\lambda - 2 \right\} \frac{\alpha}{\pi} \Gamma_0, \tag{1.5}$$

where λ is the photon mass (in units of the electron mass m). The "-2" appears explicitly in Table II, along with the finite part of the ladder graph, which is obtained from a numerical integration. In later work, Stroscio increased the precision of his vertex and double vertex results [43, 44]. These new values with his updated total are shown in Table II. Unfortunately, his new value for the double vertex graph seems to contain an error.

As can be seen in Fig. 1, the powder and vacuum experiments in 1976 are in stark disagreement with prior measurements and with the one-loop theoretical result of Stroscio and Holt [37]. A new theoretical calculation quickly followed. In 1977, Caswell *et al*. [38] recalculated the one-loop correction using the same basic approach as Stroscio and Holt. Their result, given in Table II, is below even the new lower experimental values. While the cause of the discrepancy between the earlier experiments and the newer ones has never been determined [14], the origin of the difference

TABLE II

One-Loop Contributions to the Orthopositronium Decay Rate

Graph	SH 1974	Stroscio 1975	CLS 1977	CL 1979	Adkins 1983	Adkins 1992	AFS 2000
SE	4.785(10)	4.785(10)	4.791(3)	4.791(3)	4.78499(2)	4.784984	4.784984
OV					−1.0293(7)	−1.028861	−1.028861
IV					−1.8395(9)	−1.839323	−1.839323
OV + IV	−2.90(15)	−2.8716(36)	−2.868(3)	−2.868(3)	−2.8688(12)	−2.868184	−2.868184
DV	−3.4(4)	−3.355(3)	−3.562(4)	−3.562(4)	−3.5662(7)	−3.56758(8)	−3.567629(21)
L	−2	−2	−2	−2	−2	−2	−2
	+5.8(4)	+5.8(4)	−5.90(7)	−5.818(8)	−5.8205(20)	−5.82177(52)	−5.821768(32)
A	−0.5(2)	−0.5(2)	−0.809(4)	−0.809(4)	−0.8115(8)	−0.81389(7)	−0.814057
Total	1.8(6)	1.86(45)	−10.348(70)	−10.266(11)	−10.282(3)	−10.2864(6)	−10.28665(4)

between the two theoretical results has been identified. The complete difference, apart from the usual numerical variations coming from the use of numerical techniques for integration, is in the finite part of the ladder graph. Stroscio and Holt found $+5.8(4)$ as a contribution to A_L, while Caswell, Lepage, and Sapirstein found $-5.90(7)$. The sign of Caswell, Lepage, and Sapirstein has been confirmed by a consistency check [38] and by subsequent calculations. Additional experiments in 1977 and 1978 confirmed the dramatic shift and tended to favor even lower values of the decay rate, although the theoretical result is lower yet.

The $O(\alpha^2 \ln \alpha)$ correction to the rate was obtained in 1979 by Caswell and Lepage [45]. Their result of $(1/3)\alpha^2 \ln \alpha \Gamma_0 = -0.00063\ \mu s^{-1}$ made only a small correction to the earlier one-loop value. Caswell and Lepage also improved the numerical result for the ladder graph which was the most difficult of the $O(\alpha)$ corrections. Their new one-loop result is shown in Table II. The $O(\alpha^2 \ln \alpha)$ correction was confirmed by Khriplovich and Yelkhovsky in 1990 [46].

The one-loop correction was calculated for a third time by Adkins in 1983 [47]. His results confirmed those of Caswell, Lepage, and Sapirstein, but with greater precision (see Table II). The approach used was somewhat different from that of Stroscio and Holt and of Caswell, Lepage, and Sapirstein. Instead of dealing with the annihilation cross section for free particles, Adkins worked with an electron–positron pair caught in a Coulombic bound state and with dynamics described by the Bethe–Salpeter equation. For the infrared sensitive part of the ladder graph he found

$$\Gamma_L^{IR} = \left\{ \frac{\pi}{\alpha} + 4 \ln \alpha - 2 \right\} \frac{\alpha}{\pi} \Gamma_0. \tag{1.6}$$

The π/α represents the lowest order contribution.

Stroscio initiated the era of exact calculations of one-loop corrections in 1982 when he gave the analytic value of the self-energy contribution [48]. His result was

$$\begin{aligned} A_{SE} &= 4 \ln \lambda + \frac{1}{\pi^2 - 9} \left\{ -\frac{1049}{72} \zeta(3) - \frac{775}{72} \zeta(2) \ln 2 + \frac{805}{48} \zeta(2) + \frac{67}{4} \ln 2 - \frac{21}{4} \right\} \\ &= 4 \ln \lambda + 4.784984. \end{aligned} \tag{1.7}$$

This is expressed in terms of the Riemann zeta function $\zeta(n)$ that is associated with the integration of polylogarithms [49]. Analytic results for the outer and inner vertex graphs were worked out by Adkins to be [50, 51]

$$\begin{aligned} A_{OV} &= -4 \ln \lambda + \frac{1}{\pi^2 - 9} \left\{ \frac{443}{72} \zeta(3) + \frac{3419}{144} \zeta(2) \ln 2 - \frac{485}{24} \zeta(2) - \frac{115}{4} \ln 2 + \frac{33}{2} - \frac{3}{4} R \right\} \\ &= -4 \ln \lambda - 1.028861, \end{aligned} \tag{1.8a}$$

$$\begin{aligned} A_{IV} &= -2 \ln \lambda + \frac{1}{\pi^2 - 9} \left\{ \frac{51}{160} \zeta^2(2) - \frac{3}{4} a_4 - \frac{21}{32} \zeta(3) \ln 2 + \frac{15}{8} \zeta(2) \ln^2 2 - \frac{1}{32} \ln^4 2 \right. \\ &\quad \left. + \frac{1589}{72} \zeta(3) + \frac{1253}{144} \zeta(2) \ln 2 - \frac{1417}{48} \zeta(2) - \frac{17}{2} \ln 2 + 15 \right\} \\ &= -2 \ln \lambda - 1.839323, \end{aligned} \tag{1.8b}$$

where $a_4 = \mathrm{Li}_4(1/2)$ and

$$R = \int_0^1 dx \frac{\ln(1-x)}{2-x} [\zeta(2) - \mathrm{Li}_2(1-2x)] = -1.743033833626713 \tag{1.9}$$

can easily be evaluated to any required precision [52].

The one-loop correction was recalculated using Yennie gauge by Adkins, Salahuddin, and Schalm in 1992 [53]. The purpose of this work was to develop a Bethe–Salpeter based calculational scheme that would allow for the calculation of two-loop corrections. That goal has not been realized. Nevertheless, improved results for the annihilation graph and the Feynman parts of the double vertex and ladder graphs were obtained as a consequence of this effort. The new Feynman gauge results are shown in Table II. Analytic results were obtained for the self-energy, outer vertex, and inner vertex graphs in Yennie gauge [52, 54].

The one-loop rate was calculated anew in 2000 as a part of our two-loop work in the context of nonrelativistic QED (NRQED) [55]. Results for the individual graphs are given in Table II.

The best value for the one-loop correction is

$$A = -10.286606(10) \tag{1.10}$$

obtained by Adkins [56]. This value was obtained by a significantly different approach to the calculation. Three amplitudes were identified that described the decay of o-Ps to three photons. These amplitudes were evaluated analytically, and their squares were integrated over the two-dimensional phase space to get the decay rate. The amplitude approach was used earlier by Burichenko to calculate part of the two-loop correction [57].

There are two classes of $(\alpha/\pi)^2$ corrections to the lowest order rate: those with five photons in the final state and those with three. The five photon partial rate is easiest to calculate, since the lowest order five-photon contribution has the same order in α as the two-loop correction to the lowest order three-photon decay rate. For the five-photon contribution we use $B(5-\text{photon}) = 0.187(11)$, as calculated in 1983 by Adkins and Brown [58] and by Lepage *et al.* [59]. A number of two-loop corrections to the three-photon partial rate have already been computed. All corrections involving the square of the one-loop decay amplitudes (which we will here call *class j* corrections) were estimated by Burichenko in 1993 [57]. He found $B_j = 28.8(2)$. A second calculation of this contribution by Adkins in 1996 gave $B_j = 28.860(2)$ [56]. All corrections involving vacuum polarization (our *class i*) were computed by Burichenko and Ivanov in 1995 [60]. They obtained $B_i = 0.960(3)$. A confirming evaluation by Adkins and Shiferaw in 1995 gave $B_i = 0.964960(4)$ [61]. The contribution involving a radiative correction to the electron loop on the annihilation diagram (*class h*) was obtained by Adkins and Lymberopoulos in 1995 [62, 63]. The contribution to B is $B_h = 9.0074(9)$. Class h also makes a contribution at $O(\alpha^2 \ln \alpha\Gamma_0)$. The contribution involving light-by-light scattering of two final state photons (*class k*) was evaluated by Adkins *et al.* in 2001 [64]. They found $B_k = 0.350(4)$. In the present work we complete the calculation of all $O(\alpha^2)$ corrections.

The logarithmically enhanced terms at $O(\alpha^3)$ have been evaluated. The leading logarithm at this order,

$$-\frac{3}{2}\frac{\alpha^3}{\pi}\ln^2 \alpha\Gamma_0 = -0.000032\ \mu\text{s}^{-1}, \tag{1.11}$$

was evaluated by Karshenboim in 1993 [65]. The term with a single logarithm was obtained in 2000 by three groups: Hill and Lepage [66], Kniehl and Penin [67], and Melnikov and Yelkhovsky [68]. Their result is

$$C\frac{\alpha^3}{\pi}\ln \alpha\Gamma_0 = 0.000024\ \mu\text{s}^{-1}, \tag{1.12}$$

where $C = A/3 - 229/30 + 8\ln 2 = -5.517$. The calculation of the pure $O(\alpha^3)$ corrections—term D of Eq. (1.2)—has not begun.

C. Outline of the Calculation

In this work we calculate the $O(\alpha^2)$ correction to the o-Ps decay rate—term B in Eq. (1.2). We also do a parallel calculation of the $O(\alpha^2)$ correction to the o-Ps energy due to diagrams involving annihilation into a single photon. The processes of o-Ps decay into three real photons and annihilation into one virtual photon are closely related. Both can be thought of as processes involving the annihilation of an electron–positron pair into photons followed by the recreation of the particle–antiparticle pair. In the one-photon-annihilation process, the photon is necessarily virtual. The corresponding (lowest order) energy shift

$$\Delta E_0 = \frac{m\alpha^4}{4} \tag{1.13}$$

(for the o-Ps ground state) contributes to the fine structure. We will refer to this shift as a contribution to the ground state hyperfine structure (HFS), which is the difference between the o-Ps and p-Ps energies. In the three-photon-annihilation process, the photon can be virtual or real, and the corresponding (lowest order) energy shift is complex [69]:

$$\Delta E = \left\{\left[\frac{3}{8}\zeta(3) - \frac{1}{6}\zeta(2)\ln 2 - \frac{1}{12}\zeta(2) - 2\ln 2 + \frac{3}{4}\right] - i\pi\left[\frac{2}{3}\zeta(2) - 1\right]\right\}\frac{m\alpha^6}{\pi^2}. \tag{1.14}$$

The real part contributes to the HFS. The imaginary part is related to the decay rate by the usual rule

$$\Gamma = -2Im(\Delta E), \tag{1.15}$$

which leads immediately to the Ore and Powell lowest order rate.

We use NRQED as the framework for this calculation. NRQED was proposed by Caswell and Lepage in 1986 [70] as an effective field theory [71, 72] tailored for the study of the low energy dynamics of QED. NRQED has developed in a number of directions more or less suited to the calculation of interest here. The differences of treatment are associated with the various methods for regularizing the severe ultraviolet divergences of NRQED, with the treatment of infrared divergences, and with the possibility of special treatment for ultrasoft processes. We choose an approach that meshes most easily with the earlier work of Labelle, Lepage, and Magnea on the o-Ps decay rate. [73, 74] These authors actually completed the NRQED aspect of the calculation, leaving undone only a QED calculation of the cross-section for electron–positron annihilation into three photons to two-loop order. In a sense, we are simply completing the calculation started in [73, 74]. We did the complete calculation, including both QED and NRQED parts, and in fact we found a small error in the results of [73, 74]. Our particular approach to NRQED uses a momentum cutoff as an ultraviolet regulator and a nonzero photon mass as an infrared regulator.

A closely related problem is the calculation of $O(\alpha^2)$ corrections to the p-Ps decay rate. This has been done by Czarnecki, *et al*. [75, 76] using a version of NRQED where dimensional regularization is used for both ultraviolet and infrared divergences.

D. Contents of This Work

The contents of the remainder of this article are arranged as follows. In Section II we describe the details of our implementation of NRQED and derive the forms for the various NRQED interactions and propagators. In Section III we present our calculation of the one-photon-annihilation contribution to the positronium hyperfine structure. This calculation is divided into a QED scattering calculation, a NRQED scattering calculation, the matching procedure, and a NRQED bound state perturbation theory calculation which gives the result. In Section IV we describe our calculation of the o-Ps

decay rate. The decay rate calculation follows the same steps as the hyperfine structure calculation. Section V is our conclusion.

II. CALCULATIONAL APPROACH: NRQED

We use NRQED for our calculations of the one-photon-annihilation contribution to the positronium HFS and of the o-Ps decay rate. As mentioned above, NRQED was first proposed and used for a calculation of recoil contributions to the energy levels of muonium and positronium by Caswell and Lepage [70]. Another useful reference on NRQED is [77].

A. Definition of NRQED

The implementation of NRQED used here is defined by the Lagrangian and the treatment of infrared and ultraviolet divergences. The Lagrangian has the form [77, 78]

$$\begin{aligned}\mathcal{L}_{\rm NRQED} = {} & \frac{1}{2}(\mathbf{E}^2-\mathbf{B}^2)+\psi^\dagger\Bigg[iD_t+\frac{\mathbf{D}^2}{2m}+\frac{\mathbf{D}^4}{8m^3}+\cdots+\frac{c_F e}{2m}\boldsymbol{\sigma}\cdot\mathbf{B}+\frac{c_D e}{8m^2}(\mathbf{D}\cdot\mathbf{E}-\mathbf{E}\cdot\mathbf{D}) \\ & +\frac{c_S e}{8m^2}i\boldsymbol{\sigma}\cdot(\mathbf{D}\times\mathbf{E}-\mathbf{E}\times\mathbf{D})+\cdots\Bigg]\psi+(\psi\to\chi)-\frac{d_C e^2}{4m^2}(\psi^\dagger\boldsymbol{\sigma}\sigma_2\chi^*)\cdot(\chi^T\sigma_2\boldsymbol{\sigma}\psi) \\ & +\frac{d_D e^2}{3m^4}\frac{1}{2}[(\psi^\dagger\boldsymbol{\sigma}\sigma_2\chi^*)(\chi^T\sigma_2\boldsymbol{\sigma}(-i\overleftrightarrow{\mathbf{D}}/2)^2\psi)+\text{H.C.}]+\cdots, \end{aligned} \tag{2.1}$$

where ψ and χ are the two-component electron and positron fields, $D_t=\partial_t+ieA_0$, $\mathbf{D}=\boldsymbol{\nabla}-ie\mathbf{A}$, and $\boldsymbol{\sigma}^i$ is the usual Pauli matrix. The Fermi, Darwin, spin-orbit, and the four-fermion contact and derivative couplings c_F, c_D, c_S, d_C, and d_D all have the form $1+O(\alpha)$ by matching with tree-level QED. Ultraviolet divergences are regulated by a momentum-space cutoff Λ, while infrared divergences are controlled by a nonzero photon mass λ. We make use of Coulomb gauge, in which the photon propagator has the form $1/D_\lambda(\mathbf{k})$ for Coulomb photons, where $D_\lambda(\mathbf{k})=\mathbf{k}^2+\lambda^2$, and

$$D_{ij}(k)=\frac{1}{k^2-\lambda^2+i\epsilon}\left(\delta_{ij}-\frac{k_i k_j}{D_\lambda(\mathbf{k})}\right) \tag{2.2}$$

for transverse photons. The electron propagator is

$$S(p)=\frac{1}{p_0-\mathbf{p}^2/(2m)+i\epsilon}. \tag{2.3}$$

B. Feynman Rules for Interaction Potentials

To the order of interest here the relevant NRQED electron–positron interactions (see Fig. 4) can be represented as instantaneous potentials [78]. Their values can be worked out from the corresponding QED diagrams shown in Fig. 5. We evaluate these diagrams at or near threshold using Dirac spinors normalized to represent one particle per unit volume. The appropriate incoming and outgoing electron

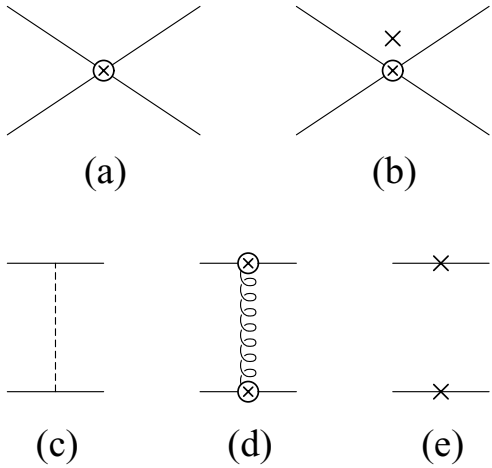

FIG. 4. The NRQED instantaneous potentials: (a) four-fermion contact, (b) four-fermion derivative, (c) Coulomb, (d) Breit–Fermi, and (e) relativistic kinetic energy.

and positron Dirac spinors are

$$u_1 = \left(\frac{E_i+m}{2E_i}\right)^{1/2}\begin{pmatrix}\psi_i\\ \frac{\boldsymbol{\sigma}\cdot\mathbf{p}_i}{E_i+m}\psi_i\end{pmatrix} = N_i\left(\frac{\gamma p_1+m}{2m}\right)\begin{pmatrix}\psi_i\\ 0\end{pmatrix}, \tag{2.4a}$$

$$\bar{u}_3 = \left(\frac{E_f+m}{2E_f}\right)^{1/2}\begin{pmatrix}\psi_f^\dagger & -\psi_f^\dagger\frac{\boldsymbol{\sigma}\cdot\mathbf{p}_f}{E_f+m}\end{pmatrix} = N_f(\psi_f^\dagger,0)\left(\frac{\gamma p_3+m}{2m}\right), \tag{2.4b}$$

$$\bar{v}_2 = \left(\frac{E_i+m}{2E_i}\right)^{1/2}\begin{pmatrix}\chi_i^\dagger\frac{\boldsymbol{\sigma}\cdot\mathbf{p}_i}{E_i+m} & \chi_i^\dagger\end{pmatrix} = N_i(0,\chi_i^\dagger)\left(\frac{-\gamma p_2+m}{2m}\right), \tag{2.4c}$$

$$v_4 = \left(\frac{E_f+m}{2E_f}\right)^{1/2}\begin{pmatrix}\frac{\boldsymbol{\sigma}\cdot\mathbf{p}_f}{E_f+m}\chi_f\\ -\chi_f\end{pmatrix} = N_f\left(\frac{-\gamma p_4+m}{2m}\right)\begin{pmatrix}0\\ -\chi_f\end{pmatrix}. \tag{2.4d}$$

We have used $E=(\mathbf{p}^2+m^2)^{1/2}$ and $N=(2m^2/(E(E+m)))^{1/2}$. The incoming (outgoing) electron momenta are $p_1=(E_i,\mathbf{p}_i)$ ($p_3=(E_f,\mathbf{p}_f)$), and the incoming (outgoing) positron momenta are $p_2=(E_i,-\mathbf{p}_i)$ ($p_4=(E_f,-\mathbf{p}_f)$) and ψ_i, ψ_f, χ_i, χ_f are appropriate initial and final state electron and positron Pauli spinors.

In order to work out the momentum-independent contribution of the four-particle contact interaction (see Fig. 5a), we use the first form of Eqs. (2.4). The amplitude corresponding to this term is

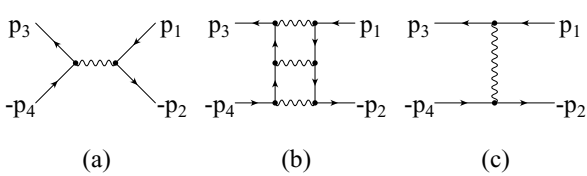

FIG. 5. QED interaction graphs used to work out the NRQED interactions potentials. The one-photon-annihilation graph (a) contributes to the real parts of the four-fermion contact and derivative interactions. The three-photon-annihilation graph (b) contributes to the imaginary parts of those interactions. The one-photon-exchange graph (c) gives the Coulomb and Breit–Fermi interactions.

$$
\begin{aligned}
i\mathcal{M} &= [\bar{u}_3(-ie\gamma^i)v_4][\bar{v}_2(-ie\gamma^j)u_1]iD_{ij}(P) \\
&= \frac{-i(4\pi\alpha)}{(2m)^2}(\psi_f^\dagger, 0)\gamma^j \begin{pmatrix} 0 \\ -\chi_f \end{pmatrix}(0, \chi_i^\dagger)\gamma^j \begin{pmatrix} \psi_i \\ 0 \end{pmatrix} \\
&= \frac{-i\pi\alpha}{m^2}\psi_f^\dagger \sigma^j \chi_f \chi_i^\dagger \sigma^j \psi_i .
\end{aligned} \tag{2.5}
$$

Note that $E_f = E_i$ by energy conservation, and $P = (2E, \mathbf{0})$. We use $\psi^\dagger \sigma^j \chi = (\chi^\dagger \sigma^j \psi)^*$ to give both spinor products the same form and turn them into traces using $\chi^\dagger \sigma^j \psi = \mathrm{tr}[\sigma^j \psi \chi^\dagger]$. Particle–antiparticle states of definite spin are formed from the constituent spinors in the usual way (see Appendix B of [79]):

$$
\psi\chi^\dagger \to \begin{cases} 1/\sqrt{2} & \text{spin 0} \\ \boldsymbol{\sigma}\cdot\hat{\epsilon}/\sqrt{2} & \text{spin 1,} \end{cases} \tag{2.6}
$$

where $\hat{\epsilon}$ is the positronium spin vector. One has

$$
i\mathcal{M} = -i\frac{2\pi\alpha}{m^2}\hat{\epsilon}_f^* \cdot \hat{\epsilon}_i . \tag{2.7}
$$

The spin average amplitude has $\hat{\epsilon}_f^* \cdot \hat{\epsilon}_i \to 1$. The corresponding potential is

$$
V_4(\mathbf{p}, \mathbf{q}) = \frac{2\pi\alpha}{m^2} d_C , \tag{2.8}
$$

where $d_C = 1 + O(\alpha)$. Higher order corrections to d_C come from more complicated graphs and are found via a matching calculation. The lowest order one-photon-annihilation energy shift is obtained from V_4 by taking its ground state expectation value (with $d_C \to 1$),

$$
\Delta E = \langle V_4 \rangle = \frac{2\pi\alpha}{m^2}|\phi_0|^2 = \frac{m\alpha^4}{4}, \tag{2.9}
$$

where the wave function at contact is $\phi_0 = (\gamma^3/\pi)^{1/2}$ with $\gamma = m\alpha/2$.

The imaginary part of V_4 is related to the decay rate. It is calculated in lowest order for o-Ps by evaluating the imaginary part of Fig. 5b. This calculation was described in detail by Labelle [74]. The result is

$$
\mathrm{Im}(d_C) = -\frac{4(\pi^2 - 9)\alpha^2}{9\pi} e_C , \tag{2.10}
$$

where $e_C = 1 + O(\alpha)$. The lowest order three-photon decay rate is given by

$$
\Gamma_0 = -2\mathrm{Im}[\langle V_4 \rangle]|\phi_0|^2 = \frac{2}{9}(\pi^2 - 9)\frac{m\alpha^6}{\pi}, \tag{2.11}
$$

the result of Ore and Powell [9].

In order to evaluate the derivative interaction $V_{4der}(\mathbf{p}_f, \mathbf{p}_i)$, we must retain the momentum dependence, at least to the first nonvanishing order. We ignore the cross-term $\mathbf{p}_f \cdot \mathbf{p}_i$ since it does not contribute when acting on the (spatially symmetric) ground state. Starting from the first form of

(2.4), one has

$$i\mathcal{M} = -i\frac{\pi\alpha}{E^2}\left(\frac{E+m}{2E}\right)^2 \psi_f^\dagger \left\{\sigma^j - \frac{\boldsymbol{\sigma}\cdot\mathbf{p}_f\sigma^j\boldsymbol{\sigma}\cdot\mathbf{p}_f}{4m^2}\right\}\chi_f\chi_i^\dagger\left\{\sigma^j - \frac{\boldsymbol{\sigma}\cdot\mathbf{p}_i\sigma^j\boldsymbol{\sigma}\cdot\mathbf{p}_i}{4m^2}\right\}\psi_i, \quad (2.12)$$

where terms of fourth order in momentum have been left out. The spin-averaged result is

$$i\bar{\mathcal{M}} = -i\frac{2\pi\alpha}{m^2}\left(1 - \frac{2}{3}\frac{\mathbf{p}_i^2+\mathbf{p}_f^2}{m^2}\right), \quad (2.13)$$

which implies

$$V_{4der}(\mathbf{p}_f, \mathbf{p}_i) = -\frac{4\pi\alpha}{3m^2}\left(\frac{\mathbf{p}_i^2+\mathbf{p}_f^2}{m^2}\right)d_D, \quad (2.14)$$

where $d_D = 1 + O(\alpha)$.

The imaginary part of V_{4der} was worked out by Labelle [74] and has been checked by us. It is given by

$$\mathrm{Im}(d_D) = -\frac{(\pi^2-9)X\alpha^2}{36\pi}, \quad (2.15)$$

where $X = (19\pi^2 - 132)/(\pi^2 - 9)$.

The Coulomb and Breit–Fermi (BF) potentials are found by looking at the basic QED one-photon-exchange interaction (see Fig. 5c). The basic spinor products are

$$\bar{u}_3\gamma^0 u_1 = \psi_f^\dagger\left\{1 - \frac{(\mathbf{p}_f-\mathbf{p}_i)^2}{8m^2} + \frac{i}{4m^2}(\mathbf{p}_f\times\mathbf{p}_i)\cdot\boldsymbol{\sigma} + \cdots\right\}\psi_i, \quad (2.16a)$$

$$\bar{u}_3\gamma^i u_1 = \psi_f^\dagger\left\{\frac{(p_f+p_i)^i}{2m} - \frac{i}{2m}\epsilon_{ian}(p_f-p_i)_a\sigma_n + \cdots\right\}\psi_i, \quad (2.16b)$$

$$\bar{v}_2\gamma^0 v_4 = \chi_i^\dagger\left\{1 - \frac{(\mathbf{p}_f-\mathbf{p}_i)^2}{8m^2} - \frac{i}{4m^2}(\mathbf{p}_f\times\mathbf{p}_i)\cdot\boldsymbol{\sigma} + \cdots\right\}\chi_f, \quad (2.16c)$$

$$\bar{v}_2\gamma^i v_4 = \chi_i^\dagger\left\{-\frac{(p_f+p_i)^i}{2m} - \frac{i}{2m}\epsilon_{ian}(p_f-p_i)_a\sigma_n + \cdots\right\}\chi_f. \quad (2.16d)$$

The interaction potential is then found from

$$-iV = (-1)[\bar{u}_3(-ie\gamma^\mu)u_1][\bar{v}_2(-ie\gamma^\nu)v_4]iD^C_{\mu\nu}(k), \quad (2.17)$$

where $k = p_f - p_i$, the Coulomb propagator is

$$D^C_{\mu\nu}(k) = \begin{pmatrix} \frac{1}{D_\lambda(\mathbf{k})} & 0 \\ 0 & \frac{-1}{D_\lambda(\mathbf{k})}\left(\delta_{ij} - \frac{k_ik_j}{D_\lambda(\mathbf{k})}\right)\end{pmatrix}_{\mu\nu}, \quad (2.18)$$

and the factor of (-1) is a fermionic minus sign. The spin average is worked out using

$$(\psi_f^\dagger A\psi_i)(\chi_i^\dagger B\chi_f) = \mathrm{tr}[(\chi_f\psi_f^\dagger)A(\psi_i\chi_i^\dagger)B] = \frac{1}{2}\mathrm{tr}[\boldsymbol{\sigma}\cdot\hat{\epsilon}_f^* A\boldsymbol{\sigma}\cdot\hat{\epsilon}_i B] \to \frac{1}{6}\mathrm{tr}[\sigma_a A\sigma_a B], \tag{2.19}$$

where the last step is the spin average. We define an order such that $\mathbf{p}_f$, $\mathbf{p}_i$, and λ each have $O(1)$. The leading interaction potential from (2.17) is the Coulomb potential of order -2:

$$V_C(\mathbf{p}_f,\mathbf{p}_i) = -\frac{4\pi\alpha}{D_\lambda(\mathbf{k})}. \tag{2.20}$$

The order 0 subleading contribution we call the BF potential. This contains the effects of transverse photon exchange as well as relativistic corrections to Coulomb photon exchange. It is

$$\tilde{V}_{BF}(\mathbf{p}_f,\mathbf{p}_i) = -\frac{4\pi\alpha}{m^2}\left\{\frac{(\mathbf{p}_f\times\mathbf{p}_i)^2}{D_\lambda^2(\mathbf{k})} + \frac{\lambda^2(\mathbf{p}_f+\mathbf{p}_i)^2}{4D_\lambda^2(\mathbf{k})} - \frac{5}{12}\frac{\mathbf{k}^2}{D_\lambda(\mathbf{k})}\right\}. \tag{2.21}$$

The states of interest to us are spherically symmetric, and so our form for the BF potential can be simplified by angular averaging, say over $\mathbf{p}_f$. We use the definitions

$$I_n = \int\frac{d\Omega_f}{4\pi}\frac{(\mathbf{p}_f\cdot\mathbf{p}_i)^n}{D_\lambda(\mathbf{k})}, \tag{2.22a}$$

$$J_n = \int\frac{d\Omega_f}{4\pi}\frac{(\mathbf{p}_f\cdot\mathbf{p}_i)^n}{D_\lambda^2(\mathbf{k})}, \tag{2.22b}$$

and the results

$$I_1 = \frac{1}{2}QI_0 - \frac{1}{2}, \tag{2.23a}$$

$$I_2 = \frac{1}{4}Q^2I_0 - \frac{1}{4}Q, \tag{2.23b}$$

$$J_0 = 1\big/\big(Q^2 - 4\mathbf{p}_f^2\mathbf{p}_i^2\big), \tag{2.23c}$$

$$J_1 = \frac{1}{2}QJ_0 - \frac{1}{2}I_0, \tag{2.23d}$$

$$J_2 = \frac{1}{4}Q^2J_0 - \frac{1}{2}QI_0 + \frac{1}{4}, \tag{2.23e}$$

where $Q = \mathbf{p}_f^2 + \mathbf{p}_i^2 + \lambda^2$. The averaged value of $\tilde{V}_{BF}$ is

$$\tilde{V}_{BF}(\mathbf{p}_f,\mathbf{p}_i) \to \frac{-4\pi\alpha}{m^2}\left\{\frac{1}{2}\big(\mathbf{p}_f^2+\mathbf{p}_i^2\big)I_0 - \frac{11}{12}(1-\lambda^2I_0) + \frac{\lambda^2}{4}\big[\big(2\big(\mathbf{p}_f^2+\mathbf{p}_i^2\big)+\lambda^2\big)J_0 - I_0\big]\right\}. \tag{2.24}$$

The expression $V_{BF}(\mathbf{p}_f,\mathbf{p}_i)$ (shown below as (2.25d)) gives the same form under averaging, and is the form that we use in the calculation.

Finally, we use δH_{kin} (shown as (2.25e)) to represent the effect of the relativistic correction to the fermion kinetic energy.

In sum, the relevant NRQED interactions, represented as instantaneous potentials, are

$$V_4(\mathbf{p}_f, \mathbf{p}_i) = \frac{2\pi\alpha}{m^2}\, d_C, \tag{2.25a}$$

$$V_{4der}(\mathbf{p}_f, \mathbf{p}_i) = -\frac{4\pi\alpha}{3m^4}\left(\mathbf{p}_f^2 + \mathbf{p}_i^2\right) d_D, \tag{2.25b}$$

$$V_C(\mathbf{p}_f, \mathbf{p}_i) = -\frac{4\pi\alpha}{D_\lambda(\mathbf{k})}, \tag{2.25c}$$

$$V_{BF}(\mathbf{p}_f, \mathbf{p}_i) = -\frac{2\pi\alpha}{m^2}\left\{\frac{\mathbf{p}_f^2 + \mathbf{p}_i^2}{D_\lambda(\mathbf{k})} - \frac{11}{6}\frac{\mathbf{k}^2}{D_\lambda(\mathbf{k})} + \frac{\lambda^2\left(\mathbf{p}_f^2 + \mathbf{p}_i^2\right)}{D_\lambda^2(\mathbf{k})} + \frac{\lambda^4}{2D_\lambda^2(\mathbf{k})} - \frac{\lambda^2}{2D_\lambda(\mathbf{k})}\right\}, \tag{2.25d}$$

$$\delta H_{kin}(\mathbf{p}_f, \mathbf{p}_i) = -(2\pi)^3\delta(\mathbf{p}_f - \mathbf{p}_i)\frac{\mathbf{p}_f^4}{4m^3}. \tag{2.25e}$$

The corresponding Feynman rules are $-i$ times the potentials.

Now we work out the electron–positron propagation factor. We let the electron and positron carry energy-momentum $(q^0 + E/2, \mathbf{q})$ and $(-q^0 + E/2, -\mathbf{q})$. We can perform the loop-energy integration simply since the interactions here are instantaneous. The propagation factor is

$$\begin{aligned}
&\int \frac{dq^0}{2\pi} iS(q^0 + E/2, \mathbf{q}) iS(-q^0 + E/2, -\mathbf{q}) \\
&\quad = i\int \frac{dq^0}{2\pi i}\, \frac{1}{q^0 + E/2 - \mathbf{q}^2/2m + i\epsilon}\, \frac{1}{q^0 - E/2 + \mathbf{q}^2/2m - i\epsilon} \\
&\quad = \frac{-im}{\mathbf{q}^2 - mE}.
\end{aligned} \tag{2.26}$$

For free particles ($E = 0$) this becomes $-im/\mathbf{q}^2$, while for particles bound in a positronium atom ($E = -\gamma^2/m$) it becomes $-im/(\mathbf{q}^2 + \gamma^2)$.

III. ONE-PHOTON-ANNIHILATION CONTRIBUTION TO THE POSITRONIUM HFS

As preparation for the decay rate calculation, we will show how the one-photon-annihilation contribution to the positronium HFS can be calculated using the methods of NRQED. Of course, the calculation of this contribution has been done before. One approach, of Adkins *et al.* [80], made use of a Bethe–Salpeter based bound state formalism [79] and Coulomb gauge. This group obtained a numerical result for the one-photon-annihilation contribution of

$$\Delta E = -0.1256481(12) m\alpha^6 = -2.344 \text{ MHz}. \tag{3.1}$$

At the same time, the group of Hoang, Labelle, and Zebarjad [78, 81] used NRQED to arrive at the analytic result

$$\Delta E = \left\{\frac{13}{32}\zeta(3) + \frac{27}{8}\zeta(2)\ln(2) - \frac{1183}{192}\zeta(2) + \frac{1477}{324}\right\}\frac{m\alpha^6}{\pi^2} = -0.1256487 m\alpha^6. \tag{3.2}$$

They made use of the two-loop vertex form factors computed by Hoang [82] and of the two-loop vacuum polarization tensor computed by Kallen and Sabry [83] and by Schwinger [84]. They

employed two infrared regularization parameters: a photon mass λ and also a parameter p_0 equal to the relativistic center-of-mass three-momentum of the electron or positron in the scattering process, with $\lambda \ll p_0 \ll m$. This infrared regularization was convenient for their matching with the QED results, which were regulated in the same manner. The agreement between the two HFS results is strong evidence that both the Bethe–Salpeter approach and the NRQED approach are well founded and were carried through without error.

We will show here a third method of calculation that reproduces the known result. This new approach is based on NRQED, but with a different infrared regulation scheme from that used above. We use simply a photon mass and keep the electron and positron strictly at threshold. There are several reasons for going through this new HFS calculation. The method is just the same as will be used in the decay rate calculation, but illustrates the method in a less complicated setting. Also, some of the integrals are identical in the HFS and decay rate calculations, including specifically the most difficult one. While this integral can be estimated numerically, a higher precision result will be obtained by comparison with the analytic HFS result of Eq. (3.2).

A. Overview

The structure of our calculation of the positronium ground state HFS is as follows. First we determine the appropriate NRQED coefficients via a matching calculation. In this matching calculation we require the agreement of the $e^- e^+ \to e^- e^+$ scattering amplitude at threshold as calculated via QED and NRQED. Then the energy shift will be obtained via a second order bound state perturbation calculation in NRQED.

The outline of our calculation is as follows. First we evaluate the zero-, one-, and two-loop scattering amplitudes from QED. This is a significant task, but is a standard type of QED calculation. Next we work out the scattering amplitude as calculated in NRQED. This one involves the as yet unknown NRQED coefficients. Comparison allows us to evaluate those coefficients. Finally we work through the bound state perturbation theory calculation and arrive at the result.

B. Calculation of the Scattering Amplitude via QED

The zero-, one-, and two-loop QED one-photon-annihilation scattering diagrams are depicted in Fig. 6. These are composed of n-loop renormalized (nR) vertex and vacuum polarization parts as shown. The renormalized vacuum polarization parts are well known, and will not be rederived here. The unrenormalized vertex parts will be evaluated using dimensional regularization and renormalized in the usual way. Infrared divergences will be regulated by use of a nonzero photon mass λ. The

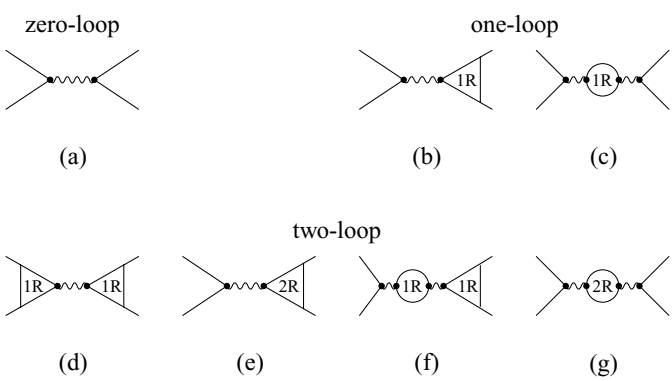

FIG. 6. Zero-, one-, and two-loop contributions to the one-photon-annihilation part of the $e^- e^+ \to e^- e^+$ scattering amplitude. Renormalized one-loop (1R) and two-loop (2R) vertex and vacuum polarization parts are indicated.

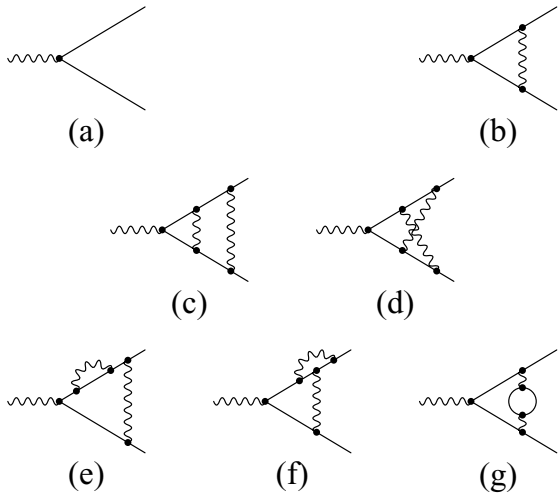

FIG. 7. Contributions to the (a) zero-loop, (b) one-loop, and (c–g) two-loop vertex parts. The two-loop contributions consist of the (c) double ladder (DL), (d) crossed ladder (CL), (e) self-energy (SE), (f) side vertex (SV), and (g) vacuum polarization (VP) graphs.

values of the one- and two-loop renormalization constants in this scheme were obtained by Adkins *et al*. [85].

The fundamental zero-loop vertex (shown in Fig. 7a) can be written as

$$A_0^m = \mathrm{tr}[(-ie(n)\gamma^m)X], \tag{3.3}$$

where $n = 4-2\epsilon$ is the dimension of spacetime, $e(n) = e\mu^\epsilon$ with μ an arbitrary mass scale introduced to keep units straight, and X is the normalized spin 1 state of polarization ϵ:

$$X = \frac{1}{\sqrt{2}}\begin{pmatrix} 0 & \boldsymbol{\sigma}\cdot\hat{\epsilon} \\ 0 & 0 \end{pmatrix}. \tag{3.4}$$

This spin state can also be written as

$$X = \frac{-1}{2}(1+\gamma^0)\gamma\epsilon\frac{1}{\sqrt{2}}, \tag{3.5}$$

where $\epsilon = (0, \hat{\epsilon})$. Thus one has

$$A_0^m = ie(n)\frac{1}{\sqrt{2}}(2\epsilon^m). \tag{3.6}$$

This is the amplitude to which all higher order corrections will be referred.

The one-loop vertex part (see Fig. 7b) is

$$\begin{aligned} A_1^m &= \int \frac{d^n q}{(2\pi)^n}\mathrm{tr}\Bigg[(-ie(n)\gamma^\mu)\frac{i}{\gamma(-q+n)-1}(-ie(n)\gamma^m) \\ &\quad\times\frac{i}{\gamma(q+n)-1}(-ie(n)\gamma_\mu)X\Bigg]\left(\frac{i}{-q^2+\lambda^2}\right) \\ &= A_0^m\left(\frac{\alpha}{\pi}\right)\left[\Omega e^{-\gamma_E}\right]^\epsilon I_1, \end{aligned} \tag{3.7}$$

where $\Omega = 4\pi\mu^2/m^2$ and γ_E is the Euler constant. (Note that we scale a factor of the electron mass m out of λ, Λ, and each momentum vector here and throughout this section and the next.) The factor $e^{-\epsilon\gamma_E}$ is extracted explicitly in order to simplify later results. The remaining factor I_1 can be written as

$$I_1 = \frac{-1}{4} e^{\epsilon\gamma_E} \int \frac{d^n q}{i\pi^{n/2}} T[(-q^2 + 2qn)(-q^2 - 2qn)(-q^2 + \lambda^2)]^{-1}, \tag{3.8}$$

where the trace T is

$$T = \frac{1}{4}\overline{\text{tr}}[\gamma^\mu(\gamma(q-n)+1)\gamma^m(\gamma(q+n)+1)\gamma_\mu(1+\gamma^0)\gamma\epsilon]. \tag{3.9}$$

We note that once the momentum integral in A_1^m is done, the result will be proportional to ϵ^m. We factor this ϵ^m out into A_0^m and define a new trace function $\overline{\text{tr}}$ such that $\text{tr}[M] = \epsilon^m \overline{\text{tr}}[M]$.

The ultraviolet sensitive part of I_1 is quadratic in q. It is infrared safe and is evaluated in the usual way via Feynman parameters. The infrared sensitive part of I_1 comes from the $q \to 0$ limit of T in which $T \to -4$. We call this (*binding piece*) I_B and find

$$\begin{aligned} I_B &= e^{\epsilon\gamma_E} \int \frac{d^n q}{i\pi^{n/2}} [(-q^2 - 2qn)(-q^2 + 2qn)(-q^2 + \lambda^2)]^{-1} \\ &= \frac{2}{\lambda}\sqrt{1 - \frac{\lambda^2}{4}} \arctan\left(\frac{2}{\lambda}\sqrt{1 - \frac{\lambda^2}{4}}\right) + \ln\lambda + O(\epsilon) \\ &= \frac{\pi}{\lambda} + \ln\lambda - 1 - \frac{1}{8}\pi\lambda + O(\lambda^2) + O(\epsilon), \end{aligned} \tag{3.10}$$

worked out via Feynman parameters. In all, we find that

$$I_1 = \frac{1}{4\epsilon} + I_B - \frac{1}{6}\pi\lambda + O(\lambda^2) + O(\epsilon). \tag{3.11}$$

Renormalization of the one-loop annihilation amplitude is accomplished by a subtraction. The one-loop vertex renormalization constant is (see [85])

$$L_1 = \left(\frac{\alpha}{\pi}\right)\left[\Omega e^{-\gamma_E}\right]^\epsilon \ell_1, \tag{3.12a}$$

$$\ell_1 = \frac{1}{4\epsilon} + \left\{\ln\lambda + 1 - \frac{3}{4}\pi\lambda + O(\lambda^2)\right\} + O(\epsilon). \tag{3.12b}$$

Then the renormalized one-loop annihilation amplitude is

$$A_{1R}^m = A_1^m - L_1 A_0^m = A_0^m \left(\frac{\alpha}{\pi}\right) I_{1R}, \tag{3.13}$$

where

$$I_{1R} = I_1 - \ell_1 = \frac{\pi}{\lambda} - 2 + \frac{11}{24}\pi\lambda + O(\lambda^2), \tag{3.14}$$

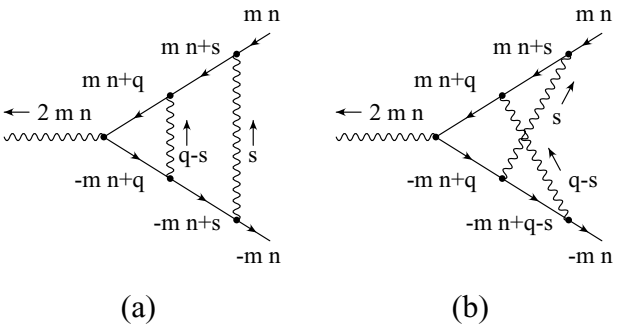

FIG. 8. The double ladder and crossed ladder graphs, showing momentum assignments. At threshold, both the electron and the positron carry in momentum $mn = (m, \mathbf{0})$.

which we rewrite for later use as

$$I_{1R} = \frac{\pi}{\lambda} + I_L(\lambda), \tag{3.15}$$

where

$$I_L(\lambda) = -2 + \frac{11}{24}\pi\lambda + O(\lambda^2). \tag{3.16}$$

Our next task is the evaluation of the five distinct two-loop annihilation amplitudes which are shown in Figs. 7c–7g.

We look first at the double ladder (DL) graph. This graph is the most difficult two-loop graph to evaluate, since it has both severe infrared divergences and two-loop ultraviolet divergences, which must be disentangled before they can be evaluated. Using the momentum labels of Fig. 8, we write

$$A^m_{DL} = A^m_0 \left(\frac{\alpha}{\pi}\right)^2 \left[\Omega e^{-\gamma_E}\right]^{2\epsilon} I_{DL}, \tag{3.17}$$

where

$$I_{DL} = \frac{1}{16} e^{2\epsilon\gamma_E} \int \frac{d^n q}{i\pi^{n/2}} \frac{d^n s}{i\pi^{n/2}} T\left[(-(q-s)+\lambda^2)(-s^2+\lambda^2)\left(-v_1^2+1\right)\right.$$
$$\left. \times \left(-v_2^2+1\right)\left(-v_3^2+1\right)\left(-v_4^2+1\right)\right]^{-1}, \tag{3.18a}$$

$$T = \frac{1}{4}\overline{\text{tr}}\left[\gamma^\mu(\gamma v_1 + 1)\gamma^\nu(\gamma v_2 + 1)\gamma^m(\gamma v_3 + 1)\gamma_\nu(\gamma v_4 + 1)\gamma_\mu(1+\gamma^0)\gamma\epsilon\right], \tag{3.18b}$$

and $v_1 = s - n$, $v_2 = q - n$, $v_3 = q + n$, $v_4 = s + n$. We note that the trace $T = T(q, s)$ is quadratic in both q and s, and define T_{nm} to be the term in $T(q, s)$ containing n powers of q and m powers of s. We note that $T_{01} = 0$, $T(0, 0) = T_{00} = 16$, $T(q, 0) - T(0, 0) = T_{10} + T_{20}$, and

$$T(q, s) = T_{00} + (T(q, 0) - T(0, 0)) + T_{02} + T_{11} + T_{b3}, \tag{3.19}$$

where

$$T_{b3} = T_{21} + T_{12} + T_{22}. \tag{3.20}$$

TABLE III

Contributions of the Double Ladder Graph to the One-Photon Annihilation Amplitude

Label	Term	Result
a0	$\frac{T(0,0)}{D(q,s)}$	I_{DL}^{a0}
a1	$\frac{T(q,0)-T(0,0)}{D(q,0)}$	$I_{1S}I_B$
a2	$(T(q,0)-T(0,0))\left(\frac{1}{D(q,s)}-\frac{1}{D(q,0)}\right)$	$-1.2339(10)$
b1	$\frac{T_{02}}{D(q,s)}$	$-\frac{\pi^2}{6}\ln\lambda - 2.282213(41)$
b2	$\frac{T_{11}}{D(q,s)}$	$-\frac{2\pi^2}{3}\ln\lambda - 17.7251(6)$
b3	$\frac{T_{b3}}{D(q,s)}$	$\frac{1}{4}(1-\epsilon)e^{\epsilon\gamma_E}\Gamma(\epsilon)I_{1S} - \frac{1}{32\epsilon^2} + \frac{9}{64\epsilon} - 0.044046(8)$

We also define $D(q,s) = -(q-s)^2 + \lambda^2$. We write the ratio $T(q,s)/D(q,s)$ as follows:

$$\frac{T(q,s)}{D(q,s)} = \frac{T(0,0)}{D(q,s)} + \frac{T(q,0)-T(0,0)}{D(q,0)} + (T(q,0)-T(0,0))\left(\frac{1}{D(q,s)}-\frac{1}{D(q,0)}\right) + \frac{T_{02}}{D(q,s)} + \frac{T_{11}}{D(q,s)} + \frac{T_{b3}}{D(q,s)}. \tag{3.21}$$

The various terms are shown in Table III along with labels and results from their evaluations. The first term $a0$ contains the two-loop binding singularity as well as an uncalculated term of order $1/\lambda$:

$$I_{DL}^{a0} = \frac{\pi^2 \ln 2}{\lambda^2} + O\left(\frac{1}{\lambda}\right). \tag{3.22}$$

We hold off on evaluating I_{DL}^{a0} any further until it can be combined with a contribution from the crossed ladder graph. The $a1$ term contains a factor of I_B (see (3.10)) from the s integral and a factor of

$$I_{1S} = I_1 - I_B = \frac{1}{4\epsilon} - \frac{1}{6}\pi\lambda + O(\lambda^2) + O(\epsilon) \tag{3.23}$$

from the q integral. The $a2$ term is finite but numerically difficult. We set $\epsilon \to 0$ and evaluated $I_{DL}^{a2}(\lambda)$ numerically using Feynman parameters for various values of λ. The reported result $I_{DL}^{a2}(0)$ was obtained by extrapolation. The $b1$ and $b2$ contributions were found by using poles (i.e., the Cauchy theorem) to do the q^0 and s^0 integrals. The logarithms were identified analytically. The remaining spatial integrals were done numerically. The ultraviolet divergent $b3$ part was worked out using Feynman parameters. The total result for the double ladder graph is

$$I_{DL} = I_{DL}^{a0} + I_{1S}I_B + \frac{1}{4}(1-\epsilon)e^{\epsilon\gamma_E}\Gamma(\epsilon)I_{1S} - \frac{1}{32\epsilon^2} + \frac{9}{64\epsilon} - \frac{5\pi^2}{6}\ln\lambda - 21.2853(12). \tag{3.24}$$

We next consider the crossed ladder (CL) graph (see Fig. 7d). Using the momentum labels of Fig. 8b, we write

$$A_{CL}^{m} = A_0^m \left(\frac{\alpha}{\pi}\right)^2 \left[\Omega e^{-\gamma_E}\right]^{2\epsilon} I_{CL}, \tag{3.25}$$

where

$$I_{CL} = \frac{1}{16} e^{2\epsilon\gamma_E} \int \frac{d^n q}{i\pi^{n/2}} \frac{d^n s}{i\pi^{n/2}} T\left[(-(q-s)+\lambda^2)(-s^2+\lambda^2)\left(-v_1^2+1\right)\right.$$
$$\left.\times \left(-v_2^2+1\right)\left(-v_3^2+1\right)\left(-v_4^2+1\right)\right]^{-1}, \tag{3.26a}$$

$$T = \frac{1}{4}\overline{\text{tr}}[\gamma^\mu(\gamma v_1+1)\gamma^\nu(\gamma v_2+1)\gamma^m(\gamma v_3+1)\gamma_\mu(\gamma v_4+1)\gamma_\nu(1+\gamma^0)\gamma\epsilon], \tag{3.26b}$$

and $v_1 = q-s-n$, $v_2 = q-n$, $v_3 = q+n$, $v_4 = s+n$. We define T_{nm} as in the DL graph and isolate terms in I_{CL} that require special treatment. The first part, I_{CL}^{a0}, which has $T \to T_{00} = 16$, is of order $1/\lambda$. We do not calculate I_{CL}^{a0} separately, but combine it with the corresponding DL contribution. The second part has $T \to T_{01}$. We use poles for the q^0 and s^0 integrals and extract a logarithmic part analytically. The result is

$$I_{CL}^{b1} = \frac{\pi^2}{2} \ln\lambda + 11.706681(44). \tag{3.27}$$

The third part has $T \to T_{10}$. This term vanishes since the integrand is odd under $q \to -q, s \to s-q$. The final part has

$$T \to T_{b3} = T - T_{00} - T_{01} - T_{10}. \tag{3.28}$$

This term has an ultraviolet divergence but is finite in the infrared. Numerical integration with $\lambda = 0$ gives

$$I_{CL}^{b3} = -\frac{1}{8\epsilon} + 1.53964(16). \tag{3.29}$$

The total for the crossed ladder graph is

$$I_{CL} = I_{CL}^{a0} - \frac{1}{8\epsilon} + \frac{\pi^2}{2}\ln\lambda + 13.24632(17). \tag{3.30}$$

For the self-energy (SE) and side vertex (SV) graphs (see Figs. 7e and 7f) we used a trick. These graphs are infrared safe but ultraviolet divergent. We tried evaluating these graphs directly in Feynman gauge, but ran into numerical difficulties. So we use Yennie gauge for the self-energy and vertex renormalization parts instead. This is allowable because the renormalized quantity represented by the diagram of Fig. 9 is independent of the gauge parameter β, where the loop photon propagator is

$$D_\beta^{\mu\nu}(k) = \frac{-1}{k^2}\left(g^{\mu\nu} + \beta\frac{k^\mu k^\nu}{k^2}\right), \tag{3.31}$$

the incoming photon is amputated, and the incoming fermion on the right is on-shell. For the self-energy and vertex parts we use the forms given in [86] and [87]. We succeeded in evaluating I_{SE}

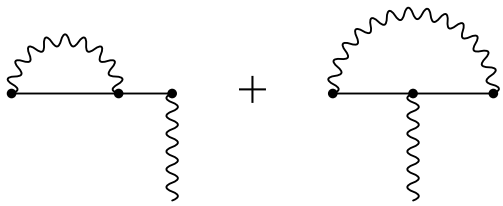

FIG. 9. Self-energy and side vertex parts of the two-loop one-photon-annihilation amplitude. These two together form a gauge-independent set when the right-hand fermion is on-shell.

analytically, but found only a numerical result for I_{SV}. Our results for these hybrid graphs (Feynman gauge for the ladder photon and Yennie gauge for the renormalization part photon) are

$$A_{SE}^m = A_0^m \left(\frac{\alpha}{\pi}\right)^2 \left[\Omega e^{-\gamma_E}\right]^{2\epsilon} I_{SE}, \tag{3.32a}$$

$$A_{SV}^m = A_0^m \left(\frac{\alpha}{\pi}\right)^2 \left[\Omega e^{-\gamma_E}\right]^{2\epsilon} I_{SV}, \tag{3.32b}$$

where

$$I_{SE} = \frac{3}{16\epsilon^2} - \frac{1}{32\epsilon} + \frac{63}{32}\zeta(2) - \frac{43}{64}, \tag{3.33a}$$

$$I_{SV} = -\frac{3}{16\epsilon^2} + \frac{1}{32\epsilon} - 7.1602742(23). \tag{3.33b}$$

The sum of these two is the same as it would be were Feynman gauge used throughout.

The vacuum polarization (VP) graph of Fig. 7g has been calculated before [88, 89]. For the unrenormalized VP contribution we found

$$A_{VP}^m = A_0^m \left(\frac{\alpha}{\pi}\right)^2 \left[\Omega e^{-\gamma_E}\right]^{2\epsilon} I_{VP}, \tag{3.34}$$

where

$$I_{VP} = -\frac{1}{16\epsilon} + \frac{2}{3}\zeta(2) - \frac{27}{32}. \tag{3.35}$$

The total for the unrenormalized one-photon-annihilation amplitude is the sum of (3.24), (3.30), (3.33a), (3.33b), and (3.35):

$$I_2 = I^{a0} + I_{1S}\left\{\frac{1}{4}(1-\epsilon)e^{\epsilon\gamma_E}\Gamma(\epsilon) + I_B\right\} - \frac{1}{32\epsilon^2} - \frac{3}{64\epsilon} - \frac{\pi^2}{3}\ln\lambda - 12.3798(13), \tag{3.36}$$

where I_{1S} and I_B are given in (3.23) and (3.10), and $I^{a0} = I_{DL}^{a0} + I_{CL}^{a0}$. The term I^{a0} was evaluated by poles, with the result

$$I^{a0} = \frac{\pi^2 \ln 2}{\lambda^2} + \left(I_B - \frac{\pi}{\lambda}\right)\frac{\pi}{\lambda} + \frac{1}{2}\ln^2\lambda - \ln\lambda + A_0. \tag{3.37}$$

The infrared singularities down to (but not including) the $\ln\lambda$ were identified analytically. The coefficient of the $\ln\lambda$ was fit numerically to be -1, and this value is required for consistency with the NRQED evaluation of the scattering amplitude. The constant A_0 was found to be

$$A_0 = -3.18(6) \tag{3.38}$$

by extrapolation of λ dependent numerical results to $\lambda = 0$.

Our next step is to renormalize the full one-photon-annihilation amplitude. We note that the renormalized vertex function Γ_R^μ is related to the unrenormalized function Γ'^μ and the vertex renormalization constant Z_1 via

$$\Gamma_R^\mu = Z_1\Gamma'^\mu = \left(\frac{1}{1+L}\right)\Gamma'^\mu. \tag{3.39}$$

On expanding in powers of α according to

$$\Gamma_R^\mu = \gamma^\mu + \Lambda_{1R}^\mu + \Lambda_{2R}^\mu + \cdots, \tag{3.40a}$$

$$\Gamma'^\mu = \gamma^\mu + \Lambda_1^\mu + \Lambda_2^\mu + \cdots, \tag{3.40b}$$

$$L = L_1 + L_2 + \cdots, \tag{3.40c}$$

one finds the one- and two-loop relations

$$\Lambda_{1R}^\mu = \Lambda_1^\mu - \gamma^\mu L_1, \tag{3.41a}$$

$$\Lambda_{2R}^\mu = \Lambda_2^\mu - \Lambda_1^\mu L_1 + \gamma^\mu\left(L_1^2 - L_2\right). \tag{3.41b}$$

These translate into corresponding relations for the annihilation amplitudes:

$$A_{1R}^m = A_1^m - A_0^m L_1, \tag{3.42a}$$

$$A_{2R}^m = A_2^m - A_1^m L_1 + A_0^m\left(L_1^2 - L_2\right). \tag{3.42b}$$

On using the definitions

$$A_i^m = A_0^m\left(\frac{\alpha}{\pi}\right)^i\left[\Omega e^{-\gamma_E}\right]^{i\epsilon} I_i, \tag{3.43a}$$

$$L_i = \left(\frac{\alpha}{\pi}\right)^i\left[\Omega e^{-\gamma_E}\right]^{i\epsilon}\ell_i, \tag{3.43b}$$

we find

$$I_{1R} = I_1 - \ell_1\,, \tag{3.44a}$$

$$I_{2R} = I_2 - I_1\ell_1 + \ell_1^2 - \ell_2. \tag{3.44b}$$

The first of these was used above in the one-loop calculation. Now the one- and two-loop

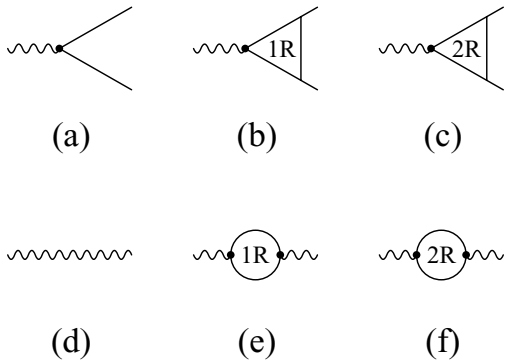

FIG. 10. Constituents of the one-photon-annihilation part of the $e^-e^+ \to e^-e^+$ amplitude. They are the (a) lowest order, (b) renormalized one-loop, and (c) renormalized two-loop annihilation amplitudes and the (d) lowest order, (e) renormalized one-loop, and (f) renormalized two-loop photon propagators.

renormalization constants are [85]

$$\ell_1 = \frac{1}{4\epsilon} + \left\{ \ln\lambda + 1 - \frac{3}{4}\pi\lambda + O(\lambda^2) \right\} + \epsilon \left\{ -\ln^2\lambda + \frac{1}{8}\zeta(2) + 2 + O(\lambda) \right\} + O(\epsilon^2), \tag{3.45a}$$

$$\ell_2 = \frac{1}{32\epsilon^2} + \frac{1}{\epsilon}\left\{ \frac{\ln\lambda}{4} + \frac{9}{64} \right\} + \left\{ \frac{1}{4}\ln^2\lambda + \ln\lambda + \frac{3}{2}\zeta(3) - 6\zeta(2)\ln 2 + \frac{221}{32}\zeta(2) - \frac{4229}{1152} + O(\lambda) \right\} + O(\epsilon). \tag{3.45b}$$

On putting all this carefully together, we find that

$$I_{2R} = \frac{\pi^2 \ln 2}{\lambda^2} + \frac{\pi}{\lambda} I_L(\lambda) - \frac{\pi^2}{3}\ln\lambda - 12.4283(13) + A_0. \tag{3.46}$$

The QED scattering amplitude can now be obtained. The complete set of constituents are given in Fig. 10. These include the zero-, one-, and two-loop renormalized annihilation amplitudes

$$A_0^m = \sqrt{2} i e \epsilon^m, \tag{3.47a}$$

$$A_{1R}^m = A_0^m \left(\frac{\alpha}{\pi}\right) I_{1R}, \tag{3.47b}$$

$$A_{2R}^m = A_0^m \left(\frac{\alpha}{\pi}\right)^2 I_{2R}, \tag{3.47c}$$

the one-photon to e^-e^+ amplitude $\bar{A}_0^m = \sqrt{2} i e \epsilon^{*m}$, the free photon propagation factor $i D^{mn}(P) \to i\delta^{mn}/(4m^2)$, and the one- and two-loop vacuum polarization corrections, which are

$$\left(\frac{\alpha}{\pi}\right) P_{1R} = \left(\frac{\alpha}{\pi}\right)\left\{ -\frac{8}{9} \right\}, \tag{3.48a}$$

$$\left(\frac{\alpha}{\pi}\right)^2 P_{2R} = \left(\frac{\alpha}{\pi}\right)^2 \left\{ \frac{\pi^2}{2}\ln\lambda + \frac{21}{8}\zeta(3) + \frac{3}{2}\zeta(2)\ln 2 - \frac{33}{16}\zeta(2) + \frac{13}{324} \right\}, \tag{3.48b}$$

times the free propagation factor. The one-loop vacuum polarization factor is easy to obtain by direct calculation. The two-loop correction was worked out by Barbieri *et al.* [90] and by Samuel [91]. The

zero-, one-, and two-loop scattering amplitudes are shown in Fig. 6. The results for the amplitudes B are

$$B_{0a}^{\rm QED} = B_0, \tag{3.49a}$$

$$B_{1b}^{\rm QED} = \left\{\frac{2\pi}{\lambda} + 2I_L(\lambda)\right\}\left(\frac{\alpha}{\pi}\right)B_0, \tag{3.49b}$$

$$B_{1c}^{\rm QED} = \left\{-\frac{8}{9}\right\}\left(\frac{\alpha}{\pi}\right)B_0, \tag{3.49c}$$

$$B_{2d}^{\rm QED} = \left\{\frac{\pi^2}{\lambda^2} + \frac{2\pi}{\lambda}I_L(\lambda) + 4\right\}\left(\frac{\alpha}{\pi}\right)^2 B_0, \tag{3.49d}$$

$$B_{2e}^{\rm QED} = \left\{\frac{2\pi^2\ln 2}{\lambda^2} + \frac{2\pi}{\lambda}I_L(\lambda) - \frac{2\pi^2}{3}\ln\lambda + 2A_0 - 24.8566(26)\right\}\left(\frac{\alpha}{\pi}\right)^2 B_0, \tag{3.49e}$$

$$B_{2f}^{\rm QED} = \left\{-\frac{16}{9}\frac{\pi}{\lambda} + \frac{32}{9}\right\}\left(\frac{\alpha}{\pi}\right)^2 B_0, \tag{3.49f}$$

$$B_{2g}^{\rm QED} = \left\{\frac{\pi^2}{2}\ln\lambda + \frac{21}{8}\zeta(3) + \frac{3}{2}\zeta(2)\ln 2 - \frac{33}{16}\zeta(2) + \frac{13}{324}\right\}\left(\frac{\alpha}{\pi}\right)^2 B_0, \tag{3.49g}$$

where

$$B_0 = -i\frac{2\pi\alpha}{m^2}. \tag{3.50}$$

So, finally, the total zero-, one-, and two-loop QED amplitudes are

$$B_0^{\rm QED} = B_0, \tag{3.51a}$$

$$B_1^{\rm QED} = \left\{\frac{2\pi}{\lambda} + 2I_L(\lambda) - \frac{8}{9}\right\}\left(\frac{\alpha}{\pi}\right)B_0, \tag{3.51b}$$

$$B_2^{\rm QED} = \left\{\frac{(2\ln 2+1)\pi^2}{\lambda^2} + \frac{4\pi}{\lambda}I_L(\lambda) - \frac{16}{9}\frac{\pi}{\lambda} - \frac{\pi^2}{6}\ln\lambda + 2A_0 - 15.7879(26)\right\}\left(\frac{\alpha}{\pi}\right)^2 B_0. \tag{3.51c}$$

C. Calculation of the Scattering Amplitude via NRQED

In this section we evaluate the zero-, one-, and two-loop contributions to the $e^-e^+ \to e^-e^+$ scattering amplitude via NRQED.

The zero-loop NRQED graphs are shown in Fig. 11. They are evaluated at threshold, that is with zero external momentum. The results are

$$B_{0a}^{\rm NRQED} = d_C B_0, \tag{3.52a}$$

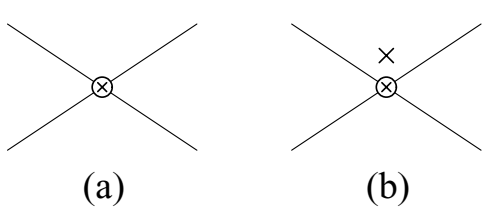

FIG. 11. The zero-loop NRQED $e^-e^+ \to e^-e^+$ scattering graphs.

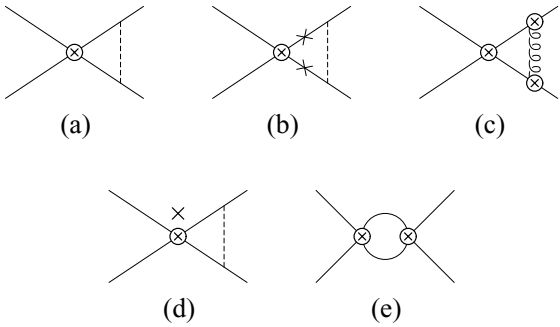

FIG. 12. The one-loop NRQED $e^-e^+ \to e^-e^+$ scattering graphs.

$$B_{0b}^{\mathrm{NRQED}} = 0, \tag{3.52b}$$

where

$$d_C = 1 + \left(\frac{\alpha}{\pi}\right) d_C^{(1)} + \left(\frac{\alpha}{\pi}\right)^2 d_C^{(2)} + O(\alpha^3). \tag{3.53}$$

Graph 11b vanishes because there is no external momentum. The total zero-loop result is

$$B_0^{\mathrm{NRQED}} = d_C B_0. \tag{3.54}$$

The one-loop NRQED graphs are shown in Fig. 12. They are evaluated at threshold. The UV divergences are regulated by a cutoff Λ on the loop three-momentum and the IR divergences by a nonzero photon mass. The necessary one-loop integrals are given in Table IV. As an example of a one-loop calculation, we evaluate the Coulomb ladder graph of Fig. 12a. It is given

TABLE IV

One-Loop Integrals $I_n = \int^{\Lambda} \frac{d^3k}{(2\pi)^3} f_n(\mathbf{k})$

n	$f_n(\mathbf{k})$	I_n
1	$\frac{1}{k^2}$	$\frac{\Lambda}{2\pi^2}$
2	$\frac{1}{k^2 D_\lambda(\mathbf{k})}$	$\frac{1}{4\pi\lambda} - \frac{1}{2\pi^2\Lambda} + O\left(\frac{\lambda^2}{\Lambda^3}\right)$
3	$\frac{1}{D_\lambda(\mathbf{k})}$	$\frac{\Lambda}{2\pi^2} - \frac{\lambda}{4\pi} + O\left(\frac{\lambda^2}{\Lambda}\right)$
4	$\frac{\mathbf{k}^2}{D_\lambda^2(\mathbf{k})}$	$\frac{\Lambda}{2\pi^2} - \frac{3\lambda}{8\pi} + O\left(\frac{\lambda^2}{\Lambda}\right)$
5	$\frac{\mathbf{k}^4}{D_\lambda^3(\mathbf{k})}$	$\frac{\Lambda}{2\pi^2} - \frac{15\lambda}{32\pi} + O\left(\frac{\lambda^2}{\Lambda}\right)$
6	$\frac{1}{D_\lambda^2(\mathbf{k}^2)}$	$\frac{1}{8\pi\lambda} + O\left(\frac{1}{\Lambda}\right)$

by

$$B_{1a}^{\mathrm{NRQED}} = 2\int \frac{d^3k}{(2\pi)^3}\left(-i\frac{2\pi\alpha}{m^2}\,d_C\right)\left(\frac{-im}{\mathbf{k}^2}\right)\left(i\frac{4\pi\alpha}{D_\lambda(\mathbf{k})}\right)$$
$$= -i\frac{16\pi^2\alpha^2}{m}\,d_C\int\frac{d^3k}{(2\pi)^3}\frac{1}{\mathbf{k}^2 D_\lambda(\mathbf{k})} = \left\{\frac{2\pi}{\lambda}\,d_C\right\}\left(\frac{\alpha}{\pi}\right)B_0. \tag{3.55}$$

The complete set of one-loop results is

$$B_{1a}^{\mathrm{NRQED}} = \left\{\frac{2\pi}{\lambda}\,d_C\right\}\left(\frac{\alpha}{\pi}\right)B_0, \tag{3.56a}$$

$$B_{1b}^{\mathrm{NRQED}} = \left\{\Lambda - \frac{1}{2}\pi\lambda + O\left(\frac{\lambda^2}{\Lambda}\right)\right\}\left(\frac{\alpha}{\pi}\right)B_0, \tag{3.56b}$$

$$B_{1c}^{\mathrm{NRQED}} = \left\{-\frac{5}{3}\Lambda + \frac{13}{12}\pi\lambda + O\left(\frac{\lambda^2}{\Lambda}\right)\right\}\left(\frac{\alpha}{\pi}\right)B_0, \tag{3.56c}$$

$$B_{1d}^{\mathrm{NRQED}} = \left\{-\frac{8}{3}\Lambda + \frac{4}{3}\pi\lambda + O\left(\frac{\lambda^2}{\Lambda}\right)\right\}\left(\frac{\alpha}{\pi}\right)B_0, \tag{3.56d}$$

$$B_{1e}^{\mathrm{NRQED}} = \{-\Lambda\}\left(\frac{\alpha}{\pi}\right)B_0. \tag{3.56e}$$

The total one-loop NRQED amplitude is

$$B_{1}^{\mathrm{NRQED}} = \left\{\frac{2\pi}{\lambda}\,d_C - \frac{13}{3}\Lambda + \frac{23}{12}\pi\lambda + O\left(\frac{\lambda^2}{\Lambda}\right)\right\}\left(\frac{\alpha}{\pi}\right)B_0. \tag{3.57}$$

The two-loop NRQED graphs are shown in Fig. 13. Many of these (b, e, h, j, k) have the form of products of one-loop graphs, whose divergences are handled as above. Those graphs containing irreducible two-loop divergences are regulated in the UV by imposing a cutoff on the innermost electron-line momentum only. (We could have implemented the cutoff differently—say on both loop

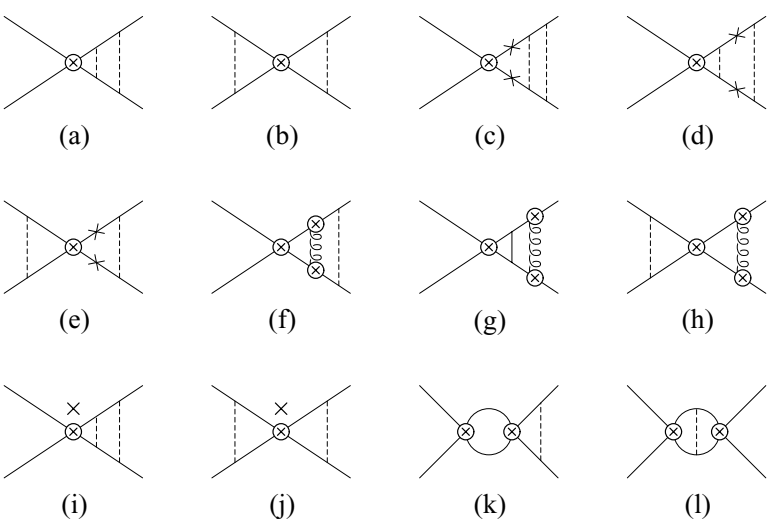

FIG. 13. The two-loop NRQED $e^-e^+ \to e^-e^+$ scattering graphs.

three-momenta—so a choice was necessary. Our choice is consistent with the choice we make for UV regulation of bound state graphs later on.) IR divergences were regulated as usual by using a photon mass. A sample two-loop calculation is that of Fig. 13g. We found that

$$\begin{aligned} B_{2g}^{\mathrm{NRQED}} &= 2\int^{\Lambda}\frac{d^3k}{(2\pi)^3}\int\frac{d^3q}{(2\pi)^3}\left(-i\frac{2\pi\alpha}{m^2}\right)\left(\frac{-im}{\mathbf{k}^2}\right)\left(i\frac{4\pi\alpha}{D_\lambda(\mathbf{k}-\mathbf{q})}\right)\left(\frac{-im}{\mathbf{q}^2}\right)\left(i\frac{2\pi\alpha}{m^2}\right) \\ &\quad\times\left\{-\frac{5}{6}\frac{\mathbf{q}^2}{D_\lambda(\mathbf{q})}+\frac{\lambda^2\mathbf{q}^2}{2D_\lambda^2(\mathbf{q})}\right\} \\ &= -i\frac{32\pi^3\alpha^3}{m^2}\int^{\Lambda}\frac{d^3k}{(2\pi)^3}\int\frac{d^3q}{(2\pi)^3}\frac{1}{\mathbf{k}^2D_\lambda(\mathbf{k}-\mathbf{q})\mathbf{q}^2}\left\{-\frac{5}{6}\frac{\mathbf{q}^2}{D_\lambda(\mathbf{q})}+\frac{\lambda^2\mathbf{q}^2}{2D_\lambda^2(\mathbf{q})}\right\} \\ &= \left\{-\frac{5}{6}\pi^2\ln\left(\frac{\Lambda}{2\lambda}\right)+\frac{\pi^2}{8}+O\left(\frac{\lambda}{\Lambda}\right)\right\}\left(\frac{\alpha}{\pi}\right)^2 B_0. \end{aligned} \tag{3.58}$$

All necessary two-loop integrals are given in Table V. The complete set of two-loop results is

$$B_{2a}^{\mathrm{NRQED}} = \left\{\frac{2\pi^2\ln 2}{\lambda^2}\right\}\left(\frac{\alpha}{\pi}\right)^2 B_0, \tag{3.59a}$$

TABLE V

Two-Loop Integrals $K_n = \int \frac{d^3k}{(2\pi)^3}\frac{d^3q}{(2\pi)^3} g_n(\mathbf{k},\mathbf{q})$

n	$g_n(\mathbf{k},\mathbf{q})$	K_n
1	$[\mathbf{k}^2D_\lambda(\mathbf{k}-\mathbf{q})\mathbf{q}^2]^{-1}$	$\frac{1}{16\pi^2}\ln\left(\frac{\Lambda}{\lambda}\right)+O\left(\frac{\lambda}{\Lambda}\right)$
2	$[\mathbf{k}^2D_\lambda(\mathbf{k}-\mathbf{q})D_\lambda(\mathbf{q})]^{-1}$	$\frac{1}{16\pi^2}\ln\left(\frac{\Lambda}{2\lambda}\right)+O\left(\frac{\lambda}{\Lambda}\right)$
3	$[D_\lambda(\mathbf{k}-\mathbf{q})\mathbf{q}^2D_\lambda(\mathbf{q})]^{-1}$	$\frac{1}{8\pi^3}\frac{\Lambda}{\lambda}-\frac{3}{32\pi^2}+O\left(\frac{\lambda}{\Lambda}\right)$
4	$[D_\lambda(\mathbf{k})(\mathbf{k}-\mathbf{q})^2D_\lambda(\mathbf{q})]^{-1}$	$\frac{1}{16\pi^2}\ln\left(\frac{\Lambda}{2\lambda}\right)+O\left(\frac{\lambda}{\Lambda}\right)$
5	$[\mathbf{k}^2(\mathbf{k}-\mathbf{q})^2D_\lambda(\mathbf{q})]^{-1}$	$\frac{1}{16\pi^2}\ln\left(\frac{\Lambda}{\lambda}\right)+O\left(\frac{\lambda}{\Lambda}\right)$
6	$[\mathbf{k}^2D_\lambda(\mathbf{k}-\mathbf{q})\mathbf{q}^2D_\lambda(\mathbf{q})]^{-1}$	$\frac{\ln 2}{16\pi^2\lambda^2}$
7	$\lambda^2\left[D_\lambda(\mathbf{k})(\mathbf{k}-\mathbf{q})^2D_\lambda^2(\mathbf{q})\right]^{-1}$	$\frac{1}{64\pi^2}$
8	$\lambda^4\left[D_\lambda(\mathbf{k})(\mathbf{k}-\mathbf{q})^2D_\lambda^3(\mathbf{q})\right]^{-1}$	$\frac{3}{512\pi^2}$
9	$\lambda^2\left[D_\lambda^2(\mathbf{k}-\mathbf{q})\mathbf{q}^2D_\lambda(\mathbf{q})\right]^{-1}$	$\frac{1}{32\pi^2}$
10	$\lambda^2\left[\mathbf{k}^2D_\lambda^2(\mathbf{k}-\mathbf{q})D_\lambda(\mathbf{q})\right]^{-1}$	$\frac{1}{64\pi^2}$
11	$\lambda^4\left[\mathbf{k}^2D_\lambda^2(\mathbf{k}-\mathbf{q})\mathbf{q}^2D_\lambda(\mathbf{q})\right]^{-1}$	$\frac{1}{64\pi^2}$
12	$\lambda^2\left[\mathbf{k}^2D_\lambda(\mathbf{k}-\mathbf{q})D_\lambda^2(\mathbf{q})\right]^{-1}$	$\frac{1}{64\pi^2}$

Note. The k integral for ultraviolet divergent integrals is cut off at upper limit Λ.

$$B_{2b}^{\rm NRQED} = \left\{\frac{\pi^2}{\lambda^2}\right\}\left(\frac{\alpha}{\pi}\right)^2 B_0, \tag{3.59b}$$

$$B_{2c}^{\rm NRQED} = \left\{\pi\frac{\Lambda}{\lambda} - \frac{3}{4}\pi^2 + O\left(\frac{\lambda}{\Lambda}\right)\right\}\left(\frac{\alpha}{\pi}\right)^2 B_0, \tag{3.59c}$$

$$B_{2d}^{\rm NRQED} = \left\{\frac{1}{2}\pi^2\ln\left(\frac{\Lambda}{2\lambda}\right) + O\left(\frac{\lambda}{\Lambda}\right)\right\}\left(\frac{\alpha}{\pi}\right)^2 B_0, \tag{3.59d}$$

$$B_{2e}^{\rm NRQED} = \left\{\pi\frac{\Lambda}{\lambda} - \frac{1}{2}\pi^2 + O\left(\frac{\lambda}{\Lambda}\right)\right\}\left(\frac{\alpha}{\pi}\right)^2 B_0, \tag{3.59e}$$

$$B_{2f}^{\rm NRQED} = \left\{-\frac{5}{3}\pi\frac{\Lambda}{\lambda} + \pi^2\ln\left(\frac{\Lambda}{\lambda}\right) + \frac{1}{3}\pi^2\ln 2 - \frac{5}{8}\pi^2 + O\left(\frac{\lambda}{\Lambda}\right)\right\}\left(\frac{\alpha}{\pi}\right)^2 B_0, \tag{3.59f}$$

$$B_{2g}^{\rm NRQED} = \left\{-\frac{5}{6}\pi^2\ln\left(\frac{\Lambda}{2\lambda}\right) + \frac{1}{8}\pi^2 + O\left(\frac{\lambda}{\Lambda}\right)\right\}\left(\frac{\alpha}{\pi}\right)^2 B_0, \tag{3.59g}$$

$$B_{2h}^{\rm NRQED} = \left\{-\frac{5}{3}\pi\frac{\Lambda}{\lambda} + \frac{13}{12}\pi^2 + O\left(\frac{\lambda}{\Lambda}\right)\right\}\left(\frac{\alpha}{\pi}\right)^2 B_0, \tag{3.59h}$$

$$B_{2i}^{\rm NRQED} = \left\{-\frac{8}{3}\pi\frac{\Lambda}{\lambda} + 2\pi^2 + O\left(\frac{\lambda}{\Lambda}\right)\right\}\left(\frac{\alpha}{\pi}\right)^2 B_0, \tag{3.59i}$$

$$B_{2j}^{\rm NRQED} = \left\{-\frac{8}{3}\pi\frac{\Lambda}{\lambda} + \frac{4}{3}\pi^2 + O\left(\frac{\lambda}{\Lambda}\right)\right\}\left(\frac{\alpha}{\pi}\right)^2 B_0, \tag{3.59j}$$

$$B_{2k}^{\rm NRQED} = \left\{-2\pi\frac{\Lambda}{\lambda} + O\left(\frac{\lambda}{\Lambda}\right)\right\}\left(\frac{\alpha}{\pi}\right)^2 B_0, \tag{3.59k}$$

$$B_{2l}^{\rm NRQED} = \left\{-\frac{1}{2}\pi^2\ln\left(\frac{\Lambda}{\lambda}\right) + O\left(\frac{\lambda}{\Lambda}\right)\right\}\left(\frac{\alpha}{\pi}\right)^2 B_0. \tag{3.59l}$$

The total two-loop NRQED amplitude is

$$B_2^{\rm NRQED} = \left\{\frac{(2\ln 2+1)\pi^2}{\lambda^2} - \frac{26}{3}\pi\frac{\Lambda}{\lambda} + \frac{\pi^2}{6}\ln\left(\frac{\Lambda}{\lambda}\right) + \frac{2}{3}\pi^2\ln 2 + \frac{8}{3}\pi^2 + O\left(\frac{\lambda}{\Lambda}\right)\right\}\left(\frac{\alpha}{\pi}\right)^2 B_0. \tag{3.60}$$

D. The Matching Calculation

The purpose of the matching calculation is to determine the coupling constants of NRQED. In our case, we need to find the $O(\alpha)$ and $O(\alpha^2)$ parts of $\mathrm{Re}(d_C)$ shown in (3.53) by matching the amplitude for $e^-e^+ \to e^-e^+$ scattering at threshold as calculated by QED and by NRQED.

We note first that at zero-loop order the matching is trivial. The zero-loop amplitudes (3.51a) and (3.54) agree as long as the $O(\alpha^0)$ part of $\mathrm{Re}(d_C)$ is one. Of course, successful matching at this order was built into the NRQED interaction (2.25a) from the start. The matching condition through one-loop order is (after dividing out a factor of $B_0 = -i2\pi\alpha/m^2$)

$$1 + \frac{\alpha}{\pi}\left\{\frac{2\pi}{\lambda} + 2I_L(\lambda) - \frac{8}{9}\right\} = d_C + \frac{\alpha}{\pi}\left\{\frac{2\pi}{\lambda} - \frac{13}{3}\frac{\Lambda}{\lambda} + \frac{23}{12}\pi\lambda\right\}, \tag{3.61}$$

which implies

$$d_C^{(1)} = \frac{13}{3}\Lambda + 2I_L(\lambda) - \frac{8}{9} - \frac{23}{12}\pi\lambda, \tag{3.62}$$

where $I_L(\lambda)$ was given in (3.16). We retain the $O(\lambda)$ term since it will become important when multiplied by $1/\lambda$ in the two-loop matching calculation. The matching condition through two-loop order is

$$\begin{aligned} &1 + \frac{\alpha}{\pi}\left\{\frac{2\pi}{\lambda} + 2I_L(\lambda) - \frac{8}{9}\right\} + \left(\frac{\alpha}{\pi}\right)^2\left\{\frac{(2\ln 2+1)\pi^2}{\lambda^2} + \frac{4\pi}{\lambda}I_L(\lambda) - \frac{16}{9}\frac{\pi}{\lambda}\right. \\ &\quad \left. - \frac{\pi^2}{6}\ln\lambda + 2A_0 - 15.7879(26)\right\} \\ &= d_C + \frac{\alpha}{\pi}\left\{\frac{2\pi}{\lambda}d_C - \frac{13}{3}\frac{\Lambda}{\lambda} + \frac{23}{12}\pi\lambda\right\} + \left(\frac{\alpha}{\pi}\right)^2\left\{\frac{(2\ln 2+1)\pi^2}{\lambda^2} - \frac{26}{3}\pi\frac{\Lambda}{\lambda}\right. \\ &\quad \left. + \frac{\pi^2}{6}\ln\left(\frac{\Lambda}{\lambda}\right) + \frac{2}{3}\pi^2\ln 2 + \frac{8}{3}\pi^2\right\}, \end{aligned} \tag{3.63}$$

which implies

$$d_C^{(2)} = -\frac{\pi^2}{6}\ln\Lambda + 2A_0 - 8.8341(26). \tag{3.64}$$

We note that d_C contains a UV divergence arising from NRQED. This will cancel eventually against a UV divergence from the bound state part of the calculation. However, d_C is finite in the infrared—the infrared singularities of QED and NRQED are the same and cancel in matching. This is natural, since NRQED is constructed to agree with QED for low energy processes. We also note that $d_C^{(1)}$ and $d_C^{(2)}$ here are real. This is expected since the one-photon-annihilation channel does not involve real intermediate states. The two-photon-annihilation channel gives an imaginary part to $d_C^{(1)}$, and the three-photon-annihilation channel gives an imaginary part to $d_C^{(2)}$ (as in Eq. (2.10)).

E. Bound State Perturbation Theory

Now that NRQED is defined to the required order, we are in position to obtain the order α^2 corrections to the energy levels. One way to do this is to base a Bethe–Salpeter formalism on the NRQED Lagrangian of (2.1). The Bethe–Salpeter kernel is considered to be the sum of a reference kernel (best taken to be simply the Coulomb interaction) and a perturbation. Then the reference Bethe–Salpeter equation

$$\left(E - \frac{\mathbf{p}^2}{m}\right)G(\mathbf{p},\mathbf{q}) - \int\frac{d^3\ell}{(2\pi)^3}\left(-\frac{4\pi\alpha}{(\mathbf{p}-\boldsymbol{\ell})^2}\right)G(\boldsymbol{\ell},\mathbf{q}) = (2\pi)^3\delta(\mathbf{p}-\mathbf{q}) \tag{3.65}$$

is identical to the nonrelativistic Schrödinger–Coulomb equation. The reference energies are the usual Bohr energies:

$$E_n = -\frac{m\alpha^2}{4n^2}. \tag{3.66}$$

The reference Bethe–Salpeter wavefunctions are found in the residues of the poles of G. They are the usual Schrödinger–Coulomb wavefunctions. The ground state wave function has the form

$$\phi(\mathbf{p}) = \phi_0 \frac{8\pi\gamma}{(\mathbf{p}^2+\gamma^2)^2} \tag{3.67}$$

times a spin factor, where $\gamma = m\alpha/2$ and $\phi_0 = \psi(\mathbf{r}=0) = (\gamma^3/\pi)^{1/2}$ is the wavefunction at contact. Bound state perturbation theory for corrections to the energy levels in this Bethe–Salpeter formalism leads to a result identical to what we would expect from ordinary second-order perturbation theory in quantum mechanics. The perturbing potentials are V_4, V_{4der}, V_{BF}, and δH_{kin}. Since we are interested in perturbations involving one-photon intermediate states, at least one factor of a four-point contact term (V_4 or V_{4der}) must be included. To the required order we find

$$\Delta E = \langle 0|V_4|0\rangle + \langle 0|V_{4der}|0\rangle + \langle 0|V_4 G' V_4|0\rangle + 2\langle 0|V_4 G' V_{BF}|0\rangle + 2\langle 0|V_4 G' \delta H_{kin}|0\rangle, \tag{3.68}$$

where $|0\rangle$ represents the spin-1 ground state, and

$$G' = \sum_{n\neq 0} \frac{|n\rangle\langle n|}{E_0 - E_n} \tag{3.69}$$

is the nonrelativistic Schrödinger–Coulomb propagator with the ground state contribution taken out. Representations for the propagator G were found by Hostler [92] and by Schwinger [93], and for the subtracted propagator G' by Caswell and Lepage [94]. For the subtracted propagator we use the form [95]

$$G'(\mathbf{p},\mathbf{q}) = \frac{-m}{D_\gamma(\mathbf{p})}(2\pi)^3\delta(\mathbf{p}-\mathbf{q}) - \frac{8\pi m\gamma}{D_\gamma(\mathbf{p})R D_\gamma(\mathbf{q})} + G'_{MP}(\mathbf{p},\mathbf{q}), \tag{3.70a}$$

$$G'_{MP}(\mathbf{p},\mathbf{q}) = \frac{-32\pi m\gamma^3}{D_\gamma^2(\mathbf{p})D_\gamma^2(\mathbf{q})}\left\{\frac{5}{2} - \frac{4\gamma^2}{D_\gamma(\mathbf{p})} - \frac{4\gamma^2}{D_\gamma(\mathbf{q})} + \frac{1}{2}\ln A + \frac{(2A-1)}{\sqrt{4A-1}}\tan^{-1}(\sqrt{4A-1})\right\}, \tag{3.70b}$$

where $D_\gamma(\mathbf{p}) = \mathbf{p}^2 + \gamma^2$, $R = (\mathbf{p}-\mathbf{q})^2$, and $A = D_\gamma(\mathbf{p})D_\gamma(\mathbf{q})/(4\gamma^2 R)$. The three parts of G' (see Fig. 14), involving zero, one, and two and more factors of the Coulomb potential, are termed respectively the zero-, one-, and many-potential terms.

The five terms in the energy shift equation (3.68) are depicted graphically in Fig. 15. The first contribution to ΔE (see Fig. 15a) is

$$\Delta E_a = \mathrm{Re}\int \frac{d^3p}{(2\pi)^3}\frac{d^3q}{(2\pi)^3}\phi^\dagger(\mathbf{p})V_4(\mathbf{p},\mathbf{q})\phi(\mathbf{q}) = \frac{2\pi\alpha}{m^2}\mathrm{Re}(d_C)|\phi_0|^2$$
$$= \left\{1 + \left(\frac{\alpha}{\pi}\right)\mathrm{Re}\big(d_C^{(1)}\big) + \left(\frac{\alpha}{\pi}\right)^2\mathrm{Re}\big(d_C^{(2)}\big)\right\}\Delta E_0, \tag{3.71}$$

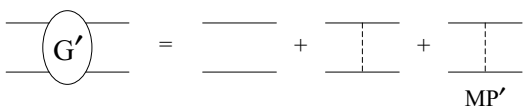

FIG. 14. The subtracted propagator G', shown as a sum of zero-, one-, and subtracted many-potential parts.

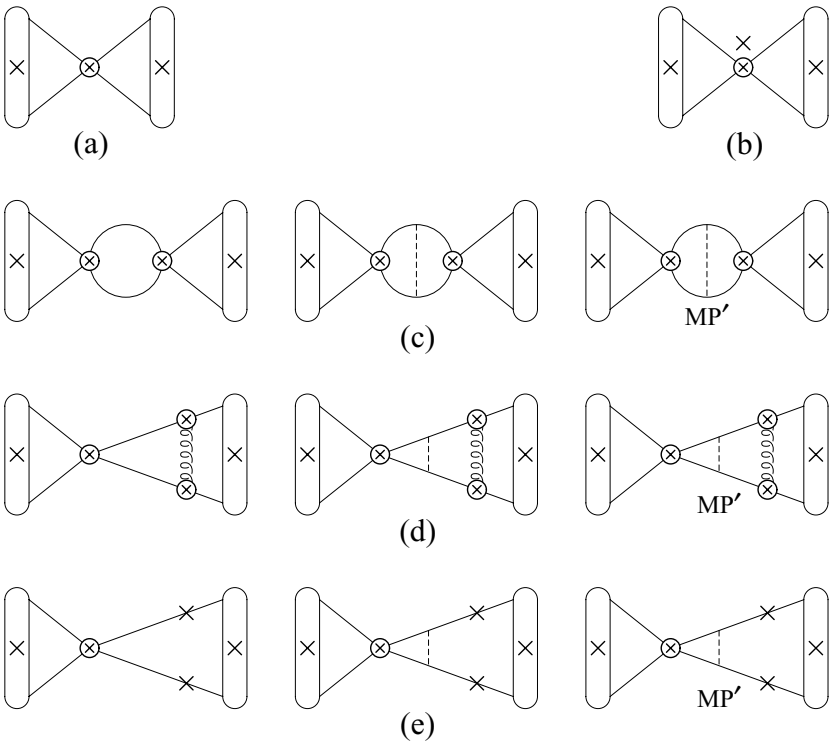

FIG. 15. The five contributions to the one-photon-annihilation energy shift. Contributions (c)–(e) are shown separated into their zero-, one-, and subtracted many-potential parts.

where

$$\Delta E_0 = \frac{m\alpha^4}{4} \tag{3.72}$$

is the lowest order one-photon-annihilation energy contribution. The second contribution to ΔE (see Fig. 15b) is

$$\begin{aligned}\Delta E_b &= \mathrm{Re}\int \frac{d^3p}{(2\pi)^3}\frac{d^3q}{(2\pi)^3}\phi^\dagger(\mathbf{p})V_{4der}(\mathbf{p},\mathbf{q})\phi(\mathbf{q})\\ &= 2\left(-\frac{4\pi\alpha}{3m^4}\right)\phi_0\int^\Lambda \frac{d^3q}{(2\pi)^3}\mathbf{q}^{\,2}\phi(\mathbf{q})\\ &= \left\{-\frac{8\alpha}{3\pi}\Lambda+\alpha^2\right\}\Delta E_0.\end{aligned} \tag{3.73}$$

The third contribution to ΔE (see Fig. 15c) contains zero-, one-, and many-potential parts. The zero-potential part is

$$\begin{aligned}\Delta E_c^0 &= \mathrm{Re}\int \frac{d^3p}{(2\pi)^3}\frac{d^3\ell}{(2\pi)^3}\frac{d^3q}{(2\pi)^3}\phi^\dagger(\mathbf{p})V_4(\mathbf{p},\boldsymbol{\ell})\left(\frac{-m}{D_\gamma(\boldsymbol{\ell})}\right)V_4(\boldsymbol{\ell},\mathbf{q})\phi(\mathbf{q})\\ &= \phi_0\left(\frac{2\pi\alpha}{m^2}\right)\left(-\frac{m\Lambda}{2\pi^2}+\frac{m\gamma}{4\pi}\right)\left(\frac{2\pi\alpha}{m^2}\right)\phi_0\\ &= \left\{-\frac{\alpha}{\pi}\Lambda+\frac{\alpha^2}{4}\right\}\Delta E_0,\end{aligned} \tag{3.74}$$

where the value of the one-loop ℓ integral was taken from Table IV. The one-potential part is

$$\begin{aligned}\Delta E_c^1 &= \mathrm{Re}\int \frac{d^3p}{(2\pi)^3}\frac{d^3k}{(2\pi)^3}\frac{d^3\ell}{(2\pi)^3}\frac{d^3q}{(2\pi)^3}\phi^\dagger(\mathbf{p})V_4(\mathbf{p},\mathbf{k})\left(\frac{-8\pi m\gamma}{D_\gamma(\mathbf{k})(\mathbf{k}-\ell)^2D_\gamma(\ell)}\right)V_4(\ell,\mathbf{q})\phi(\mathbf{q})\\ &= |\phi_0|^2\left(\frac{2\pi\alpha}{m^2}\right)^2\int^\Lambda\frac{d^3k}{(2\pi)^3}\int\frac{d^3\ell}{(2\pi)^3}\frac{-8\pi m\gamma}{D_\gamma(\mathbf{k})(\mathbf{k}-\ell)^2D_\gamma(\ell)}\\ &= \left\{-\frac{\alpha^2}{2}\ln\left(\frac{\Lambda}{2\gamma}\right)\right\}\Delta E_0,\end{aligned} \tag{3.75}$$

where the two-loop integral was taken from Table V. The many-potential part is

$$\begin{aligned}\Delta E_c^{MP} &= \mathrm{Re}\int \frac{d^3p}{(2\pi)^3}\frac{d^3k}{(2\pi)^3}\frac{d^3\ell}{(2\pi)^3}\frac{d^3q}{(2\pi)^3}\phi^\dagger(\mathbf{p})V_4(\mathbf{p},\mathbf{k})G'_{MP}(\mathbf{k},\ell)V_4(\ell,\mathbf{q})\phi(\mathbf{q})\\ &= |\phi_0|^2\left(\frac{2\pi\alpha}{m^2}\right)^2\int\frac{d^3k}{(2\pi)^3}\frac{d^3\ell}{(2\pi)^3}G'_{MP}(\mathbf{k},\ell)\\ &= \left\{-\frac{3\alpha^2}{4}\right\}\Delta E_0.\end{aligned} \tag{3.76}$$

In the last step we employed the useful formula [94]

$$\int\frac{d^3\ell}{(2\pi)^3}G'_{MP}(\mathbf{k},\ell) = \frac{-4m\gamma^2}{D_\gamma^2(\mathbf{k})}\left\{\frac{5}{2}-\ln 2-\frac{4\gamma^2}{D_\gamma(\mathbf{k})}-\frac{\gamma}{k}\tan^{-1}\left(\frac{k}{\gamma}\right)+\frac{1}{2}\ln\left(\frac{D_\gamma(\mathbf{k})}{\gamma^2}\right)\right\}. \tag{3.77}$$

The results for Figs. 15d and 15e are

$$\Delta E_d^0 = \left\{-\frac{5\alpha}{3\pi}\Lambda+\alpha^2\ln\left(\frac{\Lambda}{2\gamma}\right)-\frac{\alpha^2}{12}\right\}\Delta E_0, \tag{3.78a}$$

$$\Delta E_d^1 = \left\{-\frac{5\alpha^2}{6}\ln\left(\frac{\Lambda}{2\gamma}\right)-\frac{\alpha^2}{2}+\alpha^2\zeta(2)\right\}\Delta E_0, \tag{3.78b}$$

$$\Delta E_d^{MP} = \{\alpha^2-\alpha^2\zeta(2)\}\Delta E_0, \tag{3.78c}$$

and

$$\Delta E_e^0 = \left\{\frac{\alpha}{\pi}\Lambda-\frac{15\alpha^2}{32}\right\}\Delta E_0, \tag{3.79a}$$

$$\Delta E_e^1 = \left\{\frac{\alpha^2}{2}\ln\left(\frac{\Lambda}{2\gamma}\right)-\frac{13\alpha^2}{64}\right\}\Delta E_0, \tag{3.79b}$$

$$\Delta E_e^{MP} = \left\{\frac{51\alpha^2}{64}\right\}\Delta E_0. \tag{3.79c}$$

We summarize the results of Figs. 15a–15e as

$$\Delta E_a = \left\{1+\left(\frac{\alpha}{\pi}\right)\mathrm{Re}\big(d_C^{(1)}\big)+\left(\frac{\alpha}{\pi}\right)^2\mathrm{Re}\big(d_C^{(2)}\big)\right\}\Delta E_0, \tag{3.80a}$$

$$\Delta E_b = \left\{ -\frac{8\alpha}{3\pi}\Lambda + \alpha^2 \right\} \Delta E_0, \tag{3.80b}$$

$$\Delta E_c = \left\{ -\frac{\alpha}{\pi}\Lambda - \frac{\alpha^2}{2}\ln\left(\frac{\Lambda}{2\gamma}\right) - \frac{\alpha^2}{2} \right\} \Delta E_0, \tag{3.80c}$$

$$\Delta E_d = \left\{ -\frac{5\alpha}{3\pi}\Lambda + \frac{\alpha^2}{6}\ln\left(\frac{\Lambda}{2\gamma}\right) + \frac{5\alpha^2}{12} \right\} \Delta E_0, \tag{3.80d}$$

$$\Delta E_e = \left\{ \frac{\alpha}{\pi}\Lambda + \frac{\alpha^2}{2}\ln\left(\frac{\Lambda}{2\gamma}\right) + \frac{\alpha^2}{8} \right\} \Delta E_0. \tag{3.80e}$$

The total correction to the energy level is the sum of the above:

$$\Delta E = \left\{ 1 + \left(\frac{\alpha}{\pi}\right) \mathrm{Re}\left(d_C^{(1)}\right) + \left(\frac{\alpha}{\pi}\right)^2 \mathrm{Re}\left(d_C^{(2)}\right) \right\} \Delta E_0 + \left\{ -\frac{13\alpha}{3\pi}\Lambda + \frac{\alpha^2}{6}\ln\left(\frac{\Lambda}{2\gamma}\right) + \frac{25\alpha^2}{24} \right\} \Delta E_0. \tag{3.81}$$

F. Result for the HFS

We can now complete the calculation of the one-photon-annihilation contribution to the HFS. In the $\lambda \to 0$ limit the needed one-loop NRQED coupling constant is

$$\mathrm{Re}\left(d_C^{(1)}\right) = \frac{13}{3}\Lambda - \frac{44}{9}. \tag{3.82}$$

The two-loop coupling constant is given in (3.64). On using these in (3.81), we find

$$\Delta E = \left\{ 1 + \left(\frac{\alpha}{\pi}\right)\left[-\frac{44}{9} \right] + \left(\frac{\alpha}{\pi}\right)^2 \left[\frac{\pi^2}{6}\ln\left(\frac{1}{\alpha}\right) + 2A_0 + 1.4467(26) \right] \right\} \Delta E_0. \tag{3.83}$$

The $O(m\alpha^6)$ constant is

$$\frac{1}{4\pi^2}\{2A_0 + 1.4467(26)\} = -0.1245(31) \tag{3.84}$$

since $A_0 = -3.18(6)$. This represents an energy shift of $-2.32(6)$ MHz, since $m\alpha^6 = 18.658$ MHz. This value is consistent with the numerical result $-0.1256481(12)$ of Adkins *et al.* [80] obtained using a Bethe–Salpeter based formalism in Coulomb gauge and with the analytic result

$$\frac{1}{4\pi^2}\left\{ \frac{13}{8}\zeta(3) + \frac{27}{2}\zeta(2)\ln 2 - \frac{1183}{48}\zeta(2) + \frac{1477}{81} \right\} = -0.1256487 \tag{3.85}$$

of Hoang *et al.* [81] found using a variant of NRQED. Our new result is a third independent calculation of the one-photon-annihilation energy shift. Our method differs fundamentally from that of Adkins, Fell, and Mitrikov. It is similar to that of Hoang, Labelle, and Zebarjad, but has a different treatment of the infrared regularization in the matching calculation. The new calculation reconfirms the one-photon-annihilation energy shift result and gives strong evidence that our calculational technique and execution are correct. This is an important point, since the o-Ps decay calculation is very similar to the energy shift calculation. Also, by turning the argument around, we use the equality of (3.84)

and (3.85) to find a better value for A_0 than we were able to achieve numerically:

$$A_0 = -3.2036(13). \tag{3.86}$$

This same A_0 will be needed for the decay rate calculation.

IV. THE ORTHOPOSITRONIUM DECAY RATE

A. Overview

Our decay rate calculation follows the same outline as that for the one-photon-annihilation contribution to the energy shift. First we perform a matching calculation to determine the required coefficient of NRQED by a comparison of QED and NRQED calculations for an appropriately chosen quantity. Then we use NRQED to obtain the imaginary part of the energy shift through second order in bound state perturbation theory. The decay rate is found through $\Gamma = -2\mathrm{Im}(\Delta E)$.

The quantity to be matched is $\mathrm{Im}(A)$, the imaginary part of the $e^-e^+ \to e^-e^+$ scattering amplitude at threshold. As a notational convenience, we relate amplitude contributions to decay rate contributions through

$$\Gamma_x = -2\mathrm{Im}(\Delta E_x) = -2\mathrm{Im}(iB_x|\phi_0|^2); \tag{4.1}$$

that is, we multiply a contribution $\mathrm{Im}(iB_x)$ by $-2|\phi_0|^2$ and write this as Γ_x. But this is just notation: what is being matched is the imaginary part of the scattering amplitude.

The main part of our work is to calculate the imaginary part of the amplitude via QED. There are 83 independent graphs to evaluate, some of which are quite challenging. This work is described in Section IV.B. The rest of the calculation, which consists of a NRQED evaluation of the imaginary part of the amplitude, matching, and the NRQED calculation of the imaginary part of the energy shift, was done earlier by Labelle *et al*. [73] (modulo a small error in their work which we discuss in Section IV.F.)

B. Calculation of the Scattering Amplitude via QED

The lowest order contribution to $e^-e^+ \to e^-e^+$ involving a three-photon intermediate state is shown in Fig. 2. The imaginary part of the amplitude for this graph comes from a Cutkosky cut through all three photons, which constrains them to be on-shell [96]. Therefore the decay rate contributions can be calculated equivalently by just considering decay to three real photons from an initial spin-1 o-Ps state with no internal structure. From this point of view, the decay rate is

$$\Gamma = \frac{1}{2M}\int \frac{d^3k_1}{(2\pi)^3 2\omega_1}\frac{d^3k_2}{(2\pi)^3 2\omega_2}\frac{d^3k_3}{(2\pi)^3 2\omega_3}(2\pi)^4\delta(P-k_1-k_2-k_3)\sum_{\epsilon_1,\epsilon_2,\epsilon_3}\frac{1}{3}\sum_{\epsilon_m}\frac{1}{3!}|\mathcal{M}|^2. \tag{4.2}$$

Here $M = 2m$ is the o-Ps mass, $P = (2m, \mathbf{0})$ is the (rest-frame) o-Ps energy-momentum vector, k_i is the energy-momentum vector of the ith final-state photon with $k_i^0 = \omega_i = |\mathbf{k}_i|$, $\hat{\epsilon}_i$ is the polarization vector of the ith final state photon, and $\hat{\epsilon}_m$ is the o-Ps spin vector. The decay amplitude $\mathcal{M}$ has a zero-loop contribution from Fig. 2, one-loop contributions from Fig. 3, and many two-loop contributions.

The phase space integral for Γ is in essence only two dimensional. Energy-momentum conservation, enforced by the Dirac delta function, implies the conditions

$$2m = \omega_1 + \omega_2 + \omega_3, \tag{4.3a}$$

$$0 = \mathbf{k}_1 + \mathbf{k}_2 + \mathbf{k}_3. \tag{4.3b}$$

Use of the Dirac delta function reduces the dimensionality of the integral from nine to five. Conservation of three-momentum requires the three photons to lie in a plane. Three Euler angles describe the orientation of this decay plane in space. Since the spin-averaged differential decay rate is rotationally symmetric, these three angles can be integrated out. We are left with two variables which describe the configuration of the final state photons in the decay plane. These two variables can be taken to be proportional to the energies of two of the photons: $x_i = \omega_i/m$. The angle between any two photons is given in terms of the x's by

$$\cos(\theta_{ij}) = \frac{x_k^2 - x_i^2 - x_j^2}{2x_i x_j}, \tag{4.4}$$

where θ_{ij} is the angle between photons i and j, and k represents the third photon. The decay rate can be written as

$$\Gamma = \frac{m}{2^7\pi^3}\int_0^1 dx_1 \int_{1-x_1}^1 dx_3 \sum_{\epsilon_1,\epsilon_2,\epsilon_3}\frac{1}{3}\sum_{\epsilon_m}\frac{1}{3!}|\mathcal{M}|^2. \tag{4.5}$$

The zero-loop decay amplitude has the form

$$\mathcal{M}_0 = \sum_{\sigma\in S_3}\mathrm{tr}\left[\left(-ie\gamma\epsilon_{\sigma(3)}\right)\frac{i}{\gamma\left(-P/2+k_{\sigma(3)}\right)-m}\left(-ie\gamma\epsilon_{\sigma(2)}\right)\frac{i}{\gamma\left(P/2-k_{\sigma(1)}\right)-m}\left(-ie\gamma\epsilon_{\sigma(1)}\right)\Psi\right], \tag{4.6}$$

where the sum is over the six permutations σ of the three final state photons. The *wave function* is

$$\Psi = \sqrt{2M}\begin{pmatrix}0 & \boldsymbol{\sigma}\cdot\hat{\epsilon}_m/\sqrt{2}\\ 0 & 0\end{pmatrix}\phi_0, \tag{4.7}$$

which contains the spin-1 spin factor, a normalization factor, and the wave function at contact ϕ_0. The decay amplitude can be rewritten as

$$\mathcal{M}_0 = -i\pi\alpha^3\sum_{\sigma\in S_3}\frac{x_{\sigma(2)}}{x_1x_2x_3}\mathrm{tr}\left[\gamma\epsilon_{\sigma(3)}\left(-\gamma r_{\sigma(3)}+1\right)\gamma\epsilon_{\sigma(2)}\left(\gamma r_{\sigma(1)}+1\right)\gamma\epsilon_{\sigma(1)}\begin{pmatrix}0 & \boldsymbol{\sigma}\cdot\hat{\epsilon}_m\\ 0 & 0\end{pmatrix}\right], \tag{4.8}$$

where $r_i = n - k_i/m$ with $n = (1, \mathbf{0})$. We performed the polarization sums by

$$\sum_{\epsilon}\epsilon_\mu^*\epsilon_\nu = -g_{\mu\nu} \tag{4.9}$$

and the spin average via

$$\frac{1}{3}\sum_{\epsilon_m}\begin{pmatrix}0 & \boldsymbol{\sigma}\cdot\hat{\epsilon}_m\\ 0 & 0\end{pmatrix}^*\otimes\begin{pmatrix}0 & \boldsymbol{\sigma}\cdot\hat{\epsilon}_m\\ 0 & 0\end{pmatrix} = \frac{1}{12}[(1+\gamma_0)\gamma^\alpha]^*\otimes[(1+\gamma_0)\gamma^\beta](-g_{\alpha\beta}+n_\alpha n_\beta), \tag{4.10}$$

since ϵ_m has only spatial components. The resulting traces were evaluated using Reduce [97]. The zero-loop result is that of Ore and Powell, given in (1.3).

The lowest-order decay amplitude $\mathcal{M}_0$ is corrected by one-, two-, and higher-loop effects:

$$\mathcal{M} = \mathcal{M}_0 + \mathcal{M}_1 + \mathcal{M}_2 + \cdots. \tag{4.11}$$

The absolute square of this is

$$|\mathcal{M}|^2 = |\mathcal{M}_0|^2 + 2\mathrm{Re}[\mathcal{M}_0^*\mathcal{M}_1 + \mathcal{M}_0^*\mathcal{M}_2] + |\mathcal{M}_1|^2 + \cdots. \tag{4.12}$$

The one-loop and many of the two-loop contributions have the form $2\mathrm{Re}[\mathcal{M}_0^*\mathcal{M}_X]$. If we write the amplitude for one of these n-loop contributions as

$$\mathcal{M}_X = -i\pi\alpha^3\left(\frac{\alpha}{\pi}\right)^n \sum_{\tau\in S_3} \mathrm{tr}\left[X^{\tau}_{\mu_3,\mu_2,\mu_1}\begin{pmatrix} 0 & \boldsymbol{\sigma}\cdot\hat{\epsilon}_m \\ 0 & 0\end{pmatrix}\right]\epsilon^{\mu_3}_{\tau(3)}\epsilon^{\mu_2}_{\tau(2)}\epsilon^{\mu_1}_{\tau(1)}, \tag{4.13}$$

then the corresponding decay rate correction is

$$\Gamma_X = \frac{m\alpha^6}{\pi}\left(\frac{\alpha}{\pi}\right)^n \frac{1}{48}\int_0^1 dx_1 \int_{1-x_1}^1 dx_3 \frac{1}{x_1x_2x_3}T_X, \tag{4.14}$$

where

$$T_X = \sum_{\sigma\in S_3} x_{\sigma(2)}\frac{1}{4}\mathrm{tr}\big[\gamma^{\mu_{\sigma(3)}}\big(-\gamma r_{\sigma(3)}+1\big)\gamma^{\mu_{\sigma(2)}}\big(\gamma r_{\sigma(1)}+1\big)\gamma^{\mu_{\sigma(1)}}(1+\gamma^0)\gamma^{\alpha}\big]Y_X(g_{\alpha\beta}-n_\alpha n_\beta) \tag{4.15}$$

$$Y_X = \frac{1}{4}\mathrm{tr}\big[X^{I}_{\mu_3,\mu_2,\mu_1}(1+\gamma^0)\gamma^{\beta}\big]. \tag{4.16}$$

Since the phase space integration is symmetric under permutations of the final-state photons, it is not necessary to symmetrize in both $\mathcal{M}_0^*$ and $\mathcal{M}_X$, so for $\mathcal{M}_X$ we used 3! times the term specified by the identity permutation ($\tau = I$).

The one-loop contributions are contained in $2\mathrm{Re}[\mathcal{M}_0^*\mathcal{M}_1]$ and are shown in Fig. 3. The most difficult one-loop graph to evaluate is the ladder (see Fig. 3e). This graph is ultraviolet finite, but has an infrared binding singularity that manifests itself as a factor of $1/\lambda$. We write the ladder amplitude as

$$\begin{aligned}\mathcal{M}_L = \frac{1}{m^2}\sum_{\sigma\in S_3}\int\frac{d^4\ell}{(2\pi)^4}\mathrm{tr}\Bigg[&(-ie\gamma^{\mu})\frac{i}{\gamma(-n+\ell)-1}\big(-ie\gamma\epsilon_{\sigma(3)}\big)\frac{i}{\gamma\big(-r_{\sigma(3)}+\ell\big)-1}\\ &\times\big(-ie\gamma\epsilon_{\sigma(2)}\big)\frac{i}{\gamma\big(r_{\sigma(1)}+\ell\big)-1}\big(-ie\gamma\epsilon_{\sigma(1)}\big)\frac{i}{\gamma(n+\ell)-1}(-ie\gamma_{\mu})\Psi\Bigg]\left(\frac{-i}{\ell^2-\lambda^2}\right).\end{aligned} \tag{4.17}$$

The associated Y factor is

$$Y_L = -\int\frac{d^4\ell}{i\pi^2}\frac{N(\ell)}{H(\ell)Z(\ell)}, \tag{4.18}$$

where

$$\begin{aligned}N(\ell) = \frac{1}{4}\mathrm{tr}\big[&\gamma^{\mu}(\gamma(\ell-n)+1)\gamma^{\mu_3}(\gamma(\ell-r_3)+1)\gamma^{\mu_2}(\gamma(\ell+r_1)+1)\\ &\times\gamma^{\mu_1}(\gamma(\ell+n)+1)\gamma_{\mu}(1+\gamma^0)\gamma^{\beta}\big],\end{aligned} \tag{4.19a}$$

$$H(\ell) = (-\ell^2 + \lambda^2)(-\ell^2 + 2\ell n)(-\ell^2 - 2\ell n), \tag{4.19b}$$

$$Z(\ell) = (-(\ell - r_3)^2 + 1)(-(\ell + r_1)^2 + 1). \tag{4.19c}$$

We evaluate Y_L in two parts:

$$Y_L = -\int \frac{d^4\ell}{i\pi^2}\frac{1}{H(\ell)}\left\{\frac{N(0)}{Z(0)} + \left[\frac{N(\ell) - N(0)}{Z(\ell)} + N(0)\left(\frac{1}{Z(\ell)} - \frac{1}{Z(0)}\right)\right]\right\}, \tag{4.20}$$

where

$$Z(0) = (2x_1)(2x_3), \tag{4.21a}$$

$$N(0) = -4T_0, \tag{4.21b}$$

$$T_0 = \frac{1}{4}\mathrm{tr}\left[\gamma^{\mu_3}(-\gamma r_3 + 1)\gamma^{\mu_2}(\gamma r_1 + 1)\gamma^{\mu_1}(1 + \gamma_0)\gamma^{\beta}\right]. \tag{4.21c}$$

The first (infrared divergent) part of Y_L is

$$Y_{LB} = -\int \frac{d^4\ell}{i\pi^2}\frac{1}{H(\ell)}\frac{N(0)}{Z(0)} = \frac{T_0}{x_1 x_3} I_B, \tag{4.22}$$

where I_B was evaluated in (3.10). The corresponding contribution to Γ_L is

$$\Gamma_{LB} = 2\Gamma_0\left(\frac{\alpha}{\pi}\right) I_B = \left\{\frac{2\pi}{\lambda} + 2\ln\lambda - 2 - \frac{\pi\lambda}{4} + O(\lambda^2)\right\}\left(\frac{\alpha}{\pi}\right)\Gamma_0. \tag{4.23}$$

The second subtracted part of Y_L was evaluated numerically using Feynman parameters to do the ℓ integral. We found

$$\Gamma_{LS} = K_L(\lambda)\frac{m\alpha^7}{\pi^2}, \tag{4.24a}$$

$$K_L(\lambda) = -1.125030(6) + 2.5280(7)\lambda + O(\lambda^2). \tag{4.24b}$$

Therefore the total ladder contribution is

$$\Gamma_L = \left\{\frac{2\pi}{\lambda} + 2\ln\lambda - 7.821768(32) + 12.296(4)\lambda + O(\lambda^2)\right\}\left(\frac{\alpha}{\pi}\right)\Gamma_0. \tag{4.25}$$

Results for all of the one-loop contributions are listed in Table VI. The $O(\lambda)$ contributions come (as in the ladder graph) from the explicit λ in the photon propagator and are also induced by renormalization, since the renormalization constant has a λ dependence (see (3.45a)). We evaluated the $O(\lambda)$ corrections because, as in the one-photon-annihilation calculation, the λ-dependent one-loop results will be multiplied by factors of $1/\lambda$ in the matching process. However, again as before, we will find that the $O(\lambda)$ part of the one-loop rate cancels and does not in fact enter into the final result for the NRQED coupling constant. The total one-loop result, from Table VI, is

$$\Gamma_1^{QED} = \left\{\frac{2\pi}{\lambda} + A(\lambda)\right\}\frac{\alpha}{\pi}\Gamma_0, \tag{4.26}$$

TABLE VI

Renormalized One-Loop Contributions to the Orthopositronium Decay Rate

Contribution	$\frac{\pi}{\lambda}(\frac{\alpha}{\pi})\Gamma_0$	$\ln\lambda(\frac{\alpha}{\pi})\Gamma_0$	$\frac{\alpha}{\pi}\Gamma_0$	$\lambda\frac{\alpha}{\pi}\Gamma_0$
Γ_{SE}	0	4	4.784984	−11.0445(1)
Γ_{OV}	0	−4	−1.028861	1.8756(1)
Γ_{IV}	0	−2	−1.839323	4.7124
Γ_{DV}	0	0	−3.567629(21)	7.5499(2)
Γ_L	2	2	−7.821768(32)	12.296(4)
Γ_A	0	0	−0.8140573(3)	0.0
Total	2	0	−10.286606(10)	15.389(4)

Note. The one-loop total was taken from [56].

where

$$A(\lambda) = -10.286606(10) + 15.389(4)\lambda. \tag{4.27}$$

The two-loop contributions to $|\mathcal{M}|^2$ come in three forms. The first, from $2\mathrm{Re}[\mathcal{M}_0^*\mathcal{M}_2]$, is the set of graphs involving the zero-loop amplitude $\mathcal{M}_0^*$ multiplied by a two-loop correction $\mathcal{M}_2$. We have subdivided these contributions into classes a–i which will be described below. The second contribution, from $|\mathcal{M}_1|^2$, is the set of graphs involving the product of two one-loop corrected amplitudes. We call this class j. Finally, there are the contributions containing light-by-light scattering between two zero-loop amplitudes. While these can be thought of as arising from $2\mathrm{Re}[\mathcal{M}_0^*\mathcal{M}_2]$, for their evaluation it is better to think of them as the imaginary parts of appropriate energy contributions. These graphs we call class k. We turn now to a description of our evaluation of the various two-loop contributions.

Class a contains the two-loop vertex corrections to one or the other of the outer vertices. The class a contributions to $\mathcal{M}_2$ are shown in Fig. 16a. (Not included in class a is the vacuum polarization corrected one-loop outer vertex graph, since we collect all vacuum polarization corrections into class i.) Each class a graph is multiplied by two to account for the fact that there are two vertices to be corrected. (An additional factor of two, the "2" in $2\mathrm{Re}[\mathcal{M}_0\mathcal{M}_2^*]$, is already accounted for in formula (4.14) for the decay rate correction.) Class a graphs are free of binding singularities, but do contain two-loop ultraviolet divergences. The loop integrals are handled by use of Feynman parameters. The one-loop vertex and self-energy functions given in [85] were used to evaluate all class a graphs except for the crossed photon graph (a4). We subtracted off divergent parts proportional

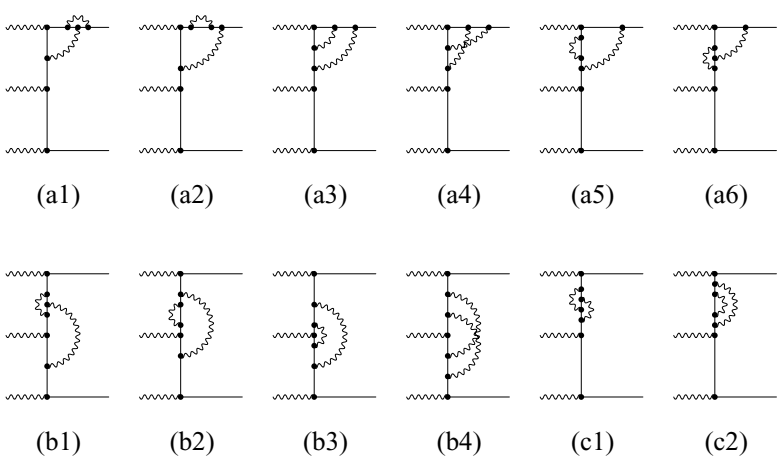

FIG. 16. Contributions of classes a, b, and c to the o-Ps decay amplitude.

TABLE VII

Unrenormalized Contributions to the Orthopositronium Decay Rate from Class a

Diagram	$\Omega^{\epsilon}\Gamma(\epsilon)(\frac{\alpha}{4\pi})\Gamma'_{\rm OV}$	$(e^{-\gamma_E}\Omega)^{2\epsilon}(\frac{\alpha}{\pi})^2\Gamma_0$	$\frac{m\alpha^8}{\pi^3}$
a1	$1-\epsilon$	$-\frac{1}{8\epsilon^2}+\frac{7}{16\epsilon}$	−0.920974(11)
a2	$\frac{-1}{1-2\epsilon}$	$\frac{1}{8\epsilon^2}+\frac{5}{16\epsilon}$	1.234266(10)
a3	$1-\epsilon$	$-\frac{1}{8\epsilon^2}+\frac{9}{16\epsilon}$	0.169211(8)
a4	0	$-\frac{1}{2\epsilon}$	0.520139(5)
a5	$\frac{-1}{1-2\epsilon}$	$\frac{1}{8\epsilon^2}+\frac{5}{16\epsilon}$	0.647231(6)
a6	$1-\epsilon$	$-\frac{1}{8\epsilon^2}+\frac{7}{16\epsilon}$	0.039065(8)
Total	$3(1-\epsilon)-\frac{2}{1-2\epsilon}$	$-\frac{1}{8\epsilon^2}+\frac{25}{16\epsilon}$	1.688938(21)

Note. Class a consists of two-loop corrections to the outer photon vertex.

to Γ_0 and to the unrenormalized one-loop outer vertex correction

$$\Gamma'_{OV}=\left(\Omega e^{-\gamma_E}\right)^{\epsilon}\left\{\frac{1}{\epsilon}+2.971139\right\}\left(\frac{\alpha}{\pi}\right)\Gamma_0 \tag{4.28}$$

and evaluated the finite remainder numerically using the adaptive iterative Monte Carlo integration routine Vegas [98]. The results for the various class a graphs are given in Table VII. The total class a unrenormalized result is

$$\Gamma'_a=\left(e^{-\gamma_E}\Omega\right)^{2\epsilon}\left\{\frac{-1}{8\epsilon^2}+\frac{25}{16\epsilon}\right\}\left(\frac{\alpha}{\pi}\right)^2\Gamma_0+\left\{3(1-\epsilon)-\frac{2}{1-2\epsilon}\right\}\Omega^{\epsilon}\Gamma(\epsilon)\times\left(\frac{\alpha}{4\pi}\right)\Gamma'_{OV}+1.688938(21)\frac{m\alpha^8}{\pi^3}. \tag{4.29}$$

The relation (3.42b) for the renormalized two-loop vertex part implies

$$\Gamma_a=\Gamma'_a-\Gamma'_{OV}L_1-4\left(\tilde{L}_2-L_1^2\right)\Gamma_0, \tag{4.30}$$

where Γ_a is the renormalized class a result, and the factor of four appears because of the two factors of two discussed above. The one-loop renormalization constant L_1 is given in (3.43b) and (3.45a). The two-loop renormalization constant (with the vacuum polarization contribution removed) is given by

$$\tilde{L}_2=\left(\frac{\alpha}{\pi}\right)^2\left[\Omega e^{-\gamma_E}\right]^{2\epsilon}\tilde{\ell}_2, \tag{4.31}$$

TABLE VIII

Unrenormalized Contributions to the Orthopositronium Decay Rate from Class b

Diagram	$\Omega^\epsilon\Gamma(\epsilon)(\frac{\alpha}{4\pi})\Gamma'_{\rm IV}$	$(e^{-\gamma_E}\Omega)^{2\epsilon}(\frac{\alpha}{\pi})^2\Gamma_0$	$\frac{m\alpha^8}{\pi^3}$
b1	$2(1-\epsilon)$	$-\frac{1}{8\epsilon^2}+\frac{7}{16\epsilon}$	0.109707(7)
b2	$\frac{-2}{1-2\epsilon}$	$\frac{1}{8\epsilon^2}+\frac{5}{16\epsilon}$	0.403240(8)
b3	$1-\epsilon$	$-\frac{1}{16\epsilon^2}+\frac{9}{32\epsilon}$	−0.023517(5)
b4	0	$-\frac{1}{4\epsilon}$	0.057609(7)
Total	$3(1-\epsilon)-\frac{2}{1-2\epsilon}$	$-\frac{1}{16\epsilon^2}+\frac{25}{32\epsilon}$	0.547039(14)

Note. Class b consists of two-loop corrections to the inner photon vertex.

where

$$\tilde{\ell}_2=\frac{1}{32\epsilon^2}+\frac{1}{\epsilon}\left\{\frac{\ln\lambda}{4}+\frac{13}{64}\right\}+\left\{\frac{1}{4}\ln^2\lambda+\ln\lambda+\frac{3}{2}\zeta(3)-6\zeta(2)\ln 2+\frac{157}{32}\zeta(2)-\frac{49}{128}\right\}+O(\epsilon). \tag{4.32}$$

Our result for the renormalized class a decay rate contribution is

$$\Gamma_a=-\ln\lambda\left(\frac{\alpha}{\pi}\right)\Gamma_{OV}+\{-2\ln^2\lambda-5.61811(11)\}\left(\frac{\alpha}{\pi}\right)^2\Gamma_0, \tag{4.33}$$

where the one-loop renormalized outer vertex decay rate contribution Γ_{OV} is given in Table VI.

Class b contains the two-loop corrections to the inner vertex. The class b contributions to $\mathcal{M}_2$ are shown in Fig. 16b. Again, no vacuum polarization effects are included in this class. The evaluation of class b is analogous to that of class a. Unrenormalized results for individual class b graphs are shown in Table VIII. The total class b unrenormalized result is

$$\Gamma'_b=\left(e^{-\gamma_E}\Omega\right)^{2\epsilon}\left\{\frac{-1}{16\epsilon^2}+\frac{25}{32\epsilon}\right\}\left(\frac{\alpha}{\pi}\right)^2\Gamma_0+\left\{3(1-\epsilon)-\frac{2}{1-2\epsilon}\right\}\Omega^\epsilon\Gamma(\epsilon)\times\left(\frac{\alpha}{4\pi}\right)\Gamma'_{IV}+0.547039(14)\frac{m\alpha^8}{\pi^3}, \tag{4.34}$$

where the unrenormalized one-loop inner vertex correction is

$$\Gamma'_{IV}=\left(\Omega e^{-\gamma_E}\right)^\epsilon\left\{\frac{1}{2\epsilon}+0.160677\right\}\left(\frac{\alpha}{\pi}\right)\Gamma_0. \tag{4.35}$$

Our result for the renormalized class b decay rate contribution is

$$\Gamma_b=-\ln\lambda\left(\frac{\alpha}{\pi}\right)\Gamma_{IV}+\{-\ln^2\lambda-0.70473(8)\}\left(\frac{\alpha}{\pi}\right)^2\Gamma_0, \tag{4.36}$$

where Γ_{IV} is given in Table VI.

Class c consists of the two-loop irreducible self-energy corrections. The class c contributions to $\mathcal{M}_2$ are shown in Fig. 16c. The *crossed rainbow* contribution $\Sigma_{CR}(p)$ to the two-loop self-energy function contains a momentum-dependent ultraviolet divergence, which makes the contribution of $\Sigma_{CR}(p)$ to the decay rate tricky to evaluate. It is easier to find the decay rate contribution of

$$\Sigma'_{CR}(p) = \Sigma_{CR}(p) + \left(\frac{\alpha}{4\pi}\right)^2 \left(\Omega e^{-\gamma_E}\right)^{\epsilon} \left(\frac{1}{\epsilon}\right) \bar{b}_2(p)(\gamma p - m), \tag{4.37}$$

which has this momentum-dependent divergence subtracted out. Here $\bar{b}_2(p)$ is the momentum-dependent part of the one-loop self-energy function defined in [85]. The modified crossed ladder decay rate contribution is

$$\Gamma_{CR'} = \left(\Omega e^{-\gamma_E}\right)^{2\epsilon} \left\{-\frac{5}{8\epsilon}\right\} \left(\frac{\alpha}{\pi}\right)^2 \Gamma_0 + (1-\epsilon)\Omega^{\epsilon}\Gamma(\epsilon) \left(\frac{\alpha}{4\pi}\right) \Gamma'_{SE} - 0.636407(15)\frac{m\alpha^8}{\pi^3}, \tag{4.38}$$

where the unrenormalized one-loop self-energy correction is

$$\Gamma'_{SE} = \left(\Omega e^{-\gamma_E}\right)^{\epsilon} \left\{-\frac{1}{\epsilon} + 0.784984\right\} \left(\frac{\alpha}{\pi}\right) \Gamma_0. \tag{4.39}$$

The double rainbow contribution (c2) is straightforward and contributes

$$\begin{aligned} \Gamma_{DR} = {} & \left(\Omega e^{-\gamma_E}\right)^{2\epsilon} \left\{-\frac{1}{8\epsilon^2} - \frac{7}{16\epsilon}\right\} \left(\frac{\alpha}{\pi}\right)^2 \Gamma_0 + \left(\frac{-1}{1-2\epsilon}\right) \Omega^{\epsilon}\Gamma(\epsilon) \\ & \times \left(\frac{\alpha}{4\pi}\right) \Gamma'_{SE} - 0.362088(39)\frac{m\alpha^8}{\pi^3}. \end{aligned} \tag{4.40}$$

The renormalized two-loop self-energy function is given by

$$\Sigma_{2R}(p) = \Sigma_2(p) + B_1\Sigma_1(p) - \left(B_2 + B_1^2\right)(\gamma p - 1). \tag{4.41}$$

We use this to find the corresponding renormalized class c decay rate contribution. We are excluding the vacuum polarization contribution from class c, so $B_1 = -L_1$, $B_2 \to -\tilde{L}_2$, and $\Sigma_2(p) \to \Sigma_{CR}(p) + \Sigma_{DR}(p)$. A part of $B_1\Sigma_1(p)$ cancels against the extra term in (4.37). For the renormalized class c decay rate contribution, we find

$$\Gamma_c = -\ln\lambda \left(\frac{\alpha}{\pi}\right) \Gamma_{SE} + \{2\ln^2\lambda + 0.05786(22)\} \left(\frac{\alpha}{\pi}\right)^2 \Gamma_0, \tag{4.42}$$

where Γ_{SE} is given in Table VI.

Class d consists of reducible combinations of one-loop self-energy and vertex corrections. The class d contributions to $\mathcal{M}_2$ are shown in Fig. 17. We worked directly with renormalized one-loop self-energy and vertex parts. For the renormalized one-loop self-energy function we used

$$\Sigma_{1R}(p) = \frac{\alpha}{4\pi}\{4\ln\lambda(\gamma p - 1) + F(\kappa)(\gamma p - 1) + G(\kappa)(\gamma p - 1)^2\}, \tag{4.43}$$

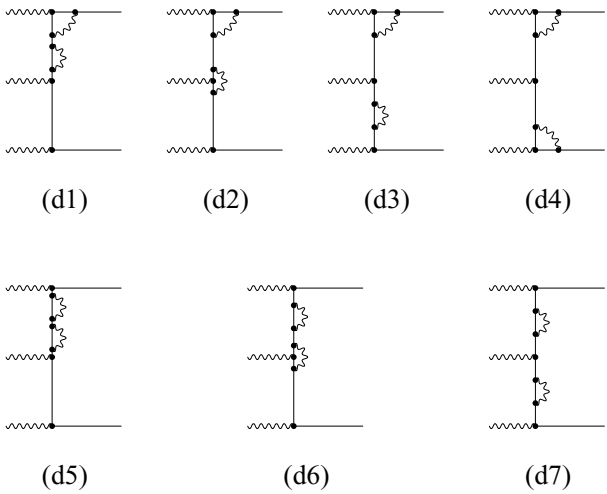

FIG. 17. Contributions of class d to the o-Ps decay amplitude.

where $\kappa = 1 - p^2$ and

$$F(\kappa) = \frac{1}{1-\kappa}\left\{(4-3\kappa) - (4-4\kappa-\kappa^2)\frac{\ln\kappa}{1-\kappa}\right\}, \tag{4.44a}$$

$$G(\kappa) = \frac{1}{1-\kappa}\left\{1 - (2-3\kappa)\frac{\ln\kappa}{1-\kappa}\right\}. \tag{4.44b}$$

The renormalized one-loop vertex function that we used is

$$\Lambda^{\lambda}_{1R}(p', p) = \frac{\alpha}{4\pi}\left\{-4\ln\lambda\gamma^{\lambda} + \int dx\, du[JN^{\lambda} + K\gamma^{\lambda}]\right\}, \tag{4.45}$$

where p' and p are the outgoing and incoming electron momenta, $J = -1/H$, $K = -5-2x\ln(H/x)$, and

$$k = p' - p, \tag{4.46a}$$

$$v = 1 - u, \tag{4.46b}$$

$$H = x - xuvk^2 + (1-x)(u(1-p'^2) + v(1-p^2)), \tag{4.46c}$$

$$Q = -x(up' + vp), \tag{4.46d}$$

$$N^{\lambda} = \gamma^{\mu}(\gamma(p'+Q)+1)\gamma^{\lambda}(\gamma(p+Q)+1)\gamma_{\mu}. \tag{4.46e}$$

The class d results are given in Table IX. Interestingly, all infrared divergences cancel in class d, leaving a finite result. The total class d decay rate contribution is

$$\Gamma_d = \{2.42123(3)\}\left(\frac{\alpha}{\pi}\right)^2\Gamma_0. \tag{4.47}$$

Class e is a set of two-loop irreducible corrections to the lowest-order decay amplitude. The class e contributions to $\mathcal{M}_2$ are shown in Fig. 18. The class e contributions are individually finite in both the infrared and the ultraviolet. They are given in Table X. Graphs (e4) and (e8), which each

TABLE IX

Renormalized Contributions to the Orthopositronium Decay Rate from Class d

Diagram	$\ln^2\lambda(\frac{\alpha}{\pi})^2\Gamma_0$	$\ln\lambda(\frac{\alpha}{\pi})\Gamma_{\rm SE}$	$\ln\lambda(\frac{\alpha}{\pi})\Gamma_{\rm OV}$	$\ln\lambda(\frac{\alpha}{\pi})\Gamma_{\rm IV}$	$\frac{m\alpha^8}{\pi^3}$
d1	4	−1	1	0	0.111780(3)
d2	−4	0	−1	−2	0.1886168(14)
d3	4	−1	1	0	−0.369613(3)
d4	−2	0	−1	0	−0.2037687(15)
d5	−4	2	0	0	0.9480621(4)
d6	4	−1	0	2	−0.9807306(15)
d7	−2	1	0	0	0.7735455(3)
Total	0	0	0	0	0.467892(5)

Note. Class d consists of products of two one-loop vertex or self-energy corrections.

TABLE X

Contributions to the Orthopositronium Decay Rate from Class e

Diagram	$\frac{m\alpha^8}{\pi^3}$
e1	−0.14045(3)
e2	0.44420(4)
e3	0.40711(17)
e4	1.83827(86)
e5	0.91155(17)
e6	−0.36691(13)
e7	−0.82448(5)
e8	−1.25105(145)
e9	0.77100(5)
Total	1.78924(172)

Note. Class e consists of ultraviolet and infrared finite two-loop corrections to the orthopositronium decay rate.

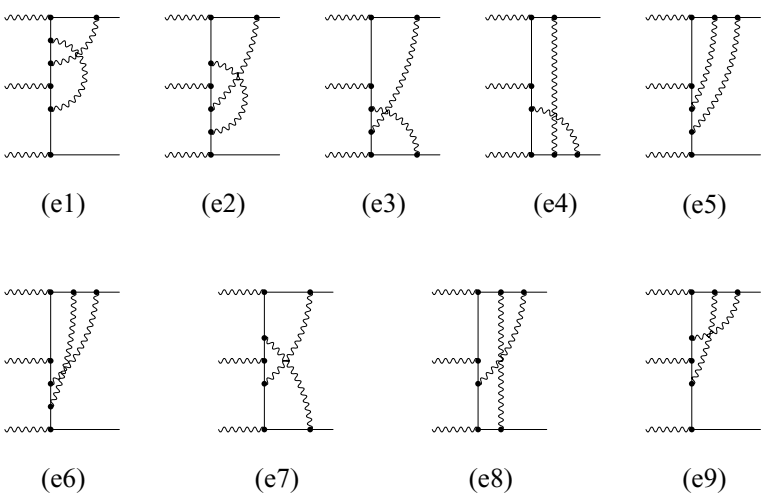

FIG. 18. Contributions of class e to the o-Ps decay amplitude.

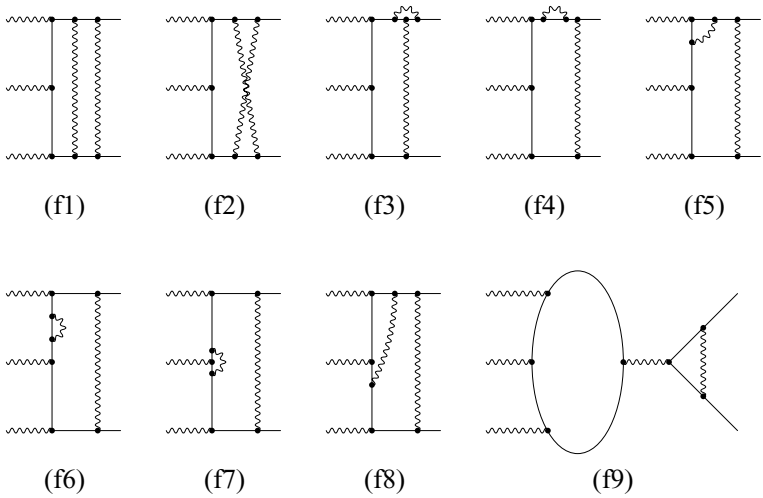

FIG. 19. Contributions of class f to the o-Ps decay amplitude. These ladder graphs contain the leading binding singularities.

contain a ladder photon, were the most difficult to evaluate numerically. The total class e decay rate contribution is

$$\Gamma_e = \{9.2589(90)\}\left(\frac{\alpha}{\pi}\right)^2 \Gamma_0. \tag{4.48}$$

Class f is the set of ladder graphs. The class f contributions to $\mathcal{M}_2$ are shown in Fig. 19. The evaluation of class f is the heart of our calculation, both because the graphs of class f contain the leading binding singularities and because these were by far the most challenging graphs to evaluate.

The double ladder graph (f1) carries the leading $1/\lambda^2$ binding singularity. It is similar in this regard to the double ladder one-photon-annihilation graph of Fig. 7c. However, the decay rate double ladder is finite in the ultraviolet. We use the momentum assignment of (f1) shown in Fig. 8a (except that (f1) has two electron propagators of momenta $q+r_1$ and $q-r_3$ between three decay photons instead of the single annihilation photon of Fig. 8a). The Y factor (see (4.16)) for (f1) is

$$Y_{f1} = \frac{1}{4}\int \frac{d^4q}{i\pi^2}\frac{d^4s}{i\pi^2}\frac{T(q,s)}{Z(q)D(q,s)H(q,s)}, \tag{4.49}$$

where

$$T(q,s) = \frac{1}{4}\mathrm{tr}\big[\gamma^\mu(\gamma(s-n)+1)\gamma^\nu(\gamma(q-n)+1)\gamma^{\mu_3}(\gamma(q-r_3)+1)\gamma^{\mu_2}(\gamma(q+r_1)+1)\gamma^{\mu_1}$$
$$\times(\gamma(q+n)+1)\gamma_\nu(\gamma(s+n)+1)\gamma_\mu(1+\gamma^0)\gamma^\beta\big], \tag{4.50a}$$
$$Z(q) = (-(q-r_3)^2+1)(-(q+r_1)^2+1), \tag{4.50b}$$
$$D(q,s) = -(q-s)^2+\lambda^2, \tag{4.50c}$$
$$H(q,s) = (-q^2+2qn)(-q^2-2qn)(-s^2+2sn)(-s^2-2sn)(-s^2+\lambda^2). \tag{4.50d}$$

As in (3.21), we find it useful to break Y_{f1} up into several parts. Our decomposition is

$$\frac{T(q,s)}{Z(q)D(q,s)} = \frac{T(0,0)}{Z(0)D(q,s)} + \left(\frac{T(q,0)}{Z(q)} - \frac{T(0,0)}{Z(0)}\right)\frac{1}{D(q,0)} + \left(\frac{T(q,0)}{Z(q)} - \frac{T(0,0)}{Z(0)}\right) \times \left(\frac{1}{D(q,s)} - \frac{1}{D(q,0)}\right) + \frac{T_{02}}{Z(q)D(q,s)} + \frac{T_{11}}{Z(q)D(q,s)} + \frac{T_{b3}}{Z(q)D(q,s)}, \quad (4.51)$$

where T_{nm} is the term in $T(q,s)$ containing n powers of q and m powers of s. We note that $T_{01} = 0$ and define

$$T_{b3} = T(q,s) - T(q,0) - T_{11} - T_{02}. \quad (4.52)$$

We label the terms in (4.51) as $a0$, $a1$, $a2$, $b1$, $b2$, $b3$. Their evaluation proceeded much as for the one-photon-annihilation double ladder graph. With the definition

$$\Gamma_{fi} = K_{fi}\frac{m\alpha^8}{\pi^3}, \quad (4.53)$$

we found that

$$K_{f1}^{a1} = K_L(\lambda)I_B(\lambda), \quad (4.54a)$$

$$K_{f1}^{a2} = 4.584(46), \quad (4.54b)$$

$$K_{f1}^{b1} = -\frac{\pi^2}{3}\ln\lambda\gamma_0 - 1.1405(19), \quad (4.54c)$$

$$K_{f1}^{b2} = -\frac{4\pi^2}{3}\ln\lambda\gamma_0 - 7.575(10), \quad (4.54d)$$

$$K_{f1}^{b3} = -0.14855(11), \quad (4.54e)$$

where $\gamma_0 = (2/9)(\pi^2 - 9)$, and $K_L(\lambda)$ and $I_B(\lambda)$ were defined in (4.24b) and (3.10). We reserve K_{f1}^{a0} to be combined with the corresponding term from the crossed ladder graph (f2). The total result for the double ladder graph (f1) is

$$K_{f1} = K_{f1}^{a0} + K_L(\lambda)I_B(\lambda) - \frac{5\pi^2}{3}\ln\lambda\gamma_0 - 4.280(48). \quad (4.55)$$

We next consider the crossed ladder graph (f2). The Y factor for this graph is

$$Y_{f2} = \frac{1}{4}\int\frac{d^4q}{i\pi^2}\frac{d^4s}{i\pi^2}\frac{T(q,s)}{Z(q)R(q,s)}, \quad (4.56)$$

where

$$T(q,s) = \frac{1}{4}\mathrm{tr}\big[\gamma^\mu(\gamma(q-s-n)+1)\gamma^\nu(\gamma(q-n)+1)\gamma^{\mu_3}(\gamma(q-r_3)+1)\gamma^{\mu_2}(\gamma(q+r_1)+1)\gamma^{\mu_1} \times(\gamma(q+n)+1)\gamma_\mu(\gamma(s+n)+1)\gamma_\nu(1+\gamma^0)\gamma^\beta\big], \quad (4.57a)$$

$$Z(q) = (-(q-r_3)^2+1)(-(q+r_1)^2+1), \quad (4.57b)$$

$$R(q,s) = (-(q+n)^2+1)(-(q-n)^2+1)(-(q-s-n)^2+1)(-(s+n)^2+1) \times (-(q-s)^2+\lambda^2)(-s^2+\lambda^2), \tag{4.57c}$$

where we have used the momentum assignments of Fig. 8b. Again we find it useful to break Y_{f2} up into several parts:

$$\frac{T(q,s)}{Z(q)} = \frac{T(0,0)}{Z(0)} + T(0,0)\left(\frac{1}{Z(q)} - \frac{1}{Z(0)}\right) + \frac{T_{01}}{Z(q)} + \frac{T_{10}}{Z(q)} + \frac{T_{b3}}{Z(q)}, \tag{4.58}$$

where

$$T_{b3} = T(q,s) - T_{00} - T_{01} - T_{10}. \tag{4.59}$$

The first term, K_{f2}^{a0}, is of $O(1/\lambda)$. We reserve it to be evaluated together with K_{f1}^{a0}. The term containing T_{01} has a logarithmic divergence, while the other three terms are finite. Our final result for the crossed ladder graph (f2) is

$$K_{f2} = K_{f2}^{a0} + \pi^2 \ln\lambda\gamma_0 + 0.7891(51). \tag{4.60}$$

The vertex and self-energy corrected ladder graphs f3 and f4 were considered together. Just as for the SV and SE one-photon-annihilation graphs, f3 and f4 contain the gauge invariant vertex and self-energy combination shown in Fig. 9. As before, we use Yennie gauge forms [86, 87] for the one-loop vertex and self-energy parts. Our results for these graphs are shown in Table XI.

The remaining class f graphs, f5–f9, are one-loop decay graphs with a ladder photon attached. These graphs have binding singularities of the form $1/\lambda$ times the one-loop decay rate contributions Γ_{SE}, Γ_{OV}, Γ_{IV}, Γ_{DV}, and Γ_A. Also, since the renormalized self-energy and vertex parts contain a factor of $\ln\lambda$, graphs f5, f6, and f7 have contributions proportional to $\ln\lambda K_L(\lambda)$. The results for these graphs are listed in Table XI.

The total class f contribution is the sum of the bottom row of Table XI and the set-aside terms

$$K_f^{a0} = K_{f1}^{a0} + K_{f2}^{a0} = 2\gamma_0 I^{a0}, \tag{4.61}$$

TABLE XI

Contributions to the Orthopositronium Decay Rate from Class f

Diagram	$K_L(\lambda)I_B(\lambda)\frac{m\alpha^8}{\pi^3}$	$(\frac{\alpha}{\pi})I_B(\lambda)$	$\ln\lambda K_L(\lambda)\frac{m\alpha^8}{\pi^3}$	$\ln\lambda\alpha^2\Gamma_0$	$\frac{\pi}{\lambda}(\frac{\alpha}{\pi})\Gamma_A$	$\frac{m\alpha^8}{\pi^3}$
f1-f1a0	1	0	0	$-\frac{5}{3}$	0	−4.280(48)
f2-f2a0	0	0	0	1	0	0.7891(51)
f3	0	0	0	0	0	−1.33550(25)
f4	0	0	0	0	0	0.206361(10)
f5	0	Γ_{OV}	−2	0	0	1.11088(51)
f6	0	Γ_{SE}	2	0	0	−3.80262(45)
f7	0	Γ_{IV}	−1	0	0	1.57005(10)
f8	0	Γ_{DV}	0	0	0	1.26019(74)
f9	0	0	0	0	1	0.314626
Total	1	$\Gamma_{SE+OV+IV+DV}$	−1	$-\frac{2}{3}$	1	−4.167(49)

Note. Class f contains the ladder graphs.

where I^{a0} was defined in (3.37). The factor of 2 appears because K_f^{a0} represents a contribution to the absolute square of $\mathcal{M}_0 + \mathcal{M}_2$, while I^{a0} represents an amplitude. The total class f decay rate contribution is

$$\Gamma_f = 2\ln 2\,\frac{\alpha^2}{\lambda^2}\,\Gamma_0 + \frac{\alpha^2}{\pi\lambda}A(\lambda)\Gamma_0 + \ln^2\lambda\left(\frac{\alpha}{\pi}\right)^2\Gamma_0 + \ln\lambda\left(\frac{\alpha}{\pi}\right)\{\Gamma_{SE} + \Gamma_{OV} + \Gamma_{IV} + \Gamma_{DV}\}$$
$$-\frac{2}{3}\ln\lambda\alpha^2\Gamma_0 - 20.50(26)\left(\frac{\alpha}{\pi}\right)^2\Gamma_0. \tag{4.62}$$

In evaluating Γ_f we found the following one-loop formula useful:

$$\Gamma_{SE} + \Gamma_{OV} + \Gamma_{IV} + \Gamma_{DV} + \Gamma_A + 2\left(I_B(\lambda) - \frac{\pi}{\lambda}\right)\frac{\alpha}{\pi}\Gamma_0 + \frac{K_L(\lambda)}{\gamma_0}\frac{\alpha}{\pi}\Gamma_0 = A(\lambda)\frac{\alpha}{\pi}\Gamma_0. \tag{4.63}$$

The infrared finite term in Γ_f was obtained from

$$-\frac{\alpha}{\pi}\left\{\Gamma_{SE} + \Gamma_{OV} + \Gamma_{IV} + \Gamma_{DV} + \frac{K_L(\lambda)}{\gamma_0}\frac{\alpha}{\pi}\Gamma_0 + 2\ln\lambda\frac{\alpha}{\pi}\Gamma_0\right\}$$
$$+\left\{2A_0 - \frac{4.167(49)}{\gamma_0}\right\}\left(\frac{\alpha}{\pi}\right)^2\Gamma_0 = -20.50(26)\left(\frac{\alpha}{\pi}\right)^2\Gamma_0. \tag{4.64}$$

Class g consists of the self-energy and vertex corrections to the double ladder graph. The class g contributions to $\mathcal{M}_2$ are shown in Fig. 20. The one-loop Feynman gauge self-energy and vertex functions were taken from [85]. Individual class g contributions are given in Table XII. The total class g decay rate contribution is

$$\Gamma_g = -\ln\lambda\left(\frac{\alpha}{\pi}\right)\Gamma_{DV} - 1.37177(49)\left(\frac{\alpha}{\pi}\right)^2\Gamma_0. \tag{4.65}$$

Class h, represented by the graphs of Fig. 21, involves radiative corrections to the annihilation graph. These graphs were evaluated earlier by Adkins and Lymberopoulos [62, 63] using the physical

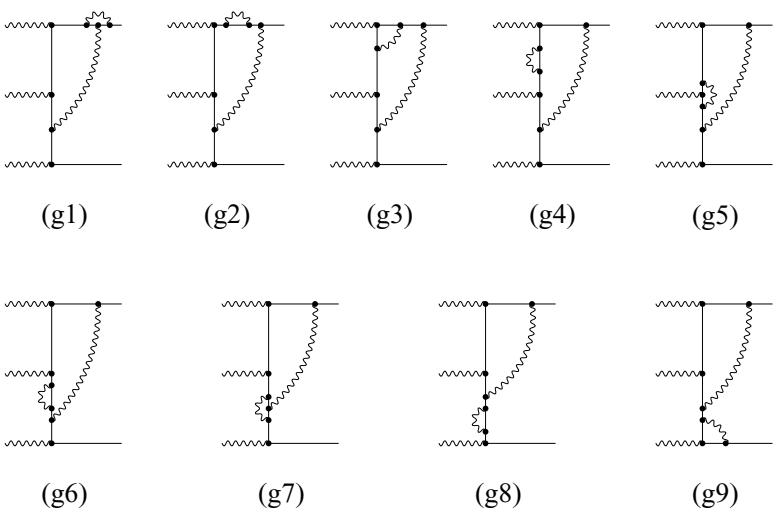

FIG. 20. Contributions of class g to the o-Ps decay amplitude.

TABLE XII

Renormalized Contributions to the Orthopositronium Decay Rate from Class g

Diagram	$\ln\lambda(\frac{\alpha}{\pi})\Gamma_{\rm DV}$	$\frac{m\alpha^8}{\pi^3}$
g1	−1	0.715025(31)
g2	1	−0.332861(44)
g3	−1	0.574056(25)
g4	1	−1.414356(56)
g5	−1	0.535009(24)
g6	1	−0.688125(31)
g7	−1	0.456777(16)
g8	1	−0.549467(11)
g9	−1	0.438853(5)
Total	−1	−0.265089(93)

Note. Class g consists of double-vertex graphs with a one-loop radiative correction.

binding of the positronium atom instead of a photon mass as an infrared regulator. The contribution of the only infrared sensitive graph, h6, with that regulator is

$$\Gamma_{h6} = \ln\alpha\alpha^2\Gamma_0 + \left\{2\Omega^{2\epsilon}\Gamma(2\epsilon)I + 1.295719(102)\right\}\frac{m\alpha^8}{\pi^3}, \tag{4.66}$$

where $I = \zeta(2)/3 - 31/48$. The only effect of the change of infrared regulator is to change $\ln\alpha$ to $\ln\lambda$. Results for the individual class h contributions are shown in Table XIII. The total class h decay rate contribution is

$$\Gamma_h = \ln\lambda\alpha^2\Gamma_0 + 9.00739(88)\left(\frac{\alpha}{\pi}\right)^2\Gamma_0. \tag{4.67}$$

Class i (see Fig. 22) contains all vacuum polarization effects. These infrared finite contributions were evaluated earlier by Burichenko and Ivanov [60] and by Adkins and Shiferaw [61]. Results for

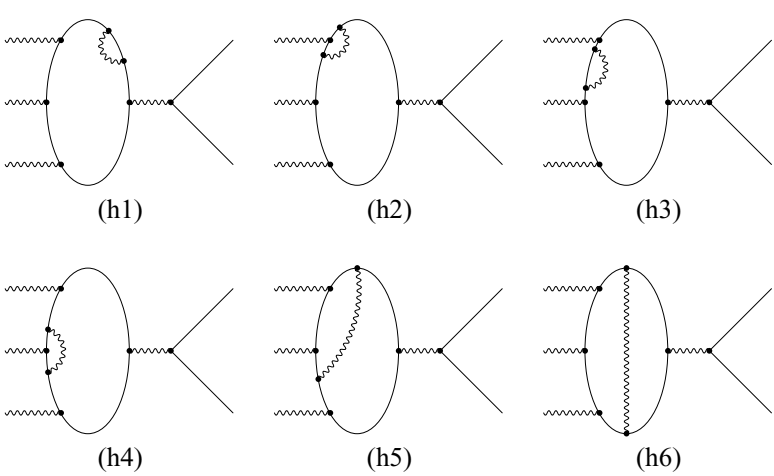

FIG. 21. Contributions of class h to the o-Ps decay amplitude.

TABLE XIII

Renormalized Contributions to the Orthopositronium Decay Rate from Class h

Diagram	$\Omega^{2\epsilon}\Gamma(2\epsilon)I\,\frac{m\alpha^8}{\pi^3}$	$\ln\lambda\alpha^2\Gamma_0$	$\frac{m\alpha^8}{\pi^3}$
h1	−1	0	0.080289(003)
h2	4	0	−1.047442(072)
h3	−1	0	0.233046(006)
h4	2	0	−0.417101(040)
h5	−6	0	1.596125(108)
h6	2	1	1.295719(102)
Total	0	1	1.740636(170)

Note. Class h consists of radiative corrections to the one-loop annihilation diagram. The I factor in the ultraviolet divergent part is $I = \zeta(2)/3 - 31/48$.

the individual class i graphs are shown in Table XIV. The total class i decay rate contribution is

$$\Gamma_i = 0.96496\left(\frac{\alpha}{\pi}\right)^2\Gamma_0. \tag{4.68}$$

Class j consists of graphs represented by the square of the one-loop amplitude $|\mathcal{M}_1|^2$. They have the form of the graph in Fig. 2 but with one of the six contributions to $\mathcal{M}_1$ (see Fig. 3) on each side. There are 21 independent graphs of this type. The class j contribution has been evaluated earlier by Burichenko [57] and by Adkins [56], who worked out expressions for the amplitudes $\mathcal{M}_1$ (all six contributions at once) and formed $|\mathcal{M}_1|^2$ directly. The one-rung ladder contributions to $\mathcal{M}_1$ lead to binding singularities. The class j contribution to the decay rate is

$$\Gamma_j = \frac{\alpha^2}{\lambda^2}\Gamma_0 + \frac{\alpha^2}{\pi\lambda}A(\lambda)\Gamma_0 + 28.860(2)\left(\frac{\alpha}{\pi}\right)^2\Gamma_0. \tag{4.69}$$

Class k consists of graphs containing a final-state light-by-light scattering process. These graphs are depicted in Fig. 23. The contribution of class k was evaluated recently by Adkins *et al*. [64]. Results for the four independent class k graphs are given in Table XV. The total class k decay rate

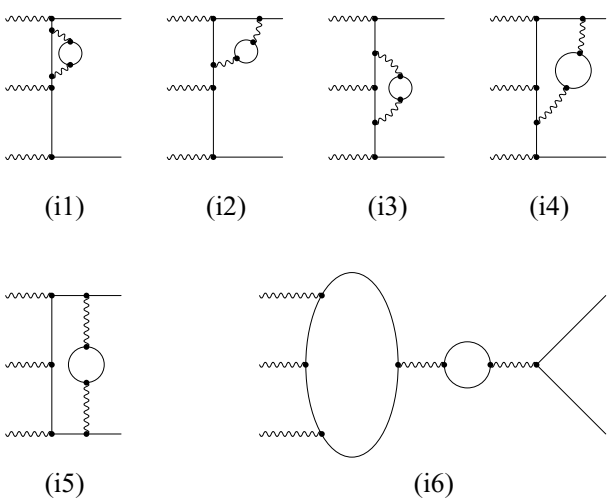

FIG. 22. Contributions of class i to the o-Ps decay amplitude.

TABLE XIV

Renormalized Contributions to the Orthopositronium Decay Rate from Class i

Diagram	Description	$\frac{m\alpha^8}{\pi^3}$
i1	Self-energy	−0.017385
i2	Outer vertex	0.040781
i3	Inner vertex	0.012167
i4	Double vertex	−0.018297
i5	Ladder	0.029375
i6	Annihilation	0.139834
Total		0.186475

Note. Class i consists of the vacuum polarization corrected one-loop diagrams. The uncertainties are everywhere smaller that one in the least significant digit.

TABLE XV

Contributions to the Orthopositronium Decay Rate from Class k

Diagram	$\frac{m\alpha^8}{\pi^3}$
k1a	0.47344(22)
k2	−0.88648(20)
k3a	−0.19198(33)
k4	0.39124(34)
Total	0.06768(69)

Note. Class k consists of the graphs involving light-by-light scattering on two of the final state photons. The results for graphs k1a and k3a must be counted twice in the total.

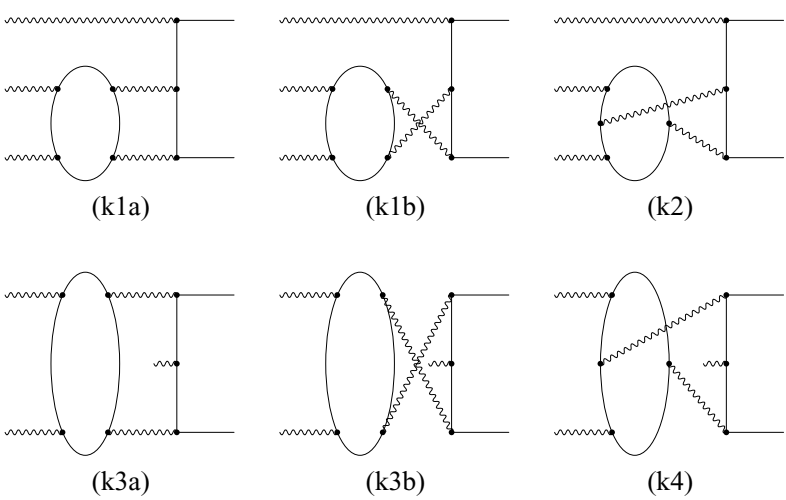

FIG. 23. Class k light-by-light scattering contributions to the o-Ps decay amplitude. Charge conjugation symmetry can be used to show that the contributions of graphs (k1a) and (k1b) are equal, as are those of (k3a) and (k3b). Additional graphs containing permutations of the final-state photons must also be included.

TABLE XVI

Two-Loop QED Contributions to the Orthopositronium Decay Rate by Class

Class	$\frac{\alpha^2}{\lambda^2}\Gamma_0$	$\frac{\alpha^2}{\pi\lambda}\Gamma_0$	$\ln\lambda\frac{\alpha}{\pi}$	$(\frac{\alpha}{\pi})^2\ln^2\lambda\Gamma_0$	$\alpha^2\ln\lambda\Gamma_0$	$(\frac{\alpha}{\pi})^2\Gamma_0$
a	0	0	$-\Gamma_{\rm OV}$	-2	0	-5.618
b	0	0	$-\Gamma_{\rm IV}$	-1	0	-0.705
c	0	0	$-\Gamma_{\rm SE}$	2	0	0.058
d	0	0	0	0	0	2.421
e	0	0	0	0	0	9.259(9)
f	$2\ln 2$	$A(\lambda)$	$\Gamma_{\rm SE+OV+IV+DV}$	1	$-2/3$	$-20.50(26)$
g	0	0	$-\Gamma_{\rm DV}$	0	0	-1.372
h	0	0	0	0	1	9.007
i	0	0	0	0	0	0.965
j	1	$A(\lambda)$	0	0	0	28.860(2)
k	0	0	0	0	0	0.350(4)
Total	$2\ln 2+1$	$2A(\lambda)$	0	0	1/3	22.73(26)

contribution is

$$\Gamma_k = 0.350(4)\left(\frac{\alpha}{\pi}\right)^2\Gamma_0. \tag{4.70}$$

This concludes our calculation of the o-Ps decay rate contributions through two-loop order. The zero-loop result is just the Ore and Powell rate of Eq. (1.3). The one-loop result was given in Eq. (4.26). The two-loop results are listed by class and summed in Table XVI. The QED decay rate results are

$$\Gamma_0^{QED} = \Gamma_0, \tag{4.71a}$$

$$\Gamma_1^{QED} = \left\{\frac{2\pi}{\lambda} + A(\lambda)\right\}\left(\frac{\alpha}{\pi}\right)\Gamma_0, \tag{4.71b}$$

$$\Gamma_2^{QED} = \left\{(2\ln 2+1)\frac{\pi^2}{\lambda^2} + 2A(\lambda)\frac{\pi}{\lambda} + \frac{\pi^2}{3}\ln\lambda + B_2\right\}\left(\frac{\alpha}{\pi}\right)^2\Gamma_0, \tag{4.71c}$$

where

$$B_2 = 22.73(26). \tag{4.72}$$

C. Calculation of the Scattering Amplitude Via NRQED

The calculation of the imaginary part of the $e^-e^+ \to e^-e^+$ scattering amplitude via NRQED is virtually identical to the calculation of the one-photon-annihilation amplitude done before (in Section III C). The only difference is that the requirement that there be at least one one-photon intermediate state is replaced by the requirement that there be a three-photon intermediate state and also that we compute the imaginary part of the amplitude instead of the real part.

The zero-loop NRQED graphs are shown in Fig. 11. As before, the results for these graphs are given in Eqs. (3.52). The zero-loop rate is (see (4.1), (3.54), and (2.10))

$$\Gamma_0^{\rm NRQED} = -2|\phi_0|^2{\rm Im}\left(i\,B_0^{\rm NRQED}\right) = e_C\,\Gamma_0, \tag{4.73}$$

where e_C is proportional to the imaginary part of d_C.

The one-loop NRQED graphs are shown in Fig. 12. Their contributions to Γ can be transcribed from (3.56) using the replacements $B_0 \to \Gamma_0$ and $d_C \to e_C$. Also, the graph of Fig. 12d picks up a factor of $X/16$ (where $X = (19\pi^2 - 132)/(\pi^2 - 9)$) because of the relation $\mathrm{Im}(d_D) = (X/16)\mathrm{Im}(d_C) + O(\alpha^3)$ between the imaginary parts of the four-fermion contact and derivative couplings. Finally, the graph of Fig. 12e picks up a factor of 2 because either one of the four-fermion vertices can contribute to the imaginary part. The total one-loop NRQED decay rate contribution is

$$\Gamma_1^{\mathrm{NRQED}} = \left\{ \frac{2\pi}{\lambda} e_C + \left(-\frac{8}{3} - \frac{X}{6} \right) \Lambda + \left(\frac{7}{12} + \frac{X}{12} \right) \pi\lambda \right\} \left(\frac{\alpha}{\pi} \right) \Gamma_0 . \tag{4.74}$$

The two-loop NRQED graphs are shown in Fig. 13. Their contribution to Γ can be obtained from (3.59) using the same replacements as before. Here, the graphs of Figs. 14i and 14j pick up additional factors of $X/16$, and the graphs of Figs. 14k and 14l pick up additional factors of 2. The total two-loop NRQED decay rate contribution is

$$\begin{aligned} \Gamma_2^{\mathrm{NRQED}} = \Bigg\{ & (2\ln 2 + 1) \frac{\pi^2}{\lambda^2} + \left(-\frac{16}{3} - \frac{X}{3} \right) \pi \frac{\Lambda}{\lambda} - \frac{\pi^2}{3} \ln\left(\frac{\Lambda}{\lambda} \right) \\ & + \frac{2\pi^2}{3} \ln 2 + \left(-\frac{2}{3} + \frac{5X}{24} \right) \pi^2 \Bigg\} \left(\frac{\alpha}{\pi} \right)^2 \Gamma_0 . \end{aligned} \tag{4.75}$$

D. The Matching Calculation

The matching calculation is used to find the $O(\alpha)$ and $O(\alpha^2)$ parts of $\mathrm{Im}(d_C)$, or equivalently, of e_C, by comparing the imaginary parts of the $e^- e^+ \to e^- e^+$ scattering amplitude in QED and in NRQED. The matching condition, through two-loop order, after dividing by Γ_0, has the form

$$\begin{aligned} & 1 + \left\{ \frac{2\pi}{\lambda} + A(\lambda) \right\} \left(\frac{\alpha}{\pi} \right) + \left\{ (2\ln 2 + 1) \frac{\pi^2}{\lambda^2} + 2A(\lambda) \frac{\pi}{\lambda} + \frac{\pi^2}{3} \ln\lambda + B_2 \right\} \left(\frac{\alpha}{\pi} \right)^2 \\ & = \left[1 + \left(\frac{\alpha}{\pi} \right) e_C^{(1)} + \left(\frac{\alpha}{\pi} \right)^2 e_C^{(2)} \right] + \left\{ \frac{2\pi}{\lambda} \left[1 + \left(\frac{\alpha}{\pi} \right) e_C^{(1)} \right] + \left(-\frac{8}{3} - \frac{X}{6} \right) \Lambda + \left(\frac{7}{12} + \frac{X}{12} \right) \pi\lambda \right\} \\ & \quad \times \left(\frac{\alpha}{\pi} \right) + \Bigg\{ (2\ln 2 + 1) \frac{\pi^2}{\lambda^2} + \left(-\frac{16}{3} - \frac{X}{3} \right) \pi \frac{\Lambda}{\lambda} - \frac{\pi^2}{3} \ln\left(\frac{\Lambda}{\lambda} \right) \\ & \quad + \frac{2\pi^2}{3} \ln 2 + \left(-\frac{2}{3} + \frac{5X}{24} \right) \pi^2 \Bigg\} \left(\frac{\alpha}{\pi} \right)^2 . \end{aligned} \tag{4.76}$$

The matching condition at $O(\alpha^0)$ is trivial because it was built into the definition of e_C. The matching condition at $O(\alpha)$ leads to

$$e_C^{(1)} = \left(\frac{8}{3} + \frac{X}{6} \right) \Lambda + A(\lambda) - \left(\frac{7}{12} + \frac{X}{12} \right) \pi\lambda . \tag{4.77}$$

We retain the term of $O(\lambda)$ since it will make a finite contribution to $e_C^{(2)}$. Finally, the matching condition at $O(\alpha^2)$ yields

$$e_C^{(2)} = \frac{\pi^2}{3} \ln\Lambda - \frac{\pi^2 X}{24} + \frac{11\pi^2}{6} - \frac{2\pi^2}{3} \ln 2 + B_2 . \tag{4.78}$$

E. Bound State Perturbation Theory

We use NRQED bound state perturbation theory to calculate the decay rate much as we used it before to obtain the one-photon-annihilation contribution to the energy shift. Here, though, we need to find the imaginary part of the energy shift and get the decay rate through $\Gamma = -2\mathrm{Im}(\Delta E)$. The same five graphs of Fig. 15 used before contribute to the imaginary part of the energy shift and so to the decay rate. The imaginary parts arise because of the imaginary parts in V_4 and V_{4der}.

The graphs of Fig. 15 make the same contributions as before (see Eq. (3.80)), but with the replacements $\Delta E_0 \to \Gamma_0$ and $d_C \to e_C$. Also, the graph of Fig. 15b is multiplied by $X/16$, and the graphs of Fig. 15c pick up a factor of 2. The result for the decay rate is

$$\Gamma = \left\{\left[1 + \left(\frac{\alpha}{\pi}\right)e_C^{(1)} + \left(\frac{\alpha}{\pi}\right)^2 e_C^{(2)}\right] + \left(-\frac{8}{3} - \frac{X}{6}\right)\left(\frac{\alpha}{\pi}\right)\Lambda + \left(-\frac{1}{3}\ln\left(\frac{\Lambda}{\alpha}\right) - \frac{11}{24} + \frac{X}{16}\right)\alpha^2\right\}\Gamma_0. \tag{4.79}$$

F. Result for the Decay Rate

Our result for the decay rate is obtained from (4.79) by use of the $\lambda \to 0$ limits of (4.77) and (4.78). We find that

$$\Gamma = \left\{1 + A(0)\left(\frac{\alpha}{\pi}\right) + \frac{\alpha^2}{3}\ln\alpha + B_{3\gamma}\left(\frac{\alpha}{\pi}\right)^2 + \cdots\right\}\Gamma_0, \tag{4.80}$$

where the three-photon final state part of B is

$$B_{3\gamma} = \left(\frac{11}{8} - \frac{2}{3}\ln 2 + \frac{X}{48}\right)\pi^2 + B_2 = 44.87(26). \tag{4.81}$$

As mentioned before, the partial rate for decay to a five-photon final state is $B_{5\gamma} = 0.187(11)$ [58, 59], so the total $O(\alpha^2)$ coefficient is

$$B = B_{3\gamma} + B_{5\gamma} = 45.06(26). \tag{4.82}$$

Our result for the part of the NRQED contribution to $B_{3\gamma}$ not due to the derivative term (that is, the part independent of X) is $\frac{11}{8} - \frac{2}{3}\ln 2 = 0.9129$. The corresponding result of Labelle *et al.* [73] was 1.16, the numerical value of $\frac{13}{8} - \frac{2}{3}\ln 2$. An additional contribution of $-\frac{1}{4}$ to this number was recently found by Labelle [99], removing the discrepancy. Also, Hill and Lepage, in the course of their calculation of the $O(\alpha^3 \ln\alpha)$ correction, obtained 0.913 for this part of the $O(\alpha^2)$ term [66]. All three NRQED calculations are in agreement.

We are in a position now to shed some light on a minor controversy concerning the effect on the decay rate of p^2/m^2 terms coming from momentum expansions. In our language, the momentum expansion terms are contained in V_{4der} and are proportional to $X = (19\pi^2 - 132)/(\pi^2 - 9)$. As noted by Khriplovich and Milstein [100, 101], the prescription

$$\left(\frac{p}{m}\right)^2 \to -\frac{\alpha^2}{4} \tag{4.83}$$

leads directly from $\Gamma_X = -2\mathrm{Im}(\Delta E_X) = -2|\phi_0|^2\mathrm{Im}(V_{4der})$ to

$$\Gamma_X = \frac{X}{48}\alpha^2\Gamma_0. \tag{4.84}$$

This is the correct contribution of V_{4der} to Γ, obtained first by Labelle *et al*. [73] and verified here. The prescription of (4.83) was also justified in the calculation of the parapositronium decay rate by Czarnecki *et al*. [75, 76] using dimensionally regularized NRQED. However, Khriplovich and Milstein apparently take the arrow in (4.83) to signify integration over the wave function $8\pi\gamma/D_\gamma^2(\mathbf{p})$ with an appropriate regularization for the ultraviolet divergence. They derive (most clearly in [101]) their prescription of

$$\left(\frac{p}{m}\right)^2 \to -\frac{3}{4}\alpha^2 \tag{4.85}$$

by evaluating the integral

$$\int \frac{d^3p}{(2\pi)^3} 8\pi\gamma \left[\frac{1}{D_\gamma^2(\mathbf{p})} - \frac{1}{p^4}\right]\left(\frac{p^2}{m^2}\right) = -\frac{3}{4}\alpha^2 \tag{4.86}$$

and arguing that the regulating term proportional to $1/p^4$ can be interpreted as merely a contribution to the known $O(\alpha)$ correction to the rate. In our calculation the contribution of V_{4der} to Γ in bound state perturbation theory (see Fig. 15b, (3.80b), and the discussion in Section IV E) is

$$\Gamma_b = \left(-\frac{8\alpha}{3\pi}\Lambda + \alpha^2\right)\frac{X}{16}\Gamma_0. \tag{4.87}$$

This was obtained by use of

$$\int^\Lambda \frac{d^3p}{(2\pi)^3}\frac{8\pi\gamma}{D_\gamma^2(\mathbf{p})}\left(\frac{p^2}{m^2}\right) = -\frac{3}{4}\alpha^2 + 2\frac{\alpha}{\pi}\frac{\Lambda}{m} \tag{4.88}$$

(see the work leading up to (3.80b). Our integral (4.88) is completely consistent with (4.86) of Khriplovich and Milstein. The difference arises because in NRQED a potential such as V_{4der} not only contributes to the decay rate directly (through the evaluation of a graph like Fig. 15b), but also indirectly through multiloop graphs (like those of Figs. 12d, 13i, and 13j) which appear in the matching procedure and affect the value of e_C. Khriplovich and Milstein did not take into account the modification that an additional p^2/m^2 potential would make to the coefficient of the momentum-independent contact potential.

Finally, we offer some thoughts on why we believe our result is correct. Our approach is based on a particular implementation of NRQED. Since its formulation in 1986 [70], NRQED and its cousin NRQCD have been used for numerous successful calculations. There is no indication that NRQED is conceptually ill-founded. We base our argument for the validity of our particular formulation of NRQED on the success of the closely related one-photon-annihilation hyperfine structure calculation. The hyperfine structure and decay rate calculations are very similar, involving in the one case the decay of a spin-1 positronium state to a single virtual photon and in the other the decay of a spin-1 positronium state to three real photons. Calculationally the two processes are completely analogous, and the NRQED parts are virtually identical. The correctness of our NRQED calculation of the hyperfine splitting is confirmed by our agreement with a calculation based on a different implementation of NRQED [78, 81] and most significantly with our agreement with the totally different Coulomb gauge Bethe–Salpeter based calculation [80] of the same correction. The NRQED part of our decay rate calculation has been confirmed through the agreement of our results with those of Labelle *et al*. [73] (as corrected) and of Hill and Lepage [66]. Our main contribution is the evaluation of the two-loop QED scattering amplitude. This was an involved and difficult piece

of work, with many opportunities for error. However, there are also numerous internal consistency conditions that were satisfied in order to achieve the cancellation of ultraviolet divergences as required by renormalization and to obtain the exact infrared structure required by NRQED. Each graph that we calculated was done independently by at least two of us. Also, some classes of graphs (i, j, and k) have been confirmed by other workers. We also mention that we saw no sign of large internal cancellations that might lead to an unusually large B coefficient in case we did make some error. In all, we believe that our results are as trustworthy as can be pending an independent check.

V. CONCLUSION

Our final result for the o-Ps decay rate is

$$\Gamma = \left\{1 + A\frac{\alpha}{\pi} + \frac{\alpha^2}{3}\ln\alpha + B\left(\frac{\alpha}{\pi}\right)^2 - \frac{3\alpha^3}{2\pi}\ln^2\alpha + C\frac{\alpha^3}{\pi}\ln\alpha + D\left(\frac{\alpha}{\pi}\right)^3 + \cdots\right\}\Gamma_0, \qquad (5.1)$$

where $A = -10.286606(10)$, $B = 45.06(26)$, and $C = A/3 - 229/30 + 8\ln 2$. Numerical values for the various contributions to the decay rate are shown in Table XVII. In looking at this table, one should keep in mind the approximate value of the current experimental uncertainty for this rate, which is $\approx 0.002\ \mu s^{-1}$. It seems clear that the perturbation series is behaving nicely, and that higher-order terms are indeed small. For example, the ratios of the $O(\alpha)$ to $O(1)$ terms and the $O(\alpha^2)$ to $O(\alpha)$ terms are

$$|A/1|\frac{\alpha}{\pi} = 0.024 \qquad (5.2)$$

$$|B/A|\frac{\alpha}{\pi} = 0.010. \qquad (5.3)$$

Now if the unknown D contribution followed roughly the same pattern, and $|D/B|\alpha/\pi = 0.010$, then one would have $D = 194$ and its contribution would be $D(\alpha/\pi)^3\Gamma_0 = 0.000018\ \mu s^{-1}$. If D

TABLE XVII

Numerical Values of Contributions to the Orthopositronium Decay Rate

Term	Contribution (in μs^{-1})
1	7.211167
$A\frac{\alpha}{\pi}$	−0.172303
$\frac{\alpha^2}{3}\ln\alpha$	−0.000630
$B\left(\frac{\alpha}{\pi}\right)^2$	0.001753(11)
$\frac{-3\alpha^3}{2\pi}\ln^2\alpha$	−0.000032
$C\frac{\alpha^3}{\pi}\ln\alpha$	0.000024
$D\left(\frac{\alpha}{\pi}\right)^3$	0.00000009D
Total	7.039979(11) + 0.00000009D

TABLE XVIII

Recent Experimental Results for the Orthopositronium Decay Rate

Medium	Place	Year	Result (in μs^{-1})	Δ	Reference
Gas	Michigan	1989	7.0514(14)	$8.1\,\sigma$	[32, 33]
Vacuum	Michigan	1990	7.0482(16)	$5.1\,\sigma$	[34]
Powder	Tokyo	1995	7.0398(29)	$-0.1\,\sigma$	[35]
Powder	Tokyo	2000	7.0399(26)	$0.0\,\sigma$	[36]

Note. The quantity Δ is the difference between the experimental and theoretical values for the rate in terms of the experimental uncertainty σ.

were 10 times this large, its contribution would still be much smaller than the present experimental uncertainty. A great many graphs contribute pure $O(\alpha^3)$ corrections, and some will be quite difficult to evaluate. Fortunately, the calculation of D is not called for at this time. Our final theoretical value, neglecting the unknown pure $O(\alpha^3)$ correction, is

$$\Gamma = 7.039\,979(11)\,\mu s^{-1}. \tag{5.4}$$

The four most recent and most precise experimental results for the o-Ps decay rate are shown in Table XVIII. The Michigan gas and vacuum results are in significant disagreement with theory, while the Tokyo powder values do not contradict the theoretical result. A recent development is an analysis of a Ps thermalization systematic in the Michigan gas experiment. The preliminary correction due to this effect brings the Michigan gas value down by approximately 3σ [102, 103]. The new value of about 7.047 μs^{-1} is in better agreement with the Michigan vacuum result, but is still well above theory.

In conclusion, with the calculation of the two-loop correction term B and the $O(\alpha^3 \ln^2 \alpha)$ and $O(\alpha^3 \ln \alpha)$ contributions, the theoretical uncertainties have been reduced to below 0.00018 μs^{-1} (corresponding to a D of 10 times 194). Even this pessimistic theoretical uncertainty is an order of magnitude smaller than the present experimental errors. Progress in solving the orthopositronium lifetime puzzle will have to come from the experimental side, with a reconciliation of the difference between the Michigan gas and vacuum experiments and the Tokyo powder experiments. If the Michigan results are confirmed, we are faced with the challenge and opportunity of a true discrepancy between theory and experiment for QED.

ACKNOWLEDGMENTS

The work of JS was partially supported by NSF Grant PHY-9870017 and that of GA by NSF Grants PHY-9711991, PHY-9722074, and PHY-0070819. GA acknowledges the hospitality of the Aspen Center for Theoretical Physics and the Physics Department of UCLA. We thank P. Labelle, G. P. Lepage, R. Hill, K. Melnikov, and A. Yelkhovsky for very useful conversations. The constant encouragement of the Michigan experimental group is gratefully acknowledged.

REFERENCES

1. M. Deutsch, *Phys. Rev.* **82** (1951), 455.
2. M. Deutsch, *in* "Positron Annihilation" (P. G. Coleman, S. C. Sharma, and L. M. Diana, Eds.), pp. 3–8, North Holland, Amsterdam, 1982.
3. M. Deutsch, *in* "The Superworld II" (A. Zichichi, Ed.), pp. 517–524, Plenum Press, New York, 1990.
4. C. D. Anderson, *Phys. Rev.* **41** (1932), 405.
5. S. Mohorovičić, *Astron. Nachr.* **253** (1934), 94.

6. A. E. Ruark, *Phys. Rev.* **68** (1945), 278.
7. J. A. Wheeler, *Ann. N.Y. Acad. Sci.* **48** (1946), 219.
8. J. Pirenne, *Arch. Sci. Phys. Nat.* **28** (1946), 233; **29** (1947), 121, 207, 265.
9. A. Ore and J. L. Powell, *Phys. Rev.* **75** (1949), 1696.
10. S. DeBenedetti and H. C. Corben, *Ann. Rev. Nucl. Sci.* **4** (1954), 191.
11. B. Maglic, *in* "Adventures in Experimental Physics," Vol. 4, pp. 64–127, World Science Education, Princeton, NJ, 1975. This reference includes "One Researcher's Personal Account" by M. Deutsch, along with reprints of many original papers and explanatory physics notes for nonspecialists.
12. M. A. Stroscio, *Phys. Rep.* **22** (1975), 215.
13. S. Berko and H. N. Pendleton, *Ann. Rev. Nucl. Part. Sci.* **30** (1980), 543.
14. A. Rich, *Rev. Mod. Phys.* **53** (1981), 127.
15. A. P. Mills, Jr. and S. Chu, *in* "Quantum Electrodynamics" (T. Kinoshita, Ed.), p. 774, World Scientific, Singapore, 1990.
16. A. Rich, R. S. Conti, D. W. Gidley, J. S. Nico, M. Skalsey, J. Van House, and P. W. Zitzewitz, *in* "New Frontiers in Quantum Electrodynamics and Quantum Optics" (A. O. Barut, Ed.), p. 257, Plenum Press, New York, 1990.
17. V. V. Dvoeglazov, R. N. Faustov, and Y. N. Tyukhtyaev, *Mod. Phys. Lett. A* **8** (1993), 3263.
18. M. I. Dobroliubov, S. N. Gninenko, A. Y. Ignatiev, and V. A. Matveev, *Int. J. Mod. Phys. A* **8** (1993), 2859.
19. M. Deutsch, *Phys. Rev.* **83** (1951), 866.
20. R. H. Beers and V. W. Hughes, *Bull. Am. Phys. Soc.* **13** (1968), 633.
21. V. W. Hughes, "Physik 1973, Plenarvortrag Physikertagung 37th," p. 123, Physik Verlag, Weinheim, Germany, 1973.
22. P. G. Coleman and T. C. Griffith, *J. Phys. B* **6** (1973), 2155.
23. D. W. Gidley, K. A. Marko, and A. Rich, *Phys. Rev. Lett.* **36** (1976), 395.
24. D. W. Gidley, P. W. Zitzewitz, K. A. Marko, and A. Rich, *Phys. Rev. Lett.* **37** (1976), 729.
25. T. C. Griffith and G. R. Heyland, *Nature* **269** (1977), 109.
26. K. F. Canter, B. O. Clark, and I. J. Rosenberg, *Phys. Lett. A* **65** (1978), 301.
27. D. W. Gidley, A. Rich, P. W. Zitzewitz, and D. A. L. Paul, *Phys. Rev. Lett.* **40** (1978), 737.
28. D. W. Gidley and P. W. Zitzewitz, *Phys. Lett. A* **69** (1978), 97.
29. T. C. Griffith, G. R. Heyland, K. S. Lines, and T. R. Twomey, *J. Phys. B* **11** (1978), L743.
30. D. W. Gidley, A. Rich, E. Sweetman, and D. West, *Phys. Rev. Lett.* **49** (1982), 525.
31. P. Hasbach, G. Hilkert, E. Klempt, and G. Werth, *Nuovo Cimento A* **97** (1987), 419.
32. C. I. Westbrook, D. W. Gidley, R. S. Conti, and A. Rich, *Phys. Rev. Lett.* **58** (1987), 1328.
33. C. I. Westbrook, D. W. Gidley, R. S. Conti, and A. Rich, *Phys. Rev. A* **40** (1989), 5489.
34. J. S. Nico, D. W. Gidley, A. Rich, and P. W. Zitzewitz, *Phys. Rev. Lett.* **65** (1990), 1344.
35. S. Asai, S. Orito, and N. Shinohara, *Phys. Lett. B* **357**, (1995), 475.
36. O. Jinnouchi, S. Asai, and T. Kobayashi, hep-ex/0011011.
37. M. A. Stroscio and J. M. Holt, *Phys. Rev. A* **10** (1974), 749.
38. W. E. Caswell, G. P. Lepage, and J. Sapirstein, *Phys. Rev. Lett.* **38** (1977), 488.
39. D. Gidley, private communication.
40. We used the values $R_\infty = 3.289841960368(25) \times 10^{15}$ Hz for the Rydberg constant and $\alpha = 7.297352533(27) \times 10^{-3}$ for the fine structure constant from "The NIST Reference on Constants, Units, and Uncertainty" (available at http://physics.nist.gov/cuu). Note that $c = \hbar = 1$ in our units.
41. I. Harris and L. M. Brown, *Phys. Rev.* **105** (1957), 1656.
42. P. Pascual and E. de Rafael, *Lett. Nuovo Cimento* **IV** (1970), 1144.
43. M. A. Stroscio, *Phys. Lett. A* **50** (1974), 81.
44. M. A. Stroscio, *Phys. Rev. A* **12** (1975), 338.
45. W. E. Caswell and G. P. Lepage, *Phys. A* **20** (1979), 36.
46. I. B. Khriplovich and A. S. Yelkhovsky, *Phys. Lett. B* **246** (1990), 520.
47. G. S. Adkins, *Ann. Phys. (N.Y.)* **146** (1983), 78.
48. M. A. Stroscio, *Phys. Rev. Lett.* **48** (1982), 571.
49. L. Lewin, "Polylogarithms and Associated Functions," North-Holland, New York, 1981.
50. G. S. Adkins, *Phys. Rev. A* **27** (1983), 530.
51. G. S. Adkins, *Phys. Rev. A* **31** (1985), 1250.
52. G. S. Adkins and D. D. Velkov, *Phys. Rev. A* **46** (1992), 7297.
53. G. S. Adkins, A. A. Salahuddin, and K. E. Schalm, *Phys. Rev. A* **45** (1992), 7774.
54. G. S. Adkins, A. A. Salahuddin, and K. E. Schalm, *Phys. Rev. A* **45** (1992), 3333.
55. G. S. Adkins, R. N. Fell, and J. Sapirstein, *Phys. Rev. Lett.* **84** (2000), 5086.
56. G. S. Adkins, *Phys. Rev. Lett.* **76** (1996), 4903.
57. A. P. Burichenko, *Yad. Fiz.* **56** (1993), 123. [*Phys. At. Nucl.* **56** (1993), 640].
58. G. S. Adkins and F. R. Brown, *Phys. Rev. A* **28** (1983), 1164.
59. G. P. Lepage, P. B. Mackenzie, K. H. Streng, and P. M. Zerwas, *Phys. Rev. A* **28** (1983), 3090.

60. A. P. Burichenko and D. Y. Ivanov, *Yad. Fiz.* **58** (1995), 898. [*Phys. At. Nucl.* **58** (1995), 832].
61. G. S. Adkins and Y. Shiferaw, *Phys. Rev. A* **52** (1995), 2442.
62. G. S. Adkins and M. Lymberopoulos, *Phys. Rev. A* **51** (1995), R875.
63. G. S. Adkins and M. Lymberopoulos, *Phys. Rev. A* **51** (1995), 2908.
64. G. S. Adkins, R. N. Fell, and J. Sapirstein, *Phys. Rev. A* **63** (2001), 032511.
65. S. G. Karshenboim, *Zh. Eksp. Teor. Fiz.* **103** (1993), 1105. [*JETP* **76** (1993), 541].
66. R. J. Hill and G. P. Lepage, *Phys. Rev. D* **62** (2000), 111301(R).
67. B. A. Kniehl and A. A. Penin, *Phys. Rev. Lett.* **85** (2000), 1210; **85** (2000), 3065(E).
68. K. Melnikov and A. Yelkhovsky, *Phys. Rev. D* **62** (2000), 116003.
69. G. S. Adkins, M. H. T. Bui, and D. Zhu, *Phys. Rev. A* **37** (1988), 4071.
70. W. E. Caswell and G. P. Lepage, *Phys. Lett. B* **167** (1986), 437.
71. A. Pich, hep-ph/9806303.
72. B. R. Holstein, hep-ph/0010033.
73. P. Labelle, G. P. Lepage, and U. Magnea, *Phys. Rev. Lett.* **72** (1994), 2006.
74. P. Labelle, Ph.D. thesis, "Order Alpha**2 Nonrelativistic Corrections to Positronium Hyperfine Splitting and Decay Rate Using Nonrelativistic Quantum Electrodynamics," Cornell University, 1994. 175. Advisor: Lepage, G. Peter.
75. A. Czarnecki, K. Melnikov, and A. Yelkhovsky, *Phys. Rev. Lett.* **83** (1999), 1135.
76. A. Czarnecki, K. Melnikov, and A. Yelkhovsky, *Phys. Rev. A* **61** (2000), 052502.
77. T. Kinoshita and M. Nio, *Phys. Rev. D* **53** (1996), 4909.
78. A. H. Hoang, P. Labelle, and S. M. Zebarjad, *Phys. Rev. A* **62** (2000), 012109.
79. G. S. Adkins and R. N. Fell, *Phys. Rev. A* **60** (1999), 4461.
80. G. S. Adkins, R. N. Fell, and P. M. Mitrikov, *Phys. Rev. Lett.* **79** (1997), 3383.
81. A. H. Hoang, P. Labelle, and S. M. Zebarjad, *Phys. Rev. Lett.* **79** (1997), 3387.
82. A. H. Hoang, *Phys. Rev. D* **56** (1997), 7276.
83. G. Källén and A. Sabry, *Dan. Mat. Fys. Medd.* **29** (1955), 1.
84. J. Schwinger, "Particles, Sources, and Fields," Vol. II, Addison-Wesley, Reading, MA, 1973.
85. G. S. Adkins, R. N. Fell, and J. Sapirstein, *Phys. Rev. D* **63** (2001), 125009.
86. G. S. Adkins, *Phys. Rev. D* **47** (1993), 3647.
87. G. S. Adkins, M. Lymberopoulos, and D. D. Velkov, *Phys. Rev. D* **50** (1994), 4194.
88. S. G. Karshenboim, *Yad. Fiz.* **56** (1993), 155. [*Phys. At. Nucl.* **56** (1993), 1710].
89. See [61] and references therein.
90. R. Barbieri, P. Christillin, and E. Remiddi, *Phys. Rev. A* **8** (1973), 2266.
91. M. A. Samuel, *Phys. Rev. A* **10** (1974), 1450.
92. L. Hostler, *J. Math. Phys.* **5** (1964), 1235.
93. J. Schwinger, *J. Math. Phys.* **5** (1964), 1606.
94. W. E. Caswell and G. P. Lepage, *Phys. Rev. A* **18** (1978), 810.
95. G. S. Adkins and J. D. Cammerata, *Phys. Rev. A* **45** (1992), 1314.
96. R. E. Cutkosky, *J. Math. Phys.* **1** (1960), 429.
97. A. C. Hearn, Rand Publication CP78, unpublished, 1985.
98. G. P. Lepage, *J. Comput. Phys.* **27** (1978), 192.
99. P. Labelle, private communication.
100. A. I. Milstein and I. B. Khriplovich, *Zh. Eksp. Teor. Fiz.* **106** (1994), 689. [*JETP* **79** (1994), 379].
101. I. B. Khriplovich and A. I. Milstein, hep-ph/9607374.
102. D. W. Gidley, April Meeting of the American Physical Society, 1998.
103. R. S. Conti, R. S. Vallery, D. W. Gidley, J. J. Engbrecht, M. Skalsey, and P. W. Zitzewitz, *in* "The Hydrogen Atom: Precision Physics of Simple Atomic Systems" (S. G. Karshenboim *et al.*, Eds.), Springer-Verlag, Berlin, 2001.